# THE UNIVERSITY of EDINBURGH

This thesis has been submitted in fulfilment of the requirements for a postgraduate degree (e.g. PhD, MPhil, DClinPsychol) at the University of Edinburgh. Please note the following terms and conditions of use:

Adaptive Waveform Design for SAR in a Crowded Spectrum

Claire Tierney

Doctor of Philosophy.
The University of Edinburgh.
July 2018

Abstract

This thesis concerns the development of an adaptive waveform design scheme for synthetic aperture radar (SAR) to support its operation in the increasingly crowded radio frequency (RF) spectrum, focusing on mitigating the effects of external RF interference.

The RF spectrum is a finite resource and the rapid expansion of the telecommunications industry has seen radar users face a significant restriction in the range of available operational frequencies. This crowded spectrum scenario leads to increased likelihood of RF interference either due to energy leakage from neighbouring spectral users or from unlicensed transmitters.

SAR is a wide bandwidth radar imaging mode which exploits the motion of the radar platform to form an image using multiple one dimensional profiles of the scene of interest known as the range profile. Due to its wideband nature, SAR is particularly vulnerable to RF interference which causes image impairments and overall reduction in quality. Altering the approach for radar energy transmission across the RF spectrum is now imperative to continue effective operation.

Adaptive waveforms have recently become feasible for implementation and offer the much needed flexibility in the choice and control over radar transmission. However, there is a critically small processing time frame between waveform reception and transmission, which necessitates the use of computationally efficient processing algorithms to use adaptivity effectively.

This simulation-based study provides a first look at adaptive waveform design for SAR to mitigate the detrimental effects of RF interference on a pulse-to-pulse basis. Standard SAR systems rely on a fixed waveform processing format on reception which restricts its potential to reap the benefits of adaptive waveform design. Firstly, to support waveform design for SAR, system identification techniques are applied to construct an alternative receive processing method which allows flexibility in waveform type. This leads to the main contribution of the thesis which is the formation of an adaptive spectral waveform design scheme.

A computationally efficient closed-form expression for the waveform spectrum that minimizes the error in the estimate of the SAR range profile on a pulse to pulse basis is derived. The range profile and the spectrum of the interference are estimated at each pulse. The interference estimate is then used to redesign the proceeding waveform for estimation of the range profile at the next radar platform position. The solution necessitates that the energy is spread across the spectrum such that it competes with the interferer. The scenario where the waveform admits gaps in the spectrum in order to mitigate the effects of the interference is also detailed and is the secondary major thesis contribution. A series of test SAR images demonstrate the efficacy of these techniques and yield reduced interference effects compared to the standard SAR waveform.

Lay Abstract

Synthetic aperture radar (SAR) is an imaging technology which provides high resolution images of the Earth surface. SAR operates at a distance using the radio frequency (RF) spectrum to transmit signals. These signals reflect off the Earth's surface and the returned signals are used to form an image. However, the RF spectrum is a finite resource and is also used heavily by the communications industry to supply internet and phone coverage, among numerous other applications. When more than one RF technology uses a similar region of the spectrum, the interactions between these signals causes interference. Signal interference can significantly reduce the resultant SAR image quality . In this "crowded RF spectrum, in part due to the rapidly developing communications industry, interference is now an ever-present threat.

The signal which the radar transmits has, until recently, been pre-determined. Advancements in physical radar components now provide potential for the signal to be designed according to its environment while "on-the-fly. With the appropriate instructions to the radar, it could operate adaptively by changing the transmission according to the RF interference.

This thesis provides a possible solution to aid the operation of SAR in the crowded spectrum by both defining new signals for transmission and a new means to process them according to the RF interference. This reduces the impact of interference on the final SAR image, restoring quality to the images.

Declaration of Originality

I declare that this thesis was composed by myself, that the work contained herein is my own except where explicitly stated otherwise in the text, and that this work has not been submitted for any other degree or professional qualification except as specified.

Claire Tierney, July 2018

Acknowledgements

Contents

List of figures

List of tables

Abbreviations & Notation

Abbreviations & Acronyms

ADC	Analogue to digital converter
APES	Amplitude and phase estimation
AR	Autoregressive
CRLB	Cramer rao lower bound
DFT	Discrete Fourier transform
FDWO	Frequency domain waveform optimization
FFT	Fast Fourier transform
FIR	Finite impulse response
FPGA	Field programmable gate array
GAPES	Gapped amplitude and phase estimation
GFDWO	Gapped frequency domain waveform optimization
GLS	generalized least squares
IRCI	Independent range cell interference
ISL	Integrated sidelobe level
LFM	Linear-frequency modulation
LMS	Least mean squares
MF	Matched filter
MI	Mutual information
MIMO	Multiple-input-multiple output
ML	Maximum likelihood
MSE	Mean square error
NLFM	Non-linear-frequency modulation
OFDM	Orthogonal frequency division multiplexing
OLS	Ordinary least squares
PSD	Power spectral density
PSL	Peak sidelobe level
PSO	particle swarm optimization
RF	Radio frequency

RFI   Radio frequency interference

SAR   Synthetic aperture radar

SINR   Signal to interference and noise ratio

SCNR   Signal to clutter and noise ratio

SNR   Signal to noise ratio

SPA   Stationary phase approximation

TCFDE   Time constrained frequency domain estimate

Notation

a lowercase mathtype denotes a scalar

$\mathbf{a}$ boldface lowercase denotes a vector

$\mathbf{A}$ boldface uppercase denotes a matrix

$(\mathbf{A})^T$ transpose operator

$(\mathbf{A})^H$ hermitian operator

$*$ Linear convolution

$\circledast$ circular convolution

$\mathrm{cov}(.)$ covariance

$\mathrm{tr}(.)$ trace

$\mathrm{diag}(.)$ diagonal (creates square matrix with non-zero entries only on the main diagonal)

$\mathrm{E}[.]$ expectation

$\hat{(.)}$ estimated value

$\mathbf{I}_n$ identity matrix of dimension n

$\mathbf{F}$ discrete Fourier transform

f frequency

t time

a waveform amplitude - time domain

$\mathbf{x}$ waveform transmission - time domain

$\mathbf{y}$ received waveform - time domain

$\mathbf{h}$ impulse response

$\mathbf{h}_c$ constrained impulse response estimate

$\boldsymbol{\Omega}$ waveform transmission - frequency domain

$\mathbf{Y}$ received waveform - frequency domain

$\mathbf{H}$ frequency response

$\mathbf{H}_c$ constrained frequency reponse estimate

$\mathbf{H}_u$ unconstrained frequency reponse estimate

$\mathbf{X}$ transmitted signal matrix

$\mathbf{X}_c$ transmitted signal cyclic matrix

$\mathbf{n}$ noise plus interference

$\mathbf{D}$ interference spectrum power

$\mathbf{R}_{nn}$ noise plus interference covariance matrix

$\mathbf{E}_i$ waveform energy spectral density

ϕ phase

B_c bandwidth

α chirp rate

τ_c pulse length

N number of waveform samples

K number of impulse response samples

M number of received waveform samples

Δr_k range resolution

r_0 slant range distance

t_i time taken to nearest range cell of interest

t_k time taken to furthest range cell of interest

$\mathbf{R}$ OFDM impulse response cyclic matrix

$\mathbf{s}$ OFDM transmitted signal

E_T total waveform energy

σ_n noise variance

ρ impulse response MSE

$\mathcal{S}$ set of samples allowing transmission in frequency domain

$\mathcal{S}^{\complement}$ complementary set disallowing transmission in frequency domain

$\hat{\mathbf{H}}_G$ gapped frequency reponse estimate

τ absolute interference threshold

τ_d relative interference threshold

Chapter 1
Introduction

1.1 Problem Description and Motivation

Synthetic Aperture Radar (SAR) is an imaging mode which can provide 2D(dimensional) or 3D images in the form of a reflectivity map [6]. Airborne SAR systems are used in either military or commercial applications and are operational day or night to provide images of the surface at a sub-metre, and more recently, sub-centimetre level. These high resolution images are obtained by using a waveform with high bandwidth and sufficient energy to discern between stronger and weaker reflectors on the surface. Since conception of the SAR system, the SAR waveform and its receive processing format has seen little change. The receive-processing, known as "deramp processing", has benefits including lower requirements on the analogue to digital converter (ADC). Additionally, deramp offers a limited level of noise suppression [7, 8], but is heavily dependent on a spectrally contiguous and flat waveform - known as the linear chirp. As a high-bandwidth mode, SAR relies on these large contiguous blocks of the radio frequency (RF) spectrum to obtain fine resolution images. However, the RF spectrum is effectively a finite resource [9, 10] - the rapid expansion of the telecommunications industry continuous to encroach towards areas of the spectrum reserved for radar, causing the need for radars to reduce transmission in areas of the spectrum. This crowded spectrum problem has lead to increased likelihood of interference from other surrounding RF users, particularly for wideband emitters. This ultimately has a negative impact on performance.

Radio frequency interference (RFI) can originate from spectral leakage from neighbouring users, unlicensed transmitters that attempt to operate in the same bandwidth as the radar or by deliberate electronic attack.The quality of a SAR image can be heavily degraded by interference. Interference in SAR has been shown to cause aberrations in the image including; false targets, blurring, creation of bright lines and reduction of the power dynamic range, meaning there is less sensitivity to discriminate between stronger

and weaker targets [3, 5, 11, 12]. In cases of very high interference, no image features are provided at all. While the 2D aspect of the imaging process allows some reduction of the impact of noise (through coherent gain), this is not possible if the source of the interference is of similar magnitude as the returns.

The ultra high frequency (UHF) and VHF bands are highly spectrally congested as this is the largely occupied by television, radio and other communications systems. SAR operation in this spectral region has many desirable applications, such as foliage penetration and sub-terrain visibility [13]. However, RF interference is a major problem as due to occupation by a large number of high power transmitters. For applications such as foliage penetration SAR, these frequencies must be removed in order to allow detection of objects under the foliage. This issue in UHF/VHF SAR led to the first attempts to mitigate interference in SAR via filtering approaches, at the cost of losing some sensitivity and resolution. As spectral congestion has become increasingly widespread, this issue of RF interference is now also pertinent to X-band and other higher frequency bands of SAR.

Low frequency SAR combined with ultra-high bandwidths have many desirable applications, such as being particularly suited to foliage penetration and allowing some sub-terrain visibility. These bands were originally in widespread use by television and radio services. The high power transmission in addition often exceeds the receiver noise, limiting system sensitivity. As spectral congestion has become increasingly widespread, this issue of RF interference is now also pertinent to X-band and other higher frequency bands of SAR.

It is clear that in the future SAR operation may be increasingly vulnerable and must consider a more flexible occupation of the spectrum - rather than the linear chirp with deramp processing which is prevalent in current SARs. Waveform agility, the ability to change waveform transmission on-the-fly [14], has become practically feasible due to the recent advancements in transmitter technology, allowing flexibility in the choice and control of transmit waveform facilitated using field-programmable gate arrays (FPGAs). Additionally, hardware advances allow faster rate ADCs which can support sampling a full bandwidth on receive, and reduces the reliance on deramp processing. In order to fully exploit this potential, computationally efficient waveform-design algorithms are required for the waveform to optimise its spectral occupation according to its environ-

ment in a responsive manner. A means to address RFI in SAR could lie in proper application of adaptive waveform design techniques.

1.2 Thesis Aims

This thesis aims to address the problem of RF interference (RFI) in SAR by adaptively designing appropriate waveforms in the spectral domain. Waveform design is a rapidly emerging field of radar spanning interest across detection [15–17], tracking [18–22] and target recognition [17, 23, 24] applications. The majority of the cutting-edge waveform design techniques are based on heavily computationally expensive iterative methods that are not always guaranteed to converge to a solution [25–28] - this poses a critical issue for on-the fly waveform design. Furthermore, there are a lack of techniques available for near-future or current radar hardware available: many waveform design techniques are designed irrespective of hardware constraints or computational burden. Another consideration which this thesis aims to address is that there is often little mention of how waveform-design procedures obtain a profile of the surrounding RFI spectrum and is usually assumed to be known [29, 30], static or given by a radio frequency environment map [25–27].

With regard to these concerns, this thesis attempts to provide an adaptive waveform design solution for SAR in the crowded spectrum which:

1. Reduces the impact of RFI on the resultant SAR image

2. Facilitates adaptivity by finding a computationally low cost solution, allowing regular re-design of the waveform on-the-fly

3. Is feasibly implementable into current electronically scanned radars

4. Is capable of estimating the interference

A first-look at a possible adaptive waveform design solution is addressed in the following work and the scope is thereby restricted to focusing on the underlying theory and demonstrating these techniques via simulation. As the techniques discussed are adaptive, obtaining real data would rely on an existing radar with waveform agility and built with the algorithms that follow herein. While the aim is to provide a solution that

could be built with current technologies, it would not be feasible to build this radar on the timescale of this study.

1.3 Organization

This thesis spans across two distinct and well-studied research fields of waveform design and interference mitigation for SAR - this thesis serves an initial bridge between these two fields.

- **Chapter 2**: Presents a literature review which firstly introduces the concept of cognitive radar and adaptive waveform design. To set-up the following review on the scope of waveform design literature, a short summary of the fundamentals of radar waveform design and SAR waveforms is included. A review of the salient works in waveform design is also included, which discusses the key ideas in waveform design and its challenges. The final section presents an overview of the existing techniques for RFI in SAR.

- **Chapter 3**: This chapter both contains the necessary background for SAR range profile estimation for this thesis but also presents a novel application of system identification methods for range-profile estimation in SAR. The discrete time-domain system model used throughout the thesis is presented here. The existing methods of range-profile estimation for SAR are discussed along with an comparative analysis of a recent study [31] on the communications-based technique of Orthogonal-frequency division multiplexing (OFDM) for SAR. There are interesting similarities between the proposed SAR system identification method and OFDM-SAR - comparisons via simulation are also demonstrated here.

- **Chapter 4**: An adaptive waveform scheme for RFI mitigation for SAR is presented here. The system identification method proposed in Chapter 3 is extended for the case of correlated interference to include RFI estimation. A spectral waveform optimization technique and a possible waveform synthesis approach is then given. Simulated SAR images are shown to demonstrate the outcome of the technique. The solution of the waveform design attempts to "fight" the interference to occupy the spectrum.

- **Chapter 5**: Expanding on the adaptive scheme proposed in Chapter 4, this section explores the case where the design solution is modified to include gaps in the spectrum; the system must decide which areas of the spectrum to occupy via a "fight or flight" mode and surrender occupation of regions of the spectrum in the interest of improving overall performance. The system identification and waveform optimization processes are modified accordingly. An analysis on the impact on performance using this technique compared to the prior is given. Existing methods for returning the lost spectral information are also applied.

- **Chapter 6**: A summary of the thesis outcomes and the possible areas for future work are discussed.

1.4   Thesis Contributions

The main contributions to knowledge in this thesis are:

- **System Identification for SAR**: Design of an alternative receive-processing algorithm for range-profile estimation replacing the traditional pulse-compression step using frequency-domain system identification techniques. A comparison to the frequency-domain system identification and OFDM-SAR is also a novel contribution.

- **Adaptive Waveform Design Scheme**: A novel formulation to optimize the estimation of the range profile on a pulse-by-pulse adaptive manner by changing the spectral content of the waveform. The solution form dictates a spectrum-competitive approach is optimal, and thereby attempts to "fight" for occupation of the spectrum.

- **Spectral "Fight or Flight" Analysis**: Modification of the novel adaptive optimization scheme to yield gaps in the spectrum in interest of enhancing the overall performance.

1.5   Publications

- C. Tierney and B. Mulgrew, "Adaptive waveform design with least-squares system identification for interference mitigation in SAR," 2017 IEEE Radar Conference (RadarConf), Seattle, WA, 2017, pp. 0180-0185.

- C. Tierney and B. Mulgrew, "Waveform independent range profile reconstruction for SAR," International Conference on Radar Systems (Radar 2017), Belfast, 2017, pp. 1-6.

- C.Tierney and B. Mulgrew, "Adaptive waveform design for interference mitigation in SAR", IEEE TAES, Revised & Re-submitted

- C.Tierney and B. Mulgrew, "Adaptive waveform design with gapped spectrum ", Proceedings of the Instititute of Acoustics, 4th SAR & Sonar Conference, Lerici, September 2018, to-appear

Chapter 2
Literature Review

2.1 Waveform Fundamentals

To understand the potential in waveform design and how it can be applied, the basic properties of radar waveforms should first be discussed. A brief introduction and review of the basic types of radar waveforms and their properties are presented in the following section. Waveform design is widely researched and a large number of waveforms are possible but the focus here is on waveforms for SAR. In SAR, one of the primary metrics of concern is the range resolution. It determines the limit on the smallest distinction between identical scatterers which can be resolved with the radar line of sight and often sets the basis for system requirements. As well as affecting range resolution, the choice of waveform directly impacts several performance metrics such as signal to noise ratio (SNR), Doppler resolution, range and Doppler sidelobes and range-Doppler coupling. The waveform properties which influence these metrics are the pulse duration τ, bandwidth, amplitude and the phase or frequency modulation applied.

2.1.1 Waveform Properties

The general expression for modeling a radar waveform is as follows

$$x(t) = a(t)\exp(2\pi j f_0 t + \phi) \tag{2.1}$$

where f_0 is the carrier frequency of the radar, $\mathbf{a}$ is the amplitude of carrier envelope and ϕ is any phase modulation that is added onto the carrier of the wave [1]. Beyond altering the carrier frequency and the duration of the pulse, the key parameters for radar waveform design are the carrier envelope $\mathbf{a}$ and ϕ. These are the significant degrees of freedom available for radar waveform design via modulation. Classically, in a fixed waveform type scenario, waveform design may rely on pulse duration or inter-pulse metrics such as pulse repetition frequency. In the adaptive waveform design framework,

the interest lies in the design of the pulse itself with respect to its amplitude and phase properties.

While it is apt to tailor an individual waveform to a specific task or radar hardware capability, there are three properties which are desirable for the general current radar system: 1) constant modulus amplitude envelope,e.g. ($\|a(t)\| = 1$), 2) continuous phase, 3) spectral containment of the waveform

1. A constant modulus amplitude is beneficial for two reasons. Firstly it avoids causing non-linear distortion at the transmitter which causes deviation from the desired waveform output. Secondly it makes full use of the amplitude at each time instant, maximizing the available power - i.e. increased power efficiency. Constant amplitude is much easier from a hardware standpoint for the class-C type amplifiers which are generally found in current radar systems [32]. Future radar systems may have amplifiers with the capability to modulate the amplitude envelope. This would offer further freedom in waveform design, but would be at the cost of reduced power-efficiency across the pulse. It is worth noting that many radar applications have a direct link between maximizing power for optimal performance, particularly in detection problems.

2. Electronically scanned radars rely on phase differences to steer the beam. Phase modulation which increases continually, allows the creation of a beam over the duration of a pulse transmission. This corresponds to the instantaneous frequency varying linearly upwards or downwards over time.

3. Spectral containment minimizes the spectral shaping that occurs at the transmitter that can result in unwanted amplitude modulation effects which can then lead to distortion and further problems encountered by directly amplitude modulation. [32]

2.1.2 Waveforms Types

Transmitting a single frequency sinusoidal radar signal without any amplitude modulation only has one degree of freedom available - pulse duration. A simple sinusoidal signal has an inherent performance trade off between energy and resolution via pulse duration control. A long pulse length is required to provide enough energy on target,

however shorter pulse lengths provide higher resolution. A high resolution waveform with a specified transmitted energy cannot be obtained. The answer to this problem lies in a process known as "pulse compression": modulating the phase over time to allow the signal to spread its energy over a band of frequencies. By modulating the frequency the waveform energy and range resolution are able to be controlled separately. The resolution in a pulse compressed waveform can be obtained with a pulse longer than that of the pure tone signal. This allows energy criteria to be met. Waveform design is one part of the solution. Correct receiver processing is also necessary to achieve the desired outcome and any associated performance gains (see Chapter 3). Dating back to the 1940's, pulse compression could be considered the original breakthrough in waveform diversity. The introduction of pulse compression allowed a significant increase of control over the transmitted waveform and performance gain.

2.1.2.1 Linear Frequency Modulation

The standard method of obtaining pulse compressed waveforms is by linearly increasing the instantaneous frequency over time - known as a "linearly frequency modulated" (LFM) or "chirped waveform". The constant rate of increase in frequency over time, allows for straightforward implementation in hardware due to its constant modulus amplitude and increasing phase sweep. It also has in-built advantages for processing on receive in terms of reducing the requirements for the analogue to digital converter (ADC) [8]. By modulating an additional frequency term with changes in time onto the centre frequency, chirps provide a method of increasing waveform bandwidth for a given pulse length without reducing the total energy transmitted. For a defined chirp period τ_c, the waveform instantaeous frequency increases across the bandwidth value from carrier frequency $f_0 - \Delta\frac{f}{2}$ to $f_0 + \Delta\frac{f}{2}$. This "sweep" in frequency is defined by the chirp rate $\alpha = \frac{B_c}{\tau_c}$. The phase of a linear chirp waveform is therefore defined as follows

$$\phi(t) = \pi \frac{B_c}{\tau_c} t^2 \tag{2.2}$$

where t denotes the time axis and B_c denotes the signal bandwidth. Where the instantaneous frequency is the time derivative of the phase:

$$F_i(t) = \frac{d\phi(t)}{dt} = \dot{\phi}(t) = \frac{1}{2\pi}\frac{B_c}{\tau_c} t \tag{2.3}$$

9

The change in the frequency at each time step is a constant linear change; the frequency increases linearly across the bandwidth B over the pulse length τ. For low bandwidth-time products the spectrum is not well defined. The higher the product the more rectangular the spectrum becomes. An example of lower and higher bandwidth products is shown in Figure 2.1 which demonstrates that for larger time-bandwidth products, the spectrum is more rectangular. As the increase in frequency over time is linear, the energy in the waveform is spread evenly across the spectrum. This creates a flat spectrum as the change in frequency over time is constant.

(a) $B\tau = 10$

(b) $B\tau = 100$
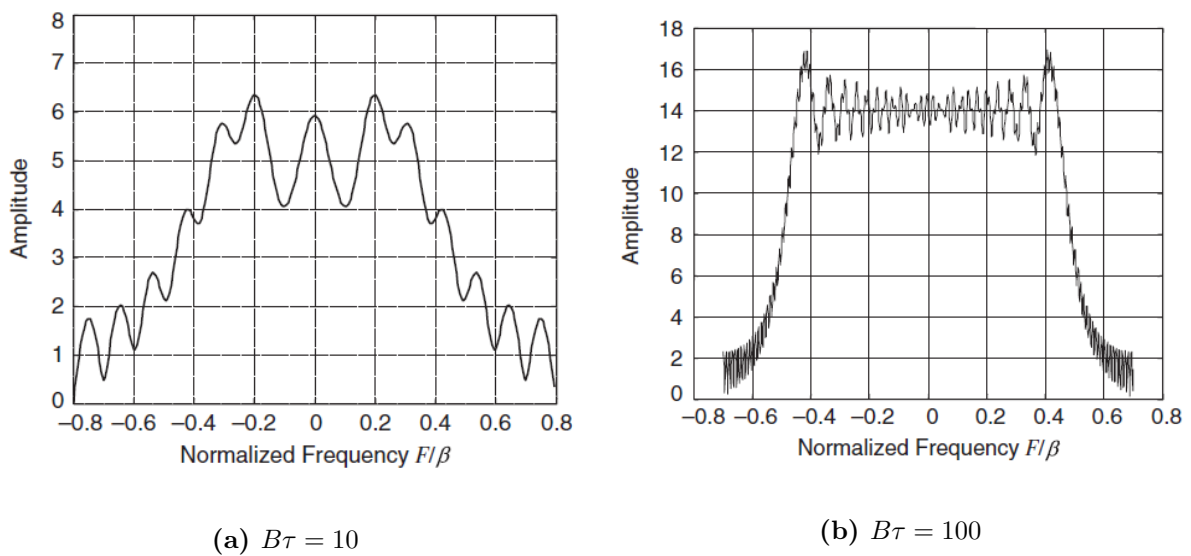
Figure 2.1: *LFM spectrum from two waveforms with low bandwidth time product (a and high product b) which has a more defined rectangular shape [1].*

The matched filter is the standard approach to obtaining the radar range information. This is achieved by correlating the known transmitted signal with the received signal. The spectral shape of the LFM is approximately rectangular, such that its time (range) domain representation is a sinc-shape and necessarily has large sidelobes. Sidelobes are problematic, particularly in the situation where there are two targets that are located closely in range - the sidelobes from the stronger reflector can mask the response from the weaker, causing a failure to detect targets. To counter the effect of high range-sidelobes, applying a window function before application of a DFT is used on receive to reduce spectral leakage effects. This reduces the height of the sidelobes, but causes a mis-match in the filter, reducing the output SNR. A measure of the sidelobes caused from matched filtering a signal can be calculated by using the autocorrelation of the
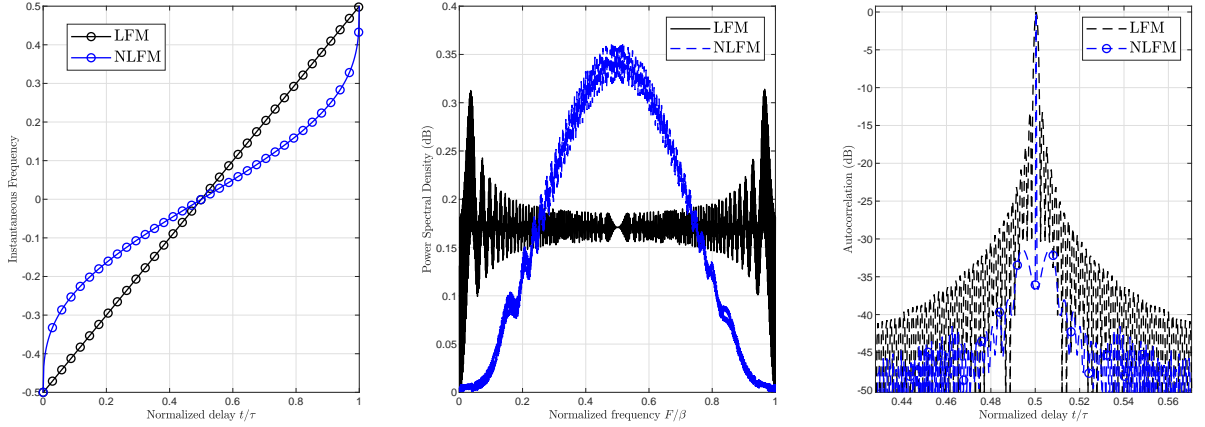
Figure 2.2: *Left-to-right: the change in frequency, PSD and autocorrelation results for LFM and NLFM waveforms of the same energy, bandwidth and pulse length*

function, which is the inverse Fourier transform of the power spectral density

$$A(t) = \mathcal{F}^{-1}[|\Omega(f)|^2] \tag{2.4}$$

where $\mathcal{F}^{-1}$ is the inverse Fourier transform and Ω is the frequency domain radar signal. If it is possible to change the spectrum of the pulse-compressed waveform, the autocorrelation result can also be modified.

2.1.2.2   Non-Linear Frequency Modulation

The LFM signal has a constant rate of change α but a non-linear frequency modulated (NLFM) signal is defined by a variable bandwidth-time sweep rate. By altering the rate of change in frequency over time, this provides a method to change the resultant spectrum, the autocorrelation properties and therefore, the sidelobe level. Due to the direct link between the waveform autocorrelation and the power-spectral density(PSD), NLFM waveforms are often designed according to a desired PSD. For example, instead of applying a window function as done in receive processing for the LFM, the NLFM spectrum can be shaped like a window function to obtain a reduction in sidelobes while maintaining maximum SNR [1]. On choosing the spectrum of an NLFM signal for waveform design, a question is raised: how to translate this PSD into a time-domain signal with constantly increasing phase and constant amplitude? Waveform synthesis

of NLFM waveforms is generally performed either by the stationary phase approximation [33] (SPA) or via various empirical methods involving look-up tables [1]. The stationary phase approximation allows a relationship to be formed between the phase in the time domain and the signal energy in the frequency domains for oscillatory signals. It originates from intractable integrals often encountered in oscillatory signals and exploits properties of the phase to approximate the integral. A comparative example between the LFM and NLFM waveforms for change in frequency, PSD and autocorrelation is shown in Figure 2.2. For this example the NLFM has been designed using SPA tailored to fit the shape of a Hann window.

2.1.2.3 Orthogonal Frequency Division Multiplexing

Orthogonal frequency division multiplexing (OFDM), widely used in digital communications applications, creates a multi-frequency signal which simultaneously transmits multiple sub-carriers to create a wideband signal. OFDM has recently attracted attention for SAR systems due to its potential ability to achieve ultra-high resolution images without the high range sidelobe effects [31, 34, 35] that are observed in standard pulse-compressed waveforms. Radar-centric studies for OFDM have suggested that it may offer enhanced range and Doppler estimation compared to standard radar signals [36, 37]. However, while this framework offers advantages including control over the spectral power, it is a variable amplitude signal in time and not readily synthesized in radar hardware. The OFDM hardware framework allows simultaneous transmission of sub-carriers, each representing a different frequency. Lower range sidelobes are then possible as they are processed separately on receive [38]. The orthogonality of the sub-carriers reduces any potential cross-talk in communications systems. If there are N OFDM sub-carriers $\mathbf{S}$ is the vector of complex weights to be transmitted across a bandwidth B, $\mathbf{S} = [S_0, S_1, \ldots, S_{N-1}]^T$ such that $\sum_{k=0}^{N-1} |S_k|^2 = N$. In discrete time, the OFDM signal is given as

$$s(t) = \frac{1}{\sqrt{N}} \sum_{k=0}^{N-1} S_k \exp\{j2\pi k \Delta f t\} \qquad t \in [0, T + T_{GI}] \tag{2.5}$$

where T is the signal duration, $\Delta f = \frac{B_c}{N} = \frac{1}{T}$ is the spacing between each of the sub-carriers and T_{GI} is the length of the guard interval known in OFDM as the cyclic prefix. Note that the waveform synthesis then directly allows design in the frequency

domain via the subcarrier weights **S**. For communications applications, the motivation for OFDM lies in reducing the cross-talk between sub-carriers which is introduced by unwanted artifacts within the transmission medium. The fundamental goal of the system is different to radar. In communications, the system needs to accurately reconstruct the transmitted signal from the received signal, however in co-located radar, the transmitted signal is known, and the aim is to accurately reconstruct the transmission medium - which is the surrounding airspace in air-to-air applications or an image of the surface in SAR or air-to-surface modes.

The transmission mode is also different. In some communications systems, such as Wi-Fi, the transmission is continuous, but in pulsed radar and SAR there are relatively large intervals between each transmission period. The guard interval in communications systems is built to be at least the same characteristic length of the transmission medium. In a SAR scenario, the scene size or resultant impulse response caused by the intersection of the radar beam on the surface is considered to be the characteristic delay of the system - the time difference between the first returned signal and the last returned signal. In communications, any delay effects caused by the transmission medium in time (an impulse response) are much less than the duration of the signal itself. OFDM employs a repetition of the signal that is the same characteristic time as the impulse response of the transmission medium which is then added to the start of the pulse and is known as a "cyclic prefix". This is then discarded on receive to remove any effects of interference between neighbouring signals caused by an impulse response in the transmission medium. In SAR, the cyclic prefix element which corresponds to the length of the scene size, is much larger than in communications applications as represented in Figure 2.3. Despite these differences there has been promising work focused on how OFDM transmit signal and impulse response times can work under SAR configuration [31, 34]. We focus our interest on one study in particular which provides an algorithm for range profile estimation using OFDM signals for the purposes of removing range-sidelobe effects as seen in the matched filter estimation and further this investigation in Chapter 3.
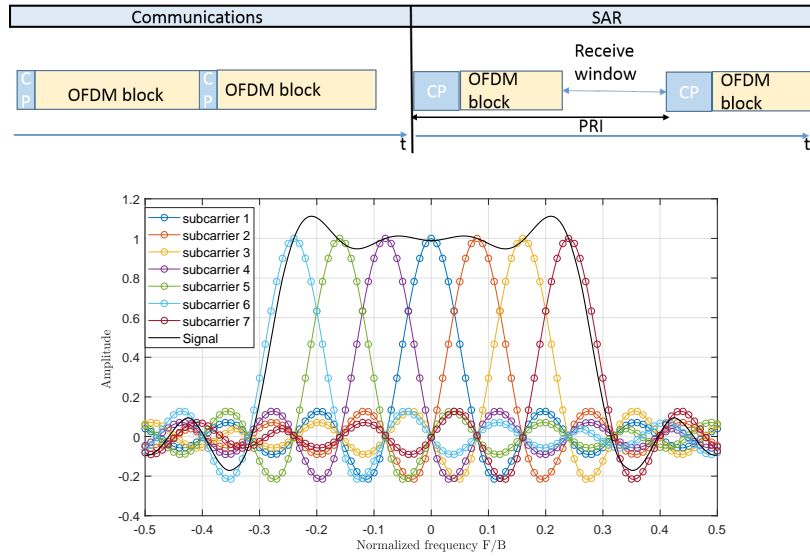
Figure 2.3: *Top:Schematic diagram comparing the transmission modes in communications and SAR. CP denotes the cyclic-prefix "guard interval". Bottom: Reprentation of frequency domain plot of individual OFDM subcarriers and resultant spectrum. Simple example with only 7 subcarriers shown.*

2.2 Cognitive Radar and Waveform Adaptivity

The airborne radar environment can be dynamic and somewhat unpredictable; targets can enter the surroundings without warning, interference may be present from other radio frequency emitters and there is the possibility of threats from electronic countermeasures. In spite of potentially volatile surroundings, traditionally radars have had limited capability to adapt to these changes and rely on manual switches in radar mode initiated by the operator. Even still, radar mode change offers little flexibility. Radar waveform transmitters have classically relied on a small selection of fixed waveforms that lack online support for adapting to the changes in the environment. Options for adaptation are limited to manually switching between waveforms - for example switching between pre-programmed modes such as search and tracking mode.

Cognitive radar and adaptive waveform systems have become of recent interest due to advancements in both transmitter technology and processor power making "on-the-fly" design of transmit waveforms feasible [14]. This provides the potential for waveforms to be specifically tailored to the surrounding RF environment and the requirements of the radar mode. At the heart of the cognitive radar concept is the ability of the radar system to learn from interacting with its environment and applying this knowledge to

new situations. Cognition itself can be defined as a collection of capabilities; perceiving, reasoning and remembering. These are applied to the radar system through sensing of the environment via the transmitter, adaptive algorithms and the concept of memory using databases. The notion of radar system capable of adapting to the surrounding environment was initially proposed in 2006 [39]. In the following years, research covered the various aspects of intelligent radar systems, which can generally be classified within one of following three areas:

1. Adaptive waveform design: focuses on retrieving maximum information from the environment by designing and transmitting waveforms based on knowledge of the scene surrounding the radar

2. Sensor management: responsible for the scheduling of waveform design and information handling over time

3. Cognitive radar: involves a full closed-loop cycle from receiving the waveform to information processing and retransmitting. Cognitive radar includes the waveform design and sensor management.

Waveform design is not an entirely new topic, but receiver advancements have traditionally been the focus of radar research with the development of digital signal processing allowing adaptive processing [14]. It has been suggested that with computationally heavy new receive processing methods, such as space-time-adaptive processing, adding waveform design to the computational load worsens the problem, unless the waveforms can be designed in a computationally simple manner. However, the full potential of waveform design is now becoming realized, in part due to the interest in cognitive radar systems. The cognitive radar concept presents closed loop waveform scheduling, which is often referred to as the perception-action cycle shown in Figure 2.4; the radar perceives its environment via waveform reception, and using this feedback acts accordingly via adapting its transmission [39, 40]. Therefore, in one processing period, the radar system is required to receive and process the return; update any relevant metrics and design and transmit the next waveform, all based on the knowledge obtained from the prior processing period. This raises one of the biggest problems for adaptive radar, limitation of processing time. There is a strict time limit between receiving a pulse, and the transmission of the next - often on the magnitude of around 100ms or less [41].

It is then imperative that waveform design for a closed loop system is computationally efficient.

One approach to this problem is designing a waveform library off-line. The waveform scheduler is then required to calculate a relevant metric, known as a measure of effectiveness(MOE) and choose from a finite selection of waveforms. This of course decreases the ability of the system to tailor the waveform and thereby may incur varying degrees of performance loss. Ideally the waveform transmitted at the end of each processing cycle is designed to be fully optimized according to the most recent information update.

Another approach to reducing computational load is to decide whether or not to redesign the waveform at each pulse. This can be done by considering application specific, information theoretic measures to determine information gain/loss from re-designing the waveform or simply transmitting the same one. In some applications, it is suitable to reduce the rate at which redesign occurs, allowing the processor longer to compute the optimal waveform. Unfortunately, particularly in tracking scenarios where the rate of information change can be high, the calculation of information theoretic metrics can themselves be challenging to compute. The best course of action is to, where possible, design computationally efficient algorithms for computation of waveforms.
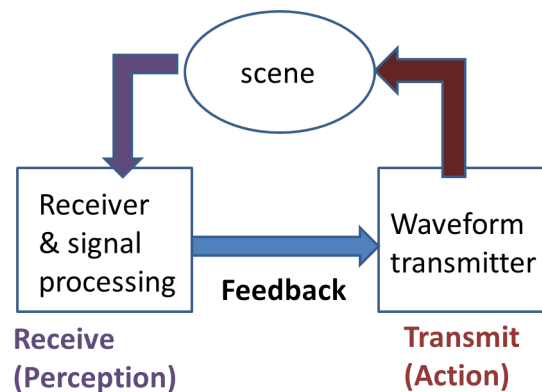
Figure 2.4: *The cognitive radar "perception-action cycle" relating to the transmitted and received signal*

2.3   Waveform Design

The renewed interest in waveform design has largely originated from three key problems: 1) interference from surrounding RF users - either through intentional jamming or unintentional means, such as due to spectral leakage, 2) the wish to optimize performance for a particular task, for example to maximize detection of targets in clutter, 3) the increasingly crowded spectrum resulting in radar systems needing to share areas of the spectrum that were previously reserved exclusively for radar.

With the progress of technology, all of these problems are intensifying. With more RF spectral users, interference is becoming more widespread, either due to energy leakage from neighbouring RF users or with increased capability of intentional jamming systems. Demands for higher specification radar are ever increasing with regards to superior mode operation, including enhanced detection, target classification and higher resolution SAR. These place pressure on all aspects of the radar system. Higher radar bandwidth allows higher resolution and enhances the ability for target classification and finer SAR resolution. Higher power provides better signal to noise and therefore enhanced detection [1]. Waveform design provides a means to leverage the best performance out of the available fundamental restrictions of the radar system. This shifts demand exclusively from increasing the specifications of the hardware potentially making the whole system more cost-effective.

While the ability to adapt to waveforms on the fly is a recent topic of research, waveform design has earlier origins. Inspired by a theory of information gain in the field of communications [42], the earliest work on radar waveform design was in 1953. It provided a definitive link between maximizing signal to noise and maximum information gain for target detection [43]. An important concept in waveform design is that an optimal waveform for one task or scenario is not necessarily optimal for all cases. Waveform design at its outset was most commonly treated as an optimization problem for a specific task. More recently waveform design trends have become spectrum-conscious; either from the perspective that the a waveform should occupy specific spectral regions for spectral coexistence or from a performance perspective where optimizing the waveform spectrum yields enhanced performance metrics. Then most recently, the cases where the waveform is spectrally limited but optimized for performance is sought. The following section will discuss the performance metrics which have driven research into

waveform design, and the next will detail the research carried out into spectral-based waveform design.

2.3.1 Performance-Driven Waveform Design

Waveform design has no one size fits all waveform - in that each has to be optimized for a specific task. However to quantify the "success" of the design, relevant metrics are required. The application of information theory to radar waveform design theory inspired further design efforts on how to improve the system performance by modifying the transmit waveform. In particular, an early application of waveform design to the problem of clutter suppression in target detection scenarios attracted research attention [44, 45] to attempt to increase the signal-to-clutter-and-noise ratio (SCNR). The spectral content of waveform design is of particular interest in clutter problems. As the clutter is signal dependent it is particularly difficult to separate from the target data in the time domain. Expanding on the work on waveform design for target detection in clutter and/or RF jamming, Kay [29] presented work on spectral design of the signal which optimized the SCNR and found the solution adheres to a "water-filling" criterion - such that the spectral energy is "filled in" across the spectrum to regions without a strong interference and/or clutter response. The concept of water-filling is prevalent in communications applications. It treats the problem of channel corruption, for example by strong interference, by considering where to allocate signal energy within its sub-channels. The water-filling method places energy in subchannels with higher SNR to maximize the overall channel condition. In this example, the water-filling is driven by an maximising the SCNR, as per the following relationship

$$\epsilon(F) = \max\left(\frac{\frac{P_n(F)}{\lambda} - P_n(F)}{P_h(F)}, 0\right) \tag{2.6}$$

where P_n is the PSD of the noise and interference and P_h is the PSD of the channel response (i.e. target and clutter interaction with the radar signal). and the "water-level" or energy contraint, is set by the value λ. The water-level and max operation enforce the water-filling nature of this method, as the optimal ESD will be zero for frequencies

$$\frac{P_n(F)}{\lambda} - P_n(F) < 0 \tag{2.7}$$

Power values greater than $\frac{1}{\lambda}$ at a given frequency component F will not have energy distributed across it such that the water-filling avoids these energies. As a result, the signal energy avoids frequencies with large noise, jamming or clutter power. An illustrative description of this case of water-filling is shown in Figure 2.5a and a resultant ESD produced using this method is shown in Figure 2.5b.
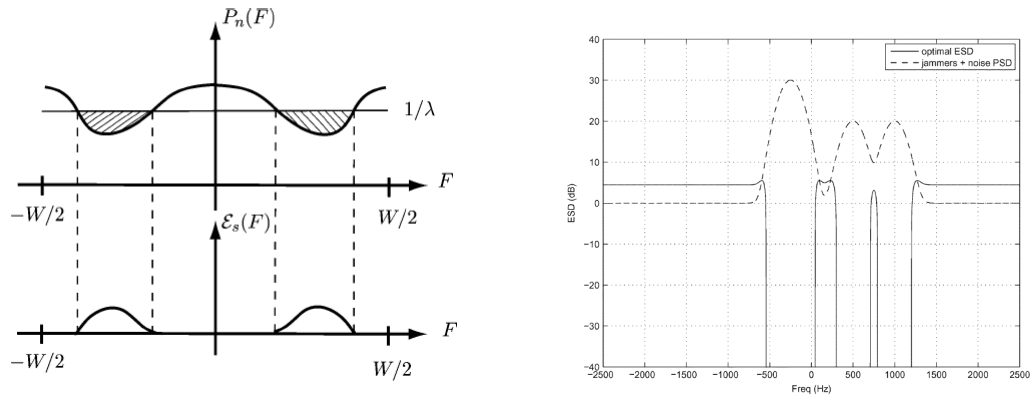
(a) *Demonstration of water-filling with a fixed energy constraint (top) , the point below which energy is "filled in", resulting in an energy spectral density (ESD) with the same resultant area as the water-filling (bottom). [29]*

(b) *Simulated output of the water-filling effect demonstrated in Kay's work on optimal target detection where the waveform energy now is filled in where the jammer energy is lowest. [29]*

While earlier approaches provided a theoretical basis into waveform design, the solutions often lacked the means to physically implement these waveforms. Using constant modulus amplitude and phase modulation, a more recent approach was able to fulfill the maximum SCNR criterion in [16], allowing an implementable solution. While the design of the waveform is often studied on its own assuming a matched filter on receive, both the optimal waveform and the receiver processing pair are studied for the clutter problem in [46].

The general detection problem is studied in the pivotal work linking waveform design and information theory by Bell [47] which is based on the original work linking maximum information and SCNR [43]. It found that optimal information extraction can be obtained when the energy is distributed among the target scattering frequencies.

19

This solution maximises the mutual information between the target measurement and the received radar waveform. As also found in the SCNR optimization route [29], the solution using mutual information also suggests a water filing approach. However, the author notes that water-filling may not be the optimal solution in a target recognition or information extraction problem. Spreading the energy out equally among the scattering frequency modes may not be the optimal solution as some target modes may contribute more to the overall information metric.

A series of studies apply the mutual information (MI) metric across various waveform design scenarios [17, 23, 48–51]. The SNR and MI metrics were used to calculate the optimal waveforms in target detection for both a known target and stochastic target [49]. In the MI waveform design field, a known target refers to a model driven by a deterministic target impulse response that is used to allow design of the subsequent waveform/receiver pairs, while a stochastic target is modelled with a random target response [47]. While target detection is more accurately described as a stochastic process, this deterministic assumption was the original basis for waveform design based on MI with later works expanding to more accurately describe and solve the problem using stochastic target models [49].

MI is used to design an optimal waveform for multiple extended targets in [50]. As suggested by Bell in [47], target recognition requires a different treatment to detection. Typically target recognition depends on some amount of prior knowledge to discern how to spread the spectral energy across the target scattering frequencies. A target recognition problem is addressed in [23] where MI is applied in conjunction with sequential hypothesis testing to operate optimally within a cognitive framework using prior information. In [15] both enhanced detection and target discrimination is treated by either maximising for the probability of detection or probability of identification respectively.

In the field of information theory, it has been shown that the MI of a Gaussian impulse response is the same as its minimum mean square error (MMSE) [52]. Both MI and MMSE are applicable in target recognition where the interest is not in a single target response range measurement, but in discriminating specific target features. Another emerging application of information theory for waveform design in radar is in the context of multiple-input multiple-output (MIMO) systems. This refers to a set up with multiple transmit and receive antennas which creates many different uncorrelated signals - the

received signal is then a superposition of many independent received signals. MIMO is often used to exploit the spatial diversity between targets. MMSE was first used as a metric for waveform design was first used in the context of MIMO, but also shown to be applicable for single transmit and receive antenna radars in [51]. The solution under both MMSE and MI criterion is shown to employ water-filling over the spatial modes of the radar scene - such that higher power is allocated to stronger targets. Other applications of MI in waveform design are used in a tracking context - such as in [53] where MI is exploited to design waveforms for tracking for a low-grazing angle. More recently it has been applied to waveform design for MIMO to support state estimation for a particle filter [54].

Another popular means of performance driven waveform design is motivated by obtaining good autocorrelation properties - usually assessed by the integrated sidelobe level (ISL) or peak sidelobe level (PSL). Minimising ISL can be treated as a non-application specific process as lower sidelobes are desirable across radar modes and is therefore a well studied problem. There is an extensive body of research applied to optimizing for good autocorrelation properties under the constant amplitude constraint - restricting modulation to phase only. [55,56]

Minimising a cost function to obtain the optimal ISL is problematic in that there are many possible ways in which the waveform can spread its energy which can lead to multiple local minima. Some approaches to this are to use stochastic optimization algorithms to exhaustively search for the optimal solution [57]. Alternatively, local minimisation using the gradient descent method can be used by choosing waveforms that are close to that of the desired solution. In [58], the authors move away from computationally intensive stochastic and gradient based methods used in prior studies, to introduce a series of cyclic algorithms which reduce the computational burden in seeking constant amplitude waveforms with low ISL.

2.3.2 Spectral Waveform Design

One of the driving factors in waveform design is the need to operate in a spectrally crowded area. It is then not surprising that a large contingent of the waveform design literature is based on spectrum centric design. Frequency based waveform design is useful not only for spectrally limited regions within the bandwidth, but additionally for

directly controlling the waveform autocorrelation via its power spectral density.

While initial works in waveform design were based around optimization for a specific task and/or performance metric, more recently the research community have largely focused on the spectral crowding problem. These solutions address suitable placement of signal energy across the bandwidth of the radar in the frequency domain. Radar waveform design where limits are imposed in given bands of the spectrum to avoid interfering with surrounding users, is of particular interest. The spectral waveform design literature generally has one of the following approaches: 1) adding small modifications to the standard LFM waveform to place nulls in the spectrum, 2) designing a waveform with forbidden bands where the spectrum cannot place energy or 3) optimizing a waveform with forbidden regions while also attempting to optimize for another performance metric. The common point across all of the following techniques is that they perform "spectral thinning" - placing gaps in the spectrum.

Designing the waveform solution purely in the frequency domain has the inevitable issue of implementation to a physically realizable time-domain signal. Designed waveforms with spectral densities which specify regions to avoid, require synthesis to discrete time constant modulus signals. Using the PSD of the signal which is band-limited and using the inverse Fourier transform will provide a time-domain sequence, but the constant modulus criteria may not be fulfilled. A section of research work aims to address this problem by starting the design with consideration of the end waveform type that the radar will use. Stepped frequency (SF) phase coding is a method of waveform formation which, similar to LFM waveforms, increases in frequency over time. Different from LFM, SF waveforms transmit a train of pulses, each with a different frequency, that increases by a step at each pulse. The drawback of SF radar is that each pulse then has associated frequency sidelobes which are vulnerable to interference. In [59] a method is presented for SF radar which places nulls at the spectral location of external RF interference by using small phase alterations which results in a small mismatch loss on receive.

As pulse compressed waveforms are common in radar systems' hardware, it is beneficial to consider options for this general pulse format. It is shown in [2] that applying small phase offsets in the standard LFM pulse can produce deep spectral nulls. An example of two spectral nulls created using this method is shown in 2.6: one notch exists in the strongest region of the signal spectrum, other at the edge where the signal
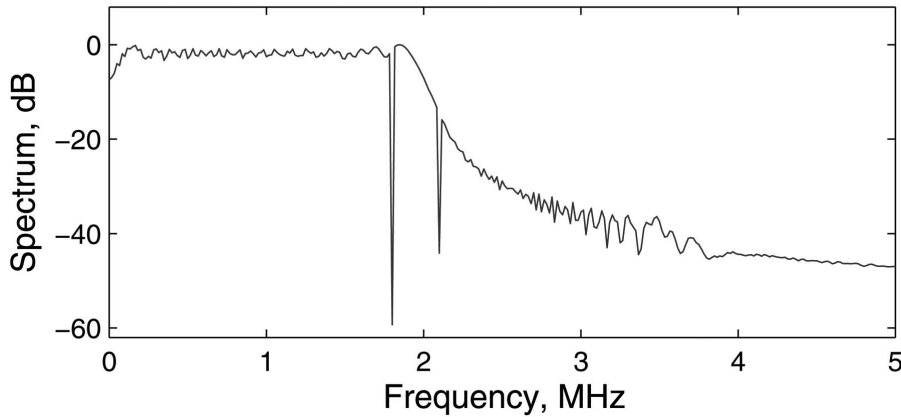
Figure 2.6: *Two deep notches produced, by the technique in [2], one of which lies in the outer-extreme of the radar bandwidth.*

strength is tapering off. By only allowing very small offsets in phase, this preserves the good autocorrelation and Doppler properties associated with the LFM waveform. This method works best on the outer extremes of the bandwidth spectrum but suffers from distortion when the offsets are applied in the main LFM band. Furthermore, the nulls that are created for the main band can be less deep than those on the outer-extreme of the bandwidth. This method shows promise for applications where neighbouring RF users have spilled interference into the region of use, of the radar of interest, but is likely not applicable for in-band interference without additional processing. Each offset corresponds to a narrowband null, and wider band nulls can be created by a combination of offsets. To create a large band gap in the middle of the band would result in a large computational expense. A similar approach to [2] also designs a waveform with small phase changes, but instead implements an iterative approach to deepen the spectral nulls [60]. In [61], this method is expanded to allow multiple-frequency notches.Per iteration, the complexity only scales in size linearly which results in a very low complexity algorithm. The algorithm is very similar in nature to another kind which uses alternate projections to allow constant-modulus waveforms with arbitrarily chosen spectral shapes - however this method does not offer as much control on the depth or placement of notches [46]. A large number of waveform design problems are analytically intractable and then rely on iterative numerical optimization methods to solve them. Computational cost at each iteration then becomes of critical importance. It often becomes the case that performance is then traded off for lower computational cost.

While many waveform designers aim to place nulls as deep as possible into the spectrum, one alternative approach is analyzing how shallow the notched spectrum can be to reasonably co-exist with surrounding interferers [10, 17]. This is a similar problem to the previous approach of spectrum thinning, but differs in that as frequency components within the bandwidth of the signal are not omitted.

The selection of algorithms presented require a set of notches rather than a chosen waveform spectra. [62] presents an iterative approach to sequentially alter the phase of the waveform until a desired spectral shape is achieved. This allows input of an arbitrary spectral shape and allows wideband notches.

Another iterative method based on phase-only modulation maintaining constant amplitude is presented in [63]. This approach allows the design of notches via user-chosen stopbands, but unlike [61], also minimizes the autocorrelation sidelobes. Using the fast Fourier transform (FFT) the complexity per iteration is kept relatively low. Two algorithms are presented in this work [63]. The second improving on the first by applying weights at the cost of more computational expense, but yielding lower autocorrelation sidelobes than the unweighted version.

Issues with iterative methods not only concern the computational complexity of the algorithm, but also its convergence behaviour. While iterative algorithms appear to work in a specific scenario, there can often be little hard evidence to suggest why this is, or whether it will converge. A study that revisits the well established problem of "phase retrieval" [43], analyses the performance of iterative algorithms for waveform optimization problems and also satisfies time domain synthesis of a given PSD under finite energy and bandwidth constraints. [64]. Phase retrieval has been applied across many fields including astronomy, crystallography and other signal processing applications. Given Fourier data and constraints, it seeks to find the Fourier phase function to satisfy the constraints. Patton describes how the solution to these types of problems is suitable in the radar waveform problem. Using the best fitting algorithm for the type of problem, known as Gerchberg-Saxton (GSA), Patton explains the success of previous radar waveform optimization problems such as [64]. He also demonstrates that the GSA algorithm has lower computational complexity and addresses the problem where the time-domian sample number has to be equal to the frequency-domain number.

Generally when the only constraints placed on the transmit waveform are finite energy and bandwidth, the power spectral density is the only metric through which performance is affected, as this is also directly related to the autocorrelation. Optimizing waveform design solely for good autocorrelation properties has already been discussed and is a difficult problem. The complexity of the problem only increases when adding spectral gaps. Expanding on prior work on cyclic algorithms, stopband constraints are added in [63]. Phase-based waveform design methods are currently at the stage where they are simultaneously addressing stop-band constraints and autocorrelation properties all while attempting to be relatively feasible for implementation. The main struggle is reducing computational burden.An iterative pattern search study has recently shown promising results for high convergence speeds [65], compared with the cyclic algorithm approach.

With each constraint impacting the other, the problem still remains a difficult one to solve completely. The aim is to find a waveform which exhibits constant modulus amplitude, increasing phase while fitting a desired PSD with deep spectral notches. For a chosen PSD there may not exist a solution where the sets intersect. A thread of research analyses the feasibility of waveform optimization under multiple constraints. In these works, the problem is defined as non-convex quadratic optimization in [25–27,56]. These could be considered the current "state of the art" in radar waveform design. Analysis of the possible intersections under various waveform degrees of freedom is carried out. There are numerous studies under this framework; one which allows amplitude modulation [25], one study optimizes for SINR while avoiding specific frequency bands and constrains the total energy plus an additional performance related constraint. Finally, it is demonstrated that the performance parameters are generally competing against the each other.

A similarity constraint is added to allow some control performance related characteristics such as range-Doppler resolution, signal modulus and peak sidelobe level. This particular approach is set up and is re-expressed as a convex optimization problem which then allows use of semi-definite programming. This results in a relatively computationally inexpensive algorithm which scales in polynomial time. Results showed that a closer match to the desired PSD was obtained by trading off the similarity constraint metric relating to sidelobe levels and range-Doppler resolution via the autocorrelation

function.

Summary

The main challenge for waveform design in radar is the need to synthesize a physically feasible waveform that is able to occupy the spectrum where appropriate, while also optimizing its performance for the desired task. This is not a simple feat, and in general the solutions either address one problem or the other. The set of solutions which address both are computationally complex and designed for a static problem that can be treated offline. Current state of the art solutions treat detection problems with assumed knowledge of the surrounding spectral environment. There is a notable absence of work for waveform design in SAR. This could be due to: 1) the inflexibility of the current SAR processing to novel waveforms and 2) the detection problem is not the same as the imaging problem, so spectral thinning worsens the performance as opposed to improving it 3) historically SAR has treated interference mitigation issues on receive which will be discussed in the following section.

2.4   RFI Suppression for SAR

Detrimental effects of interference in SAR are significant and can include: 1) decreased signal to interference and noise (SINR) of echoes which reduces the dynamic range of the image, causing reduced capability to image weaker reflectors (such as terrain), 2) Increased range sidelobes -also reduces dynamic range and can mask neighbouring reflector response if it is weaker, 3) increased artifacts i.e. creation of false targets or bright lines and blurring of the image, 4) decreased functionality of further SAR uses, such as target detection and identification 5) phase distortion affecting post-processing applications such as interferometry. Examples of RFI impact on SAR images from the open literature are shown in Figure 2.7. Figure 2.7a taken from [4] is heavily distorted with narrowband RFI masking the image features with the introduction of bright lines compared with the non-corrupted image and 2.7c shows the effects of image blurring and reduced image sensitivity.

(a)

(b)

(c)

(d)
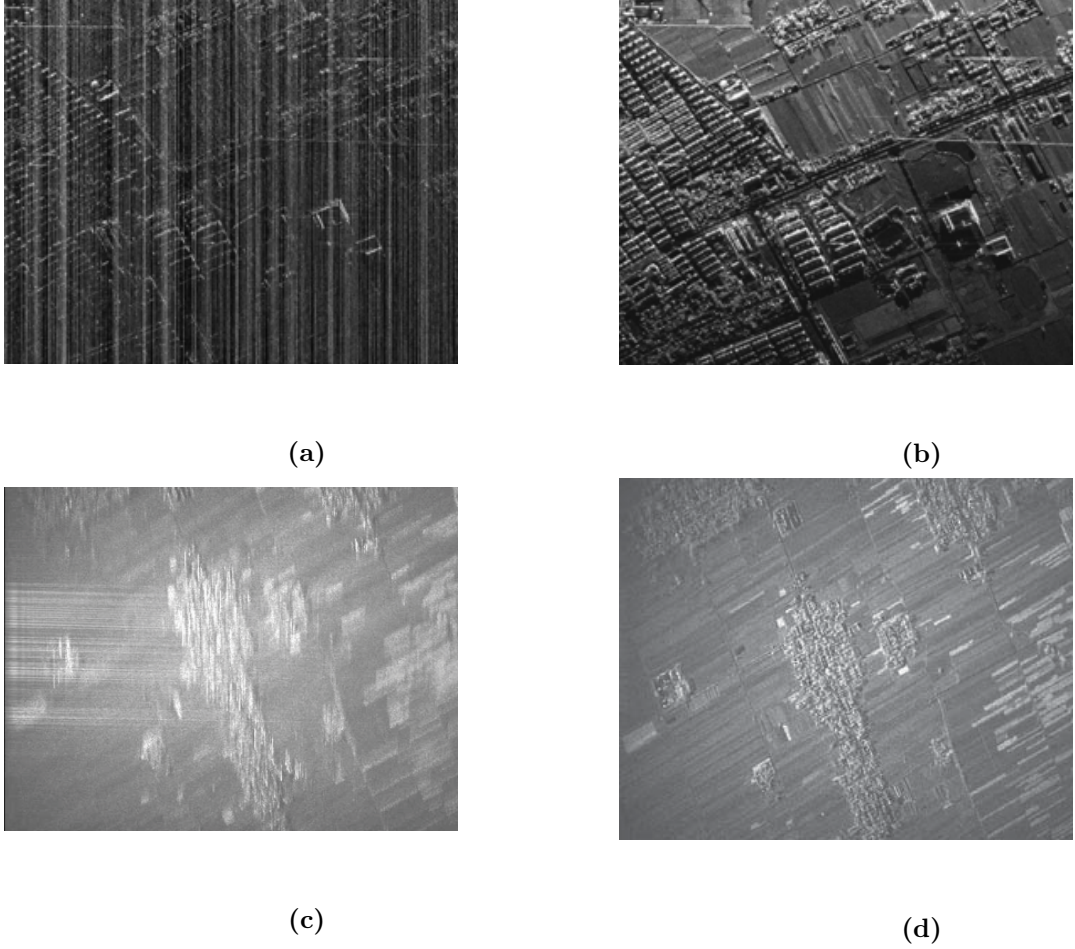
Figure 2.7: *Example SAR images corrupted (left) and without RFI (right)*

The SAR imaging mode has to some extent an inbuilt noise suppression ability via its image formation process. This process combines many observations of the scene from different platform locations which results in an improved overall SNR. While this provides some level of interference suppression, if the RFI power is on a similar same scale as the target response returns, significant degradation of the image can occur. Another convenient tool which SAR processing has relied on is stretch processing on receive [8] which allows additional noise suppression through bandwidth reduction on receive [7]. However, this approach is heavily reliant on the LFM waveform. With the advent of waveform design, it is desirable to move away from these strict requirements on waveform estimation.

RFI mitigation can be regarded as a two stage process, initially by identifying the

frequency content of the RFI then subsequently removing and correcting for the RFI. Earlier methods for RFI suppression were based on its removal from the received signal via filtering. Newer methods attempt to model RFI and remove it while attempting to minimize the overall detriment to imaging metrics. Methods for RFI suppression can generally be categorized according to the method of processing the signal as either parametric or non-parametric. Parametric methods model RFI as a linear combination of individual frequency components then attempt to reconstruct the RFI by estimating the content of each component. The RFI is then subtracted from the raw received data. Non-parametric methods exploit the statistical differences between the scene impulse response response and the RFI then apply filtering in the frequency or time domain.

2.4.1 Filtering

RFI suppression via a linear notched filter is generally implemented in the frequency domain by thresholding and removing the samples with more energy than the rest of the received data. This works well for very narrow-band interferers and a small number of emitters. However there are consequences from notching out parts of the received signal when the number of frequencies removed increases. Negative effects caused by notching include adding to the time-domain sidelobes, reducing the overall image intensity and reduction of range resolution. The filter transients also cause reduced data record length which increases the required data rate for a fixed scene length. In SAR images, the notched data can cause reduction in image intensity, reduction of range resolution and raising the time-sidelobes. A method based on least mean squares (LMS) presented in [12] uses a single filter to perform both the interference suppression and the equalization used to remedy the distortions caused by the notching function. A similar approach was presented by [66]. Both of these methods make the assumption that the transmitted waveform and interference signal are known.

An alternative method to the fixed linear notch technique is use of adaptive filters to iteratively separate the desired radar signal from the unwanted RFI. Adaptive filters are desirable over fixed filters in that they can alter their own tap weights automatically using the input data. These methods have been applied to interference suppression problems without requiring specific parameters on the signal of interest. These algorithms rely on the assumption that the interference can be constructed from a summation of

sinusoids. This is a very common assumption for interference suppression algorithms and is the basis for the collection of parametric-type algorithms. [3, 7, 67–70]
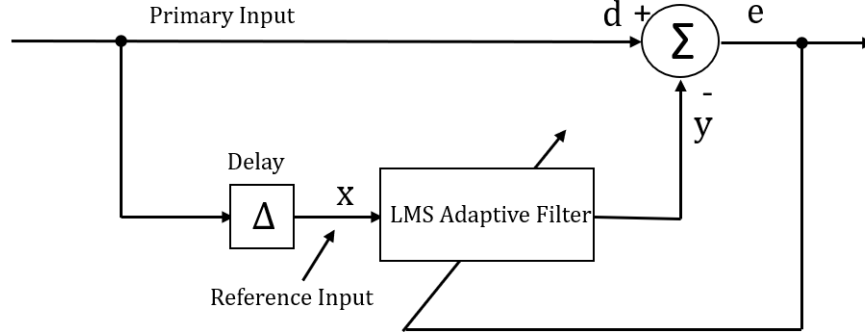
Figure 2.8: *Least Mean Square (LMS) filter where the input is the radar signal combined with interference, the filter output is the estimated RFI signal and the error output is the desired radar signal*

There are various methods to implement these adaptive filters for the RFI suppression problem. The most popular of which is the LMS adaptive filter which has been widely covered in the literature - both within and outside the radar context [11, 66, 71–74]. The LMS adaptive filter requires a primary input and obtains its reference signal by delaying the primary signal.

The adaptive LMS method requires a primary input signal, in the RFI context, this is the combined returned radar signal and the RFI signal. A time delay is then applied to the input signal to provide a reference input to the adaptive filter. The adaptive filter operates by iteratively altering the filter weights vector $\mathbf{W}_i$ to minimize the mean-square-error between the filter output and the primary input signal as shown in (2.9). A system diagram of this method is shown in Figure 2.8. The output of the adaptive filter is the estimate of the RFI. The estimate is constructed from the inner product of the adaptive filter weights $\mathbf{W}_i$ and the reference signal vector $\mathbf{X}_i$

$$y(i) = \mathbf{W}_i.\mathbf{X}_i^T \tag{2.8}$$

Finally, the error signal between the primary input and the output of the adaptive filter is the cleaned radar signal.

$$e(i) = d(i) - y(i) \tag{2.9}$$

Another LMS based approach is demonstrated by Abend and McCorkle [71] where an over-determined system produces a FIR filter with tap number that is independent of the number of interfering signals. This is also combined with an iterative technique to reduce the range sidelobes caused by the filter's impulse response. However, the filtering causes edge effects which results in reduced data record length. These adaptive LMS algorithms have the capability to remove a large number of interferers simultaneously as there is no dependence on number of sinusoidal frequencies. The major issue encountered by filtering methods for RFI are the resultant sidelobes. As such filtering methods should be paired with a suitable method to deal with the raised sidelobe levels. Included in the autoregressive approach to modeling and removing interference is a sidelobe reduction method [71]. This partially alleviates the impact of the sidelobes but with additional computational cost.

One study on the LMS adaptive filter concluded that it can significantly suppress RF interference, but further techniques are required to mitigate the increased sidelobes [11]. Representative examples are shown in Figure 2.9. The results demonstrate that there is significant improvment on the compressed and uncompressed contaminated signal, but comparing the compressed ideal and cleaned signal (d and f), there is a notable increase in sidelobes. Furthering this technique an integrated LMS and range-Doppler algorithm with in-built sidelobe reduction was proposed to complement the adaptive LMS technique [73] at a lower computational cost than previously attempted in [71]. Stages of the resultant outputs from this algorithm in [73] are shown in 2.10, from the original RFI contaminated signal, to the interference cleaned signal and finally the sidelobe suppressed output.

These methods all operate by using the time variations in the input signal. A different approach is to apply the adaptive LMS algorithm in the frequency domain, as demonstrated in [75]. To compensate for numerical instability which can be problematic in adaptive algorithms, an amplitude normalization step is also included.

2.4.2 Parametric Methods

Interference suppression is carried out in the following methods by modeling RFI as a superposition of pure tone signals and then attempting to estimate the individual RFI parameters for frequency, phase and amplitude. These components are then sub-
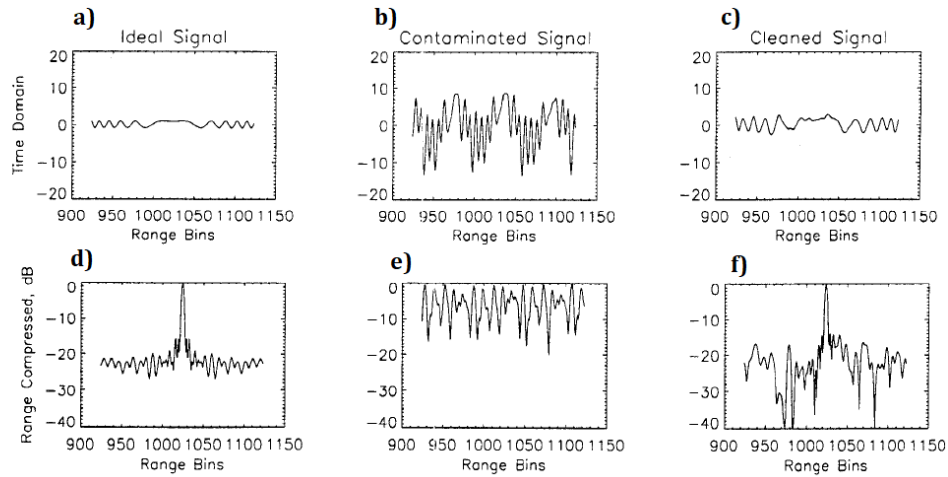
Figure 2.9: *Time domain compressed and uncompressed signals, without RFI, with RFI and cleaned using an adaptive LMS filter. Top: Uncompressed signals shown without RFI, with RFI and post LMS clean-up. Bottom: Range-compressed signals.*

tracted from the corrupted wideband radar signal. These methods generally exhibit lower signal distortion than some filtering techniques and can provide good interference suppression. Methods for estimating the RFI generally depend on "sniff" pulses where the radar listens beforehand to obtain data on the interference. Directly estimating and subtracting the RFI is an approach used in a series of works in what is known as "estimate and subtract" methods [7, 69]. Along with the assumption that RFI is a sum of sinusoidal frequencies, the observed wideband radar signal return plus thermal noise is assumed to be Gaussian white-noise - thereby relying on the approximately flat spectral nature of the LFM. The least-squares estimate of the RFI parameters including frequencies, amplitudes and phase can be expressed as the maximum likelihood estimate [69]. Directly calculating the maximum likelihood (ML) has two main drawbacks:target signals causing errors or bias in RFI estimation and high computational cost. For RFI with multiple individual sinusoids the problem becomes non-linear and analytically intractable, and then relies on an iteratively improving an initial guess at the interference parameters of amplitude, frequency and phase.

Methods exist which instead calculate the approximate ML estimates and use iterative optimization to estimate and subtract RFI. In [7] an alternative parametric ML (PML) algorithm is applied for RFI estimation, which has lower computational cost than direct ML, if the number of RFI tones is small. The more sinusoidal tones estimated, the more
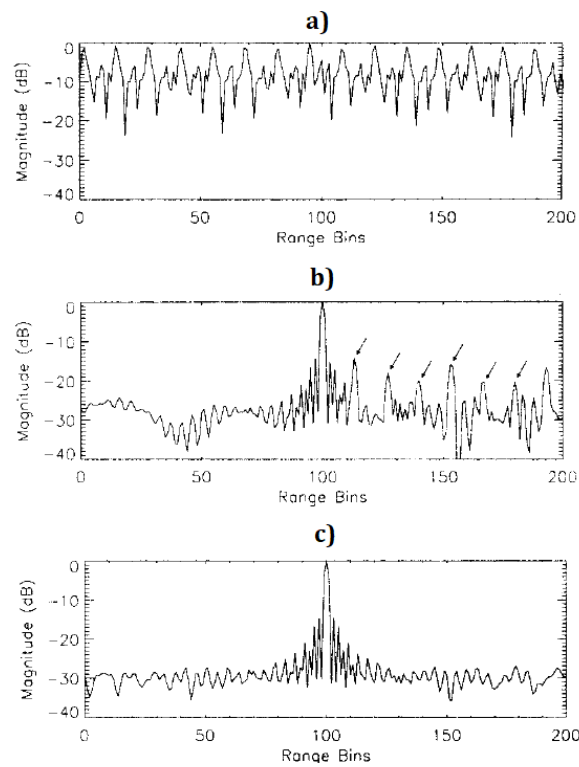
Figure 2.10: *Stages of interference processing using LMS filter with sidelobe supression: a) RFI contaminated signal, b) LMS filter output c) Sidelobe supression.*

iterations PML requires.

Another least-squares approach integrated with the LFM signal is [70]. To reduce the effects of estimation bias due to targets, prior knowledge is used in combination with the estimate and subtract approach [3]. Estimates of the wideband targets are subtracted from the received signal before interference estimation and then subtraction is allowed. The estimates of the targets are obtained based on the assumption that target responses will not change substantially from pulse to pulse. The received real part of the signal can be modelled as

$$x(t_n) = s(t_n) + \eta(t_n) + \sum_{i=1}^{L} A_i \sin(\omega_i t_n + \phi_i) \qquad n = 0, \cdots, N-1 \qquad (2.10)$$

where N is the number of time-domain samples, $\mathbf{s}$ is the target return, η is the random background noise signal and finally the interference signal is represented by L sinusoids with amplitudes A_i, phases ϕ_i and normalized frequencies $\omega_i = 2\pi f_i T$ where T is the sampling period and f_i is the continuous-time frequency. In addition to using prior knowledge of targets, the algorithm assumptions also include that the interference bandwidth is small compared to that of the radar (i.e. NBI) and that target signals are wideband, so therefore narrow peaks in time.

The interference signal is then separated into distinct groups of sinusidal components; for L_1, it is assumed that the frequencies ω_i are not modulated from pulse to pulse and are therefore considered to be both known and fixed across the period of data collection. The other groups L_2 and L_3 have no assumption that they are fixed or have associated prior knowledge so are estimated on a pulse-to-pulse basis. The L_2 group frequencies are assigned to those in the commercial FM band, while L_3 is the group of all remaining unknown frequencies. A system-flow diagram for this procedure are the subsequent processing is shown in Figure 2.11.

Initially, using the prior target knowledge, estimates of the targets are removed from the received signal. Then, the interference removal is comprised of two stages, the known-frequency estimation and subtraction, then the unknown-frequency removal and subtraction. The "known frequencies" in group L_1 are obtained from an RFI measurement. From this, sinusoids are generates at these observed frequencies and orthonormal basis vectors are computed. Interfering signals are extracted using orthogonal projection.
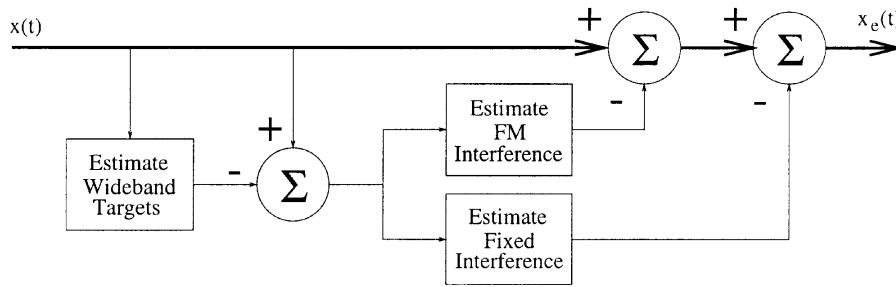
Figure 2.11: *Example systems flow chart for parametric interferefernce estimate and subtract method demonstrated in [3].*

The components with the most energy are used to form an estimate of the interference signal from group L_1. Group $L2$ uses a frequency-transform based technique, rather than using orthogonal projection. This method estimates the amplitude, frequency and phase of the largest FM sinuoids, then in the frequency domain this contribution is removed from the signal and the next highest energy contributing signal is removed. This iteration is continued until a pre-determined number of sinusoidal contributors has been removed by this process. Once interference removal has been completed, the algorithm then updates the target estimates for the next received pulse.

Compared to filtering methods, this algorithm presents lower sidelobes via both a spectrally efficient estimate and subtract algorithm, paired with iterative signal removal reducing sidelobes even further. The CLEAN algorithm is a similar approach and iteratively removes interference from the peak amplitudes of an oversampled FFT. It also sees the same negative effects of estimation bias and high computational expense [76].

These methods are shown to perform well, if the modeling assumptions are correct. Overall, parametric based methods rely heavily on the quality of observed data and that the spectrum consists of a known number of sinusoids in white noise.

2.4.3 Non-Parametric Methods

Non-parametric interference suppression methods are classified as those which use spectral estimation methods to distinguish RFI from return signals and then filter out the noise. As previously highlighted, one of the key stages in interference mitigation is the identification of the RFI. RFI detection is particularly important in parametric models in order to avoid model mismatch. Recent work has proposed that enhanced

characterization of RFI, in combination with the standard notch filtering approach, allows a significant reduction in interference removal [77]. Meyer [77] provides a method to analyse the returned signal in the frequency domain and then notches are placed over the contaminated frequency components. This approach like other non-parametric methods, does not rely on modeling the RFI, so does not suffer from estimation bias. However, like the original filtering methods, it does incur higher sidelobes time-domain. A similar notching based approach is presented in [78].

The statistical differences between the radar echoes and the RFI is a basis for many of the proceeding non-parametric methods [4, 5, 79–82] Three of the dominant non-parametric methods in the literature feature the use of what is known as the "Eigen-subspace method", "Complex Empirical Mode Decomposition" (CEMD) and "Independent Component Analysis" (ICA) which are detailed below.

An example of an eigensubspace technique for interference supression is presented in [4]. A block diagram of the algorithm application is shown in 2.12.Initially, the algorithm must detect whether or not there is NBI present, this is done by assessing the magnitude of change in the frequency domain across range samples, a large change denotes the presence of RFI. The received signal data $\mathbf{x}$ of length $M \times 1$ can then be separated into K subvectors of dimension L with $K = M - L + 1$, such that the sub-vector is written $\mathbf{x}_k = [x_k, x_k + 1, \cdots, x_k + L - 1]^T$. Each of these subvectors are then stored in a data matrix $\mathbf{X} = [x_1, x_2, \cdots, x_k]$ of dimension $L \times K$ such that all K subvectors are stored. This now allows construction of the covariance matrix which then allows the eigenvalue decomposition. The eigenvalues are used to construct their corresponding eigenvectors. The largest eigenvalues are used to construct the interference subspace. These components in the interference subspace are assumed to have much larger value than those of the scene signal, which then allows the assumption that the complement subspace is spanned by the scene signal and background noise only. The received signal x_k is projected onto the interference subspace $\mathbf{F}$ to give the vector f_k, so that finally the RFI free data can be obtained as follows

$$\hat{\mathbf{x}}_{\mathbf{k}} = \mathbf{x}_k - \mathbf{f}_k \tag{2.11}$$

where $\hat{\mathbf{x}}_k$ is the RFI suppressed radar signal. This is performed for all subvectors, and a new RFI free data matrix $\mathbf{X}'$ of the same structure as $\mathbf{X}$ is constructed, to then provide

the final full cleaned signal $\mathbf{x}'$ of dimension $M \times 1$ This process is repeated for all pulses within the data collection N.
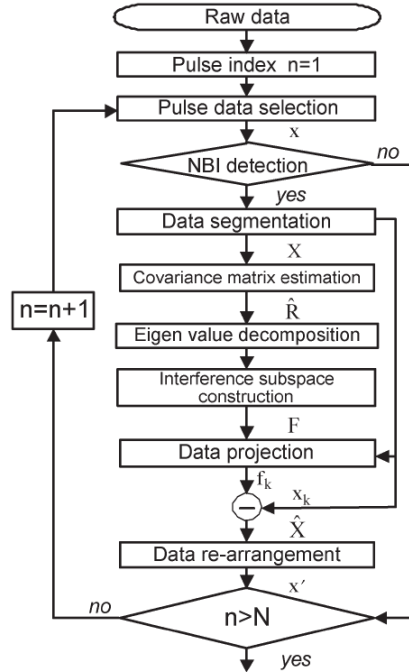
Figure 2.12: *Example systems flow chart for non-parametric eigensubspace interfer-efernce estimate and subtract method as demonstrated in [4]*

The major drawbacks of the eigensubspace method are that if the RFI power and target echo power are similar, the subspaces will not be obtainable.

CEMD is the approach used to remove RFI by decomposing NBI-contaminated radar echoes into a sum of basis functions . A similar approach is also demonstrated in [79]using intrinsic mode functions (IMF) - in each of these functions there is a single frequency component and each of these functions are orthogonal to the others. RFI and target echoes can be separated using blind source separation as they can both be classified as independent signals. The RFI is initially identified in the frequency domain. The returns with NBI present are then filtered in the time domain and whitened. At this stage independent component analysis (ICA) is used which decomposes the echoes into a series of basis signals. The RFI is then identified by performing thresholding. [81,82]

Another method proposes an interference detection method analyzing the statistics of the spectral content of the return pulses [5]. Using the kurtosis of the returned

spectral data, a decision is made to whether RFI exists in the spectrum, as shown in Figure(2.13). If interference is detected, the ICA and eigensubspace filtering methods are applied. The eigensubspace method explores the energy difference using second order statistics.This method is limited in that if the RFI power and target echo power are similar, the subspaces may not be obtainable. ICA assumes that the target echoes are Gaussian distributed and calculates the statistical difference between the RFI and the echoes. This method may then not be applicable if the returns are non-Gaussian.
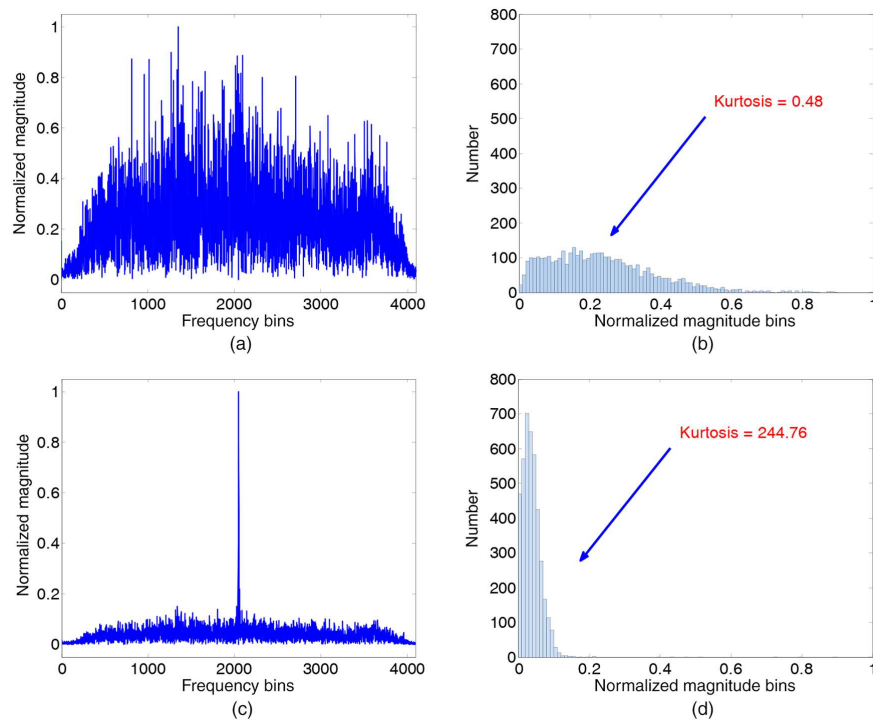
Figure 2.13: *Kurtosis of range-frequency profile with and without NBI [5].*

Independent subspace analysis (ISA) is an extension of the theory of ICA, but is based on reducing the redundancy in time-frequency representation [83]. ISA provides a method to solve for the separation problem in the time-frequency domain. If NBI is found to be present using the kurtosis detection method, the single pulse is projected onto the time-frequency domain using the short-time Fourier transform. The previous method using ICA alone requires there to be at least as many mixture signals as sources.

When the RFI is observed to be time-variant, this restricts the number of samples that can be used when estimating its spectrum. This restriction of samples negatively effects the potential performance of the eigensubspace method. One method successfully esti-

mates the RFI power spectrum with reduced dependence on a large number of samples to perform the classification and mitigation of RFI. The RFI is estimated adaptively and iteratively and the RFI is then filtered using orthogonal subspace projection. [84]

The methods discussed so far are suitable for narrow-band interference which is classified as interference which occupies less than 1% of the total radar bandwidth. For wider-band interferences, these methods struggle due to much higher computational expense and the resultant distortion and possible artifacts introduced, caused by filtering out large portions of the spectrum.To address this, there are some emerging techniques to deal with interference which is wider than 1% of the band. As the wideband interference can be detected in either the time or frequency domain, the short-time Fourier transform is used to represent the interference in the time-frequency domain, This then allows the problem to be expressed as a series of instantaneous spectrum narrow band mitigation problems. Then, similar statistical tests can be performed, as discussed for the narrow band case. [85] Another recent approach which uses the short-time Fourier transform to exploit a sparse representation in the time-frequency domain. A joint-estimation approach is presented which performs WBI suppression and signal of interest recovery via sparse representations [86].This topic continues to be an area of ongoing research, both in identifying and separating the interference, and also in reducing the computational expense of these algorithms.

2.4.4 Missing Data Problem

The interference mitigation approaches discussed, either completely remove the samples with interference present, thereby also losing the samples with scene information, or aim to reconstruct or separate the interference from the desired signal. The filtering case often provides computationally cheap and easily implementable solutions, but the major drawback lies in the degradation in performance, associated with missing data in the spectrum. A set of general signal processing methods exist for the reconstruction of spectral information from gapped data. These methods are generally based on the principle of iteratively estimating the spectrum and updating the missing samples in a way that could be described as interpolation. While a selection of these methods have been directly applied to SAR, there are many other pre-existing algorithms for spectral estimation . These techniques can also be readily applied to missing spectrum

data for SAR. As SAR raw data is often random, non-parametric approaches generally perform better than parametric methods as no assumptions on the content are imposed on the problem. However, this performance gap between applying non-parametric and parametric techniques was not seen to be large in one comparitive study [87].

Of particular interest are the three methods which dominate the literature for missing data SAR; Papoulis-Gerchberg algorithm, AR-Burg and the gapped amplitude and phase estimation (GAPES) method. The first estimates the spectrum of the complete signal by interactively removing the high frequency components present due to the loss of information in the time-domain. This is an iterative based algorithm which is guaranteed to converge if a ratio between the available samples and the nulled-samples is satisfied. Furthermore, it is able to reconstruct the spectrum without any assumptions placed on the scene content. A significant drawback of this method, is that the number of iterations required for a suitable performance output is in the order of several thousand [88].

Autoregressive methods are often applied in order to compute the coefficients of an adaptive filter which is applied to interpolate the data. The AR-Burg method uses the Burg interpolation method to construct the AR filter coefficients which then filters the spectral data to estimate the missing spectrum [89].

The amplitude and phase estimation (APES) algorithm was developed as a spectral estimation algorithm [58], but later extended to include capability for missing data interpolation GAPES [90]. GAPES makes an assumption that the missing data has the same spectral content as the existing data set, which is a fairly natural assumption for the SAR scene model. The GAPES method offers some advantages over the AR-Burg algorithm as there is a less restrictive model assumed, but at the cost of higher computational expense. GAPES has been observed to generally outperform AR-Burg, but this is dependent on the oversampling ratios. For small oversampling rates, GAPES only performs slightly better than AR-Burg. Alternative non-parametric methods have been proposed, but with notably higher computational expense. These methods are based on an iterative adaptive approach or sparse learning via iterative minimization. Overall the most promising methods for implementation are the AR-Burg and GAPES algorithm, which have both demonstrated their applicability to the SAR missing data problem. The main drawback of these methods is the inability to properly reconstruct spectrally-

flat, non-sparse scenes. This has higher significance for applications such as bi-static SAR and interferometry. However for many applications, imaging the strongest targets in the scene is adequate. There is also growing interest in the application of compressive sensing techniques to attempt to reconstruct sparse scenes in the case of missing data. The performance is dependant on a number of finely tuned parameters and the type of CS algorithm applied. The performance can be very good, but computational expense and restriction to sparse scenes are the main drawbacks [91, 91].

2.4.5 Summary

There is evidently a large spread of possible methods for RFI mitigation in SAR, each with its own strengths and setbacks. Filtering methods, especially adaptive filtering, can be effective at reducing the presence of RFI but risks causing a rise in sidelobes - one of the initial effects of RFI, so these methods are only partially effective unless used alongside a sidelobe reduction algorithm. Filtering methods could be especially effective combined with spectrum re-filling methods such as GAPES or AR-burg, if the scene is suitably sparse. Parametric approaches depend on the ability to model the RFI as sinusoidal waves, but must do so fairly accurately in order to avoid introducing estimation bias causing disruption to the full modelling and estimation process. Non-parametric methods are more robust to error, but often highly computationally expensive or place requirements that may not always be true, i.e. that the RFI eigenvalue bases are separable. Both parametric methods and non-parametric methods are generally restricted to dealing with very narrowband interference ($< 1\%$ of radar bandwidth).

2.5 Chapter Summary

The waveform design and RFI mitigation for SAR approaches are localized to specific parts of the processing chain. Waveform design places energy around the areas of the lowest RFI power in the interest of maximising the SINR in a spectral avoidant approach. This is problematic for SAR, as this region of the frequency response is then unknown and lowers resolution. The RFI mitigation methods for SAR attempt to remove this interference on receive. In light of new adaptive techniques for waveform design and the full processing chain, it would then be pertinent to combine both the

transmit and receive aspects of the process to fully optimize the cycle for SAR. The main challenges in these areas still apply. An adept solution should: provide low range-sidelobes and minimize interference to provide a full dynamic range to the SAR image, provide high-resolution imaging, be computationally feasible to meet the adaptivity timing constraints laid out in [41].

The main restriction in dealing with RFI is the narrow-band assumption, as shown, this is the failing point for both parametric, in terms of computational expense and non-parametric as the interference cannot be easily separated from the desired radar signal. With current methods not addressing these problems, a new solution that does not inherently require on the bandwidth to be signficantly less than the radar bandwidth is necessary. In addition it would be desirable for the computational complexity of the RFI mitigation technique to be indepedent of RFI bandwidth. For a dynamic radar environment where the interference may change pulse-to-pulse, a computationally cheap solution is especially crucial. The following work in Chapter 4 & 5 will discuss a waveform-design driven interference mitigation method that can work for larger than RFI 1% of the radar bandwidth and is low computational complexity, which scales independently of RFI frequency components. Chapter 3 continues to describe the system model and estimation necessary to facilitate this waveform-RFI mitigation driven technique.

Chapter 3

Range Profile Estimation

3.1 Introduction

This chapter presents a frequency-domain based processing method for waveform reception to complement the subsequent work on waveform design for SAR. In addition, the relevant background on receive processing, obtaining the range profile, will be discussed alongside the discrete radar signal model. The concept of the waveform-estimator pair is an important theme throughout this work; waveform design can only yield performance gains when designed with respect to the appropriate estimator. The proposed range-profile estimator replaces the stretch-processing receive step (deramp-on receive) in standard SAR receive processing. The motivation for using a new filter lies in the need to move away from LFM-dependent receive filters to facilitate waveform diversity. This method, named the time-constrained frequency domain estimate (TCFDE), is based on system identification methods and exploits a factorization to the discrete Fourier transform in an approach similar to OFDM. This modification in the frequency domain and projection to the time domain to obtain the constrained SAR range profile is a novel thesis contribution. Comparisons are drawn between OFDM-SAR and TCFDE with respect to energy usage, sidelobe level, noise-suppression, system timing and assumptions used in the algorithms. It is shown, that similar to OFDM, TCFDE produces a high resolution range profile with low sidelobes, maximizing the use of the available bandwidth due to an effect known as "inter-range cell interference (IRCI)-free" estimation [31]. The limiting operational factors of TCFDE are analyzed via a simulation to test its Doppler tolerance and where the range profile cannot be modeled as finite.

3.2 Radar Range Profile

3.2.1 Radar Signal Model and Range Profile

Radar range estimation at its most fundamental is the process of one-dimensional echo-location using the time taken for a transmitted signal to reflect off a scattering point and return to the radar. The received signal then has embedded relative distance and reflector strength information. The representation of target amplitudes and their delay constitutes the range profile. This complex valued reflectivity can be used to represent the relative strength compared to other targets in the scene and also holds phase information. The range profile is defined as a time-delimited one dimensional array of the reflectivity of the corresponding range-cells on the ground of the scene of interest. The physical extent of the range profile depends on the radar operational mode.

It is common practice for radar targets to be modeled as point targets of infinitesimal physical extent which results in the reflected radar waveform being a time delayed signal with amplitude attenuation. The true nature of superposition of scattered electromagnetic radar signals is a multi-faceted problem requiring knowledge of many variables and their underlying interactions including, but not limited to; waveform polarization, propagation medium characteristics such as cloud content, scattering angle of targets and the dependency on frequency of the target reflectivity [8]. As inclusion of these factors would distract from the intent of the following work, the standard discrete scattering model that is used in many radar applications is used here and throughout instead.

For a single scatterer, the returned signal is an amplitude scaled version of the original signal, shifted according to its relative time delay. For a continuum of scatterers the returned signal is a linear superposition of each of the signals and resulting from their separation in space, the returned waveforms are also separated in phase. The radar environment and the physical RF waveforms are most accurately represented in continuous-time through the following received signal model across a physical extent in range of r, where r is related to propogation time by the speed of the RF waveform c, $r = ct$

$$y(t) = \int_t h(t)x\left(t - \frac{2r}{c}\right) + n(t)\mathrm{d}t \tag{3.1}$$

such that $y(t)$ is the returned signal, $x(t)$ is the transmitted signal, r denotes the relative

44

distance of a target reflector, such that $\frac{2r_n}{c}$ is the round-trip time taken for the signal to travel to-and-from the target and the scene range profile $h(t)$ is written as

$$h(t) = A\nu_n(t) \tag{3.2}$$

where A can be used in a model to account for signal attenuation or antenna pattern considerations, but will generally assumed to be $A = 1$. It is assumed for now that the physical extent of the range profile is finite, but will be discussed further in this Chapter.

3.2.2 Discrete Time Signal Model

Continuous models are infeasible for representation in digital systems and for computational modeling, therefore a discrete-time model is more practical both for modeling and to represent the digital signal processing in the radar. Discretization is carried out at the front-end of the radar by the analogue-to-digital converter (ADC), according to a sampling rate f_s, which must satisfy at least the Nyquist rate. The transmitted signal of length τ_c is therefore represented digitally in N samples such that

$$N = \tau f_s \tag{3.3}$$

The observed received discretized signal from a transmission $x(t)$ is a superposition of multiple scaled and time delayed signals can be expressed generally as follows

$$y(t) = \sum_n h_n x\left(t - \frac{2r_n}{c}\right) + n(t) \tag{3.4}$$

such that the basic components of the radar measurement process can be represented as a time-series by; the transmitted signal, $x(t)$, ν_n is the complex valued reflectivity value of a single scatterer , the received signal $y(t)$ and noise in the system $n(t)$ resulting from internal radar hardware noise and any additional interference sources. Note that this received signal does not represent any of the additional receive processing such as band-band conversion or "deramping". In this discrete time representation the range profile is then discretized according to the waveform resolution, which is determined by the bandwidth of the transmitted signal. In Chapter 2, the concept of modulating frequencies to the main RF signal to obtain higher range resolution proportional to the

bandwidth of the resultant signal was introduced. Range imaging can then be achieved by using the different frequencies present in the signal to obtain high resolution. The true range profile is continuous but it is physically impossible to measure this with the necessarily band-limited radar signal $\mathbf{x}$. This imposes a limit on the possible resolution of the imaging process

$$\Delta r_k = \frac{c}{2B_c} \tag{3.5}$$

Therefore, for a physical range extent of r, the number of discrete points in the range profile is given as

$$K = \frac{r}{\Delta r_k} \tag{3.6}$$

The interaction of the range profile with the transmitted signal can, equally to (3.4), be expressed as a linear convolution, due to the "shifting" mechanism in time. Therefore, the observations at the receiver can be expressed as the linear time-domain convolution of the transmitted signal and the range profile vector $\mathbf{h}$ as

$$y(k) \quad = \quad [h(k) * x(k)] + n(k) \tag{3.7}$$

where the transmitted waveform is $\mathbf{x} = \begin{bmatrix} x(0) & x(1) & \cdots & x(k) & \cdots & x(N-1) \end{bmatrix}^T$, k is the kth sample of transmitted waveform where $k = (0, 1, \cdots, N-1)$. The range profile is $\mathbf{h} = \begin{bmatrix} h(0) & h(1) & ... & h(K-1) \end{bmatrix}^T$. The noise plus interference vector $\mathbf{n}$ is an $(N + K - 1)$ dimensional vector with covariance matrix $\mathbf{R}_{nn} = E[\mathbf{n}\mathbf{n}^H]$. The linear convolution can also be expressed in matrix form as follows

$$\mathbf{y} = \mathbf{X}\mathbf{h} + \mathbf{n} \tag{3.8}$$

where $\mathbf{X}$ is a $(N + K - 1) \times K$ rectangular and Toeplitz matrix where columns contain time shifted versions of the transmitted signal $\mathbf{x}$ and the received signal is of corresponding length $(N + K - 1)$. The terms after the data vector can be zero as they correspond to before or after the transmitted signal.

$$\mathbf{X} = \begin{bmatrix} x(0) & 0 & \dots & 0 \\ x(1) & x(0) & \dots & 0 \\ \vdots & & & \\ & \vdots & \ddots & \\ x(K-1) & x(K-2) & \dots & x(0) \\ x(K) & x(K-1) & \dots & x(1) \\ \vdots & & & \\ x(N-1) & x(N-2) & \dots & x(N-K) \\ 0 & x(N-1) & \dots & x(N-K+1) \\ \vdots & & & \\ 0 & 0 & \dots & x(N-1) \end{bmatrix}$$

3.2.3 SAR Range Profile

Synthetic aperture radar (SAR) processing is fundamentally different from classic radar modes such as detection and tracking in that the aim is to gather and process information on the ground clutter, which forms the image. The observed returned signal from the ground is then a superposition of many scattering points rather than a small number in detection scenarios. Desirable features of a SAR range profile would consist of many fine resolution cells with low sidelobe levels and a low noise level. The higher the sidelobes are, the more likely that less reflective surfaces will not be sufficiently imaged as they become buried in the response from brighter targets. This is difficult to achieve, as each range cell with a scattering target contributes its own sidelobes due to the auto-correlation function of the transmitted signal. Sidelobes from each target cell then spills over into the neighbouring cells in an effect known as inter-range-cell-interference (IRCI). With an increasing number of range cells the IRCI worsens and has the effect of reducing the resultant range resolution [31].

In a SAR mode, the radar antenna main-beam is focused onto a patch on the ground which then forms the corresponding range profile. This is usually of a pre-determined length according to the scene size of interest, known as the range swath R_w. The number of range cells denoted as K is then given by (3.6), where r represents the range swath R_w. A returned range sample consists of a summation of all reflectivity points

47
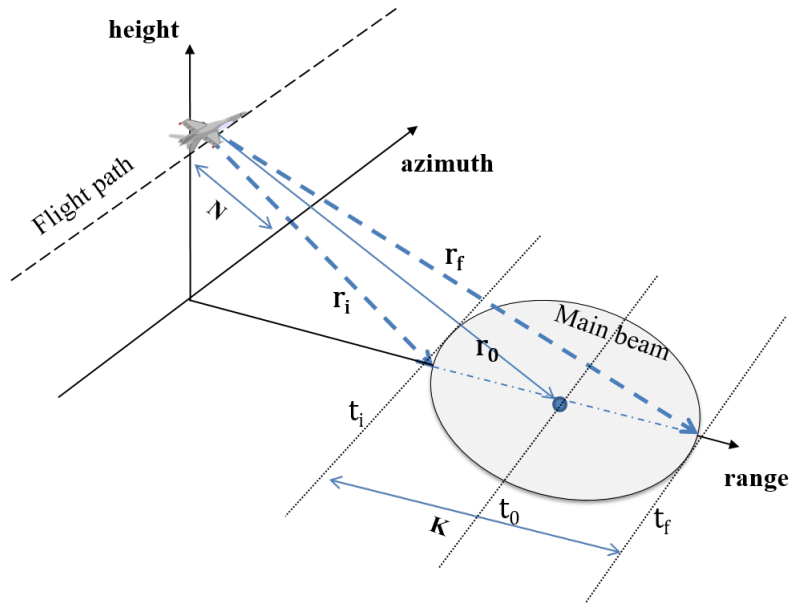
Figure 3.1: *Example of spotlight data collection showing the range and azimuth directions.*

for the corresponding time sample - this amounts to summing across other samples in the azimuth direction, providing a 1D slice across the scene in the range dimension. The central point of a SAR scene, the scene centre, is commonly used as the reference point for other signal returns. In Figure 3.1, the slant range distance r_0 to the scene centre is given as $t_0 = \frac{r_0}{c}$. The ground patch propagation time is the difference in delay between the nearest range cell of interest t_i and the furthest range cell t_f, $t_k = t_f - t_i$, which then corresponds to the time taken for the signal to propagate across the scene.

3.2.3.1   Cross-Range

A returned range sample consists of a summation of all reflectivity points for the corresponding time sample - these targets must be separated in the cross-range, also known as azimuth direction. In addition to using a large bandwidth to obtain high range resolution, the defining property of the SAR mode is the use of a sidelooking radar beam to obtain multiple 1D range-profiles, each differing in content, which are then processed to obtain a 2D image. Formation of the one-dimensional range profile is carried out at successive steps in the cross-range, also known as azimuth direction. There are a number of methods in which the cross-range data can be gathered, the major modes being **stripmap** which does not change the beam direction and in effect builds up the

image by sliding along the cross range and **spotlight** mode, which focuses on one patch of ground and changes look angle along the flight-path (aperture) to obtain different angle views of the same scene. Spot-light SAR is chosen to be the primary mode for application for its general application to shorter scene sizes which will be discussed later in this chapter. It is noted that these techniques could also be applied to other imaging modes. Figure 3.1 depicts spotlight mode operation where the same patch on the ground is illuminated by the main radar beam at each successive azimuth position and called from hereon the "scene of interest". SAR operates on a low pulse-repetition rate (LPRF) and does not suffer range-ambiguities. As the platform moves to gather the image, two successive pulses are then represent successive azimuth positions and are then subject to some amount of change.

3.3 Range Profile Estimation Methods

Estimation of the range profile can be described as a inverse problem; where the range profile is to be determined from the input and output of the system. It can also be described as a deconvolution process - the scene has been linearly convolved with the transmitted signal, and using the received signal, we wish to deconvolve the two signals.The following section discusses the principle methods used for reconstructing the SAR range profile.

3.3.1 Matched Filter

The matched filter is ubiquitous across radar signal processing and has particular merit in detection applications. It is designed such that it optimizes the SNR based on the response from a single target response. In Gaussian white noise, the detection probability is maximized and is by its definition the optimal estimator for detection [92]. As noted in the previous section, it is crucial to note that the SAR mode is not a detection mode, but instead aims to reconstruct the radar range profile from the summation of many return signals. Therefore, it is no longer optimally matched to each individual return. The matched filter performs the time-domain deconvolution of the return and transmitted signals.

$$\hat{h}(t) = y(t) * x^H(-t) \tag{3.9}$$

where, in effect, the received signal is being matched to the original signal which is time reversed and conjugated due to its directional difference (retreating from radar rather than returning). The matched filer is then looking for the points of correlation where the time delay of the correlations can then be translated to the target range. The performance of the matched filter is limited by the point-spread function (PSF) - this value can also be interpreted as the auto-correlation function, which drives the design of NLFM waveforms as discussed in Chapter 2.

For the proceeding discussion on alternative estimators which are presented in matrix format, it is useful to also write the matched filter in this way. It can be expressed in matrix form by a bank of matched filters, each matched to a particular column of the transmitted signal matrix $\mathbf{X}$, and therefore to each element of the range profile impulse response.

$$\mathbf{y} = \mathbf{X}\mathbf{h} + \mathbf{n} \tag{3.10}$$

$$\mathbf{X}^H\mathbf{y} = \left\{\mathbf{X}^H\mathbf{X}\right\}\mathbf{h} + \mathbf{X}^H\mathbf{n} \tag{3.11}$$

If the following is approximately true

$$\mathbf{X}^H\mathbf{X} \approx C\mathbf{I} \tag{3.12}$$

where $\mathbf{I}$ is the identity matrix of dimension $N \times N$, C is a constant, the range profile can be evaluated via the following approximation, neglecting the noise term and assuming the identity matrix

$$\hat{\mathbf{h}} \approx \mathbf{X}^H\mathbf{y} \tag{3.13}$$

which corresponds to the same processing shown in the time domain, as the rows of $\mathbf{X}^H$ contain time delayed and conjugated versions of the transmitted signal. As (3.12) is an approximation, this causes the observed sidelobes - another way of expressing the resultant sidelobes from the autocorrelation.

3.3.2 Stretch Processing

In SAR applications, it is common to have very long pulse lengths in order to obtain long distance imaging by creating a high energy, low power signal. Stretch processing - also known as deramp processing - inherently depends on the waveform being a LFM

signal. Built into its analysis is the time taken for signals to propagate between the scene and the radar - if the total patch propagation time is less than the length of the chirp signal $t_k < \tau$ ($K < N$) a lower sampling rate can be used at the ADC due to the resultant smaller spread of frequencies on receive. The form of the transmitted LFM signal is given as

$$x_c(t) = [a(t) - a(t - \tau_c)]\exp(2\pi j \phi_L(t)) \tag{3.14}$$

where a(.) denotes the signal envelope and for notational simplicity, the LFM phase term is denoted $\phi_L(t) = (f_c t + \frac{1}{2}\alpha t^2)$, recalling from Chapter 2, $\alpha = \frac{B_c}{\tau_c}$ refers to the change in frequency over time (chirp rate). Then considering that each of these transmission signals are shifted in time according to the distance of their round-trip delay t_n

$$y(t) = \sum_n \nu_n x_c(t - t_n) \tag{3.15}$$

such that the received signal is a summation of the shifted and time-delayed transmitted signal $\mathbf{x}_c$. In order to perform the reconstruction, the conjugate of the receive signal is mixed with a "deramp" LFM signal set up according to the arrival times of the target echoes. It is assumed here that the receiver has knowledge of the patch propagation time and that n target signals will arrive between t_i and t_f. The deramp waveform $\mathbf{x}_d$ starts at time t_i and ends at $t_f + \tau_c$

$$x_d(t) = [a(t_i) - a(t - t_f)]\exp(2\pi j \phi_L(t - t_i)) \tag{3.16}$$

The received signal is then mixed with the conjugate of the deramp signal

$$s_{\text{deramp}} = y(t) x_d^*(t) \tag{3.17}$$

giving the resultant deramped signal. Owing to the constant chirp term α, phase terms combine and cancel [8] (not shown here) to give a frequency term which separates out each of the target returns as a result of the linear chirp term α

$$s_{\text{deramp}} = \sum_n \nu_n \exp(2\pi j(\underbrace{\alpha(t_i - t_n)}_{f_n}(t - t_n))) \times [a(t - t_n) - a(t - (t_f + \tau_c))] \tag{3.18}$$

This signal, known as the deramped signal, is a superposition of many sinusodial waves, each scaled and increasing in frequency, as denoted by f_n, according to the time of the

carrier t_n. The spread of frequencies present is then proportional to the spread of the range swath. Like any multi-frequency signal, this can be easily interpreted in the frequency domain by application of a Fourier transform. Applying a Fourier transform to the deramped signal, the absolute modulus of which is a top-hat rectangular function, results in a sinc function denoted as $A(f)$, which is then shifted by the resultant corresponding phases

$$S_{\text{deramp}}(t) = \sum_n A(f - 4\alpha t_n)\nu_n \exp[2\pi j(\phi_L - f t_n)] \tag{3.19}$$

The result is that the target distance can then be calculated from the frequency at the peak of the corresponding sinc function such that the range profile can be mapped onto by a given frequency via the following relationship

$$t_n = \frac{f_n \pi}{\alpha} \tag{3.20}$$

Stretch processing can be considered as a Fourier technique and was historically considered a computationally cheap method via use of a fast Fourier transform (although traditional radars performed this in hardware). Its strongest feature however was the reduced requirements for the ADC if the duration of the chirp is much longer than the scene propagation time. This is true for spotlight SAR, but generally is not the case for stripmap mode. The main drawbacks for stretch-processing is its inflexibility to alternative waveforms. The need to synthesize non-linear and alternative waveform structures to facilitate both adaptivity to the surrounding environment and additionally to reap performance benefits may force the use of alternative range profile estimators. However, it should also be noted that there has been some research effort to support the use of NLFMs in combination with the stretch processor [93].

3.3.3   Orthogonal Frequency Division Multiplexing

A problem that higher bandwidth SAR systems may face is the problem of IRCI - sidelobes that are formed from each range cell which propagate along the full range profile - for more range cells, there are more respective sidelobes. The need to reduce IRCI is the motivation for design of a SAR-specific receive filter for OFDM proposed in [31]. In the following section an OFDM-SAR application which recognizes the need to

modify the receive processing to fully exploit the use of OFDM-waveforms. As discussed in the previous Chapter, OFDM has significant potential for SAR in that it may be able to provide ultra-low sidelobe levels and allows design in the frequency domain. As the sub-carriers do not have to occupy a contiguous block they can easily allow large gaps in the frequency domain.

3.3.3.1 Discrete Fourier Transform,Cyclic Prefix and OFDM

Sinusoidal signals are eigenfunctions of LTI systems, so if the range profile is considered to be linear and invariant, then an infinite duration signal is an eigenfunction of this system. This is one of the reasons for using the waveform cyclic prefix. The definition of the DFT states that a circular convolution of two signals in time will then be a multiplication in the frequency domain.

$$\mathbf{F}\left\{ y[n] = x[n] \circledast h[n] \right\} = X[i]H[i], \quad 0 < i < N - 1 \tag{3.21}$$

The DFT matrix is defined

$$\mathbf{F} = \frac{1}{\sqrt{N}} \begin{bmatrix} 1 & 1 & 1 & \cdots & 1 \\ 1 & W_N & W_N^2 & \cdots & W_N^{N-1} \\ \vdots & \vdots & \vdots & \ddots & \vdots \\ 1 & W_N^{N-1} & W_N^{2(N-1)} & \cdots & W_N^{(N-1)^2} \end{bmatrix}$$

such that $W_N = \exp[-j2\pi/N]$ and the IDFT $\mathbf{F}^{-1}$ is defined accordingly so that $\mathbf{F}^H\mathbf{F} = \mathbf{I_N}$, where $\mathbf{I}$ is the $N \times N$ identity matrix. There are often many advantages to operation in the frequency domain, namely efficiency via simple point-to-point multiplication as opposed to matrix computation of convolutions.However, the interaction of a finite transmitted signal and a transmission medium cannot be described as a circular convolution, rather it is a linear convolution process. By creating a cyclic prefix as the input to the impulse response, the process can then be approximately represented by a circular convolution. This then allows multiplication in the frequency domain on application of the DFT.

$$Y[i] = \mathbf{F}\left\{ y[n] = x[n] \circledast h[n] \right\} = X[i]H[i], \quad 0 < i < N - 1 \tag{3.22}$$

As introduced in Chapter 2, the addition of the cyclic prefix acts a guard interval between each of the sub-signals to prevent self-interference between the signals within the transmission medium, known as intersymbol interference (ISI). The addition of the cyclic prefix then allows both 1) removal of ISI 2) approximating circular convolution allowing simple calculations. The first K samples relating to the length of the cyclic prefix are removed on waveform reception. This sets up the following linear model

$$\mathbf{y} = \mathbf{R}\mathbf{s} + \mathbf{n} \tag{3.23}$$

where $\mathbf{R}$ is a $K \times K$ square and Toeplitz matrix which is a cyclic-matrix representation of the impulse response (described in full in the next section), $\mathbf{s}$ is the OFDM waveform and the truncated received signal $\mathbf{y}$ is of corresponding length (K). The cyclic prefix allows the frequency response of the scene to be modeled as a circulant convolution matrix. This matrix, due to its Toeplitz and square dimensions, can be said to be normal such that $\mathbf{R^H R} = \mathbf{R R}^H$ and has an eigen-decomposition $\mathbf{R} = \mathbf{M\Lambda M}^H$ where Λ is a diagonal matrix of eigenvalues of $\mathbf{D}$ and $\mathbf{M}$ is a unit matrix where the columns are eigenvectors of $\mathbf{R}$. Given that the $\mathbf{R}$ is a circulant matrix, this allows the following eigen-decomposition with the DFT matrix $\mathbf{F}$ to also be true $\mathbf{R} = \mathbf{F}^H \Lambda \mathbf{F}$. This yields the following relationship, which then allows application of the DFT according to definition (21) in the context of circular convolution [94]

$$\mathbf{R} = \mathbf{F}^H \text{diag}\left\{\mathbf{F r}_1\right\} \mathbf{F} \tag{3.24}$$

where $\mathbf{r_1}$ is the first column of the matrix $\mathbf{R}$ Applying the DFT to (3.23)

$$\mathbf{Fy} = \mathbf{F}[\mathbf{R}\mathbf{s} + \mathbf{n}] \tag{3.25}$$

$$\mathbf{Y} = \mathbf{F R F}^H \mathbf{F}[\mathbf{s}] + \mathbf{N}$$

$$\mathbf{Y} = \mathbf{F F}^H \text{diag}\left\{\mathbf{F r}_1\right\} \mathbf{F F}^H \mathbf{S} + \mathbf{N}$$

$$\mathbf{Y} = \text{diag}\left\{\mathbf{F r}_1\right\} \mathbf{S} + \mathbf{N}$$

$$\mathbf{Y} = \mathbf{D S} + \mathbf{N} \tag{3.26}$$

where $\mathbf{D}$ is the representation of $\mathbf{R}$ in the frequency domain.

3.3.3.2 OFDM-SAR

This application [31] is of particular interest as it highlights the requirement of using a suitable receive process to fully exploit performance enhancements from using a particular waveform. Previous attempts to integrate OFDM with radar use the matched filter, but these results are subject to IRCI [35]. Like stretch processing, the algorithm requires the knowledge of the scene size and operates in the limit where the signal vector length is greater than the respective scene signal vector length such that $N > K$. This is the condition under which the IRCI is suppressed. The following presents the range profile estimation algorithm from [31].

OFDM waveforms exploit use of a cyclic extension, a repetition of the signal added to the start of the transmission to act as a guard interval and is removed on waveform reception.In the following analysis, the OFDM transmit signal is written such that the cyclic prefix is removed and is represented by the "tail" section of the signal such that

$$\mathbf{s}' = \Big[s(K-1), s(K), \cdots, s(N+K-2) \Big]^T$$

On receive, the first $K-1$ samples relating to the cyclic prefix are removed, and the signal is modeled as an $N \times 1$ vector such that

$$\mathbf{y} = \mathbf{R}\mathbf{s} + \mathbf{n} \tag{3.27}$$

where $\mathbf{y} = \Big[y(N-1) \quad y(N) \quad ... \quad y(N+K) \Big]^T$, the target strength coefficients d can be given by the following cyclic, square and Toeplitz matrix of dimension $N \times N$

$$\mathbf{R} = \begin{bmatrix} d(0) & 0 & \cdots & 0 & d(K-1) & ... & d(1) \\ d(1) & d(0) & \cdots & 0 & d(K-1) & ... & d(2) \\ \vdots & \ddots & \ddots & \vdots & \ddots & ... & \vdots \\ d(K-2) & \cdots & d(0) & 0 & \cdots & 0 & d(K-1) \\ d(K-1) & d(K-2) & \cdots & d(0) & \cdots & 0 & 0 \\ 0 & \ddots & \ddots & \vdots & \ddots & \ddots & \vdots \\ 0 & \ddots & d(K-1) & d(K-2) & ... & d(0) & 0 \\ d(1) & \cdots & 0 & d(K-1) & d(K-2) & \cdots & d(0) \end{bmatrix}$$

which consists of cyclically shifted copies of the N dimensional weighting target strength

coefficient vector, which is analogous to the estimated range profile $\hat{\mathbf{h}}$

$$\mathbf{d} = \left[d(0), d(1), \cdots, d(K-1), 0, \cdots, 0 \right]^T$$

and where the number of zeros at the end of the vector is $N - K$. For an OFDM system, the demodulator performs the DFT on the received signal, to give

$$\mathbf{Y} = \mathbf{DS}' + \mathbf{N} \tag{3.28}$$

where $\mathbf{S}'$ is the FFT of the the time domain truncated vector $\mathbf{s}'$. The estimate of $\mathbf{D}$ is then given simply as a division of each of the vectors of the same dimension

$$\hat{\mathbf{D}} = \frac{\mathbf{Y}}{\mathbf{S}'} \tag{3.29}$$

So that then the range profile estimate can be obtained by applying the N-point inverse DFT (IDFT)

$$\hat{\mathbf{d}} = \mathbf{F}^{-1} \{\mathbf{D}\} \tag{3.30}$$

3.3.3.3 Insufficient Cyclic Prefix

However, due the matrix sizing of the circulant matrix, it can only be represented by a maximum of N elements. When the signal size becomes smaller than the swath width $N < K$, there is no longer one range cell mapped onto the coefficient vector $\mathbf{d}$ which results in reduced resolution

$$\mathbf{R} = \begin{bmatrix} \tilde{d}(0) & \tilde{d}(N-1) & \cdots & \tilde{d}(1) \\ \tilde{d}(1) & \tilde{d}(0) & \cdots & \tilde{d}(2) \\ \vdots & \vdots & \ddots & \vdots \\ \tilde{d}(N-1) & \tilde{d}(N-2) & \cdots & \tilde{d}(0) \end{bmatrix}$$

each $\tilde{\mathbf{d}}$ value given as

$$\tilde{d}(n) = \sum_{i:0<iN+n<M-1} d_{iN+n}, \qquad (n = 0, \cdots, N-1) \tag{3.31}$$

The weighting vector becomes a summation of reflectivity coefficients from several range cells, which results in energy from neighboring range cells contributing to each estimated
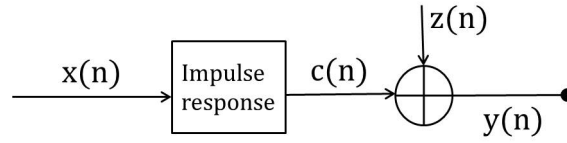
Figure 3.2: *Basic flow chart of system identification process*

$\tilde{d}(n)$ value. This results in reduced range resolution. So while this OFDM-SAR method is capable of reduced sidelobes, this is only possible up to the condition of range-swath matching where $N = K$.

3.4 Least Squares System Identification

System identification can be described, in a general sense, to be concerned with tasks of parameter estimation based on observations originating from a dynamical system. For system identification problems which can be described as linear in the parameters, the least squares method is a suitable for their estimation. The radar profile estimation system can be described as a linear problem, and is as such, suitable for estimation via least-squares approximation. In 1960, [95] described the optimal estimation of an impulse response of a linear time-invariant system (LTI) in the presence of white noise using knowledge of the input and output over a specified interval of time. The radar estimation problem - in particular the SAR range-profile estimation problem meets this criteria. Leading from this work, the next section presents the salient aspects of this work and integrates this to the radar range-profile problem in the time domain, and is then expanded on to formulate a frequency domain least-squares estimator. While this result has now been exploited and used across many areas of control theory and system identification, it has not been applied to the SAR range profile estimation problem.

3.4.1 Time Domain Model

The least squares methodology uses a set of inputs $\mathbf{x}$, observations $\mathbf{y}$ and estimates the model parameters $\boldsymbol{\beta}$ which approximate the smallest sum of squared residuals between the observations and the estimated output using model parameters.

The input and output can be continuous but require discretization. The input is as-

sumed to be known and the resulting output $c(n)$ is then modified by additive noise $z(n)$ caused by internal measurement errors and/or an additional non-observable system input

$$y(n) = c(n) + z(n) = \sum_{p=0}^{\infty} \boldsymbol{\beta}(p) x(n - p) + z(n) \tag{3.32}$$

An example system flow chart is given in 3.2. Since in reality the input and output are finite values, the impulse response must also be approximated by a finite set of values. Approximating an infinite impulse response as finite can induce some level of error which is system dependent, but generally reported to be small [96].In order to proceed with impulse response estimation, the following model assumptions are made

1. $h(p) = 0$ for $p > P$, such that the impulse response is assumed to be zero outside the measurement interval

2. $x(n)$ is observed for $0 \leq n \leq N$ and is not identically zero in this interval

3. $x(n) = 0$ for $n < 0$ and $n > N$

4. $y(n)$ is observed for $0 \leq n \leq N + P$

These model assumptions are readily applicable to the SAR case: 1. in stretch processing, it is already assumed that the range impulse response is of finite length and zero outside the range of interest for 2. and 3. the transmitted waveform $x(n)$ is non-zero across the relevant intervals and 4. represents the corresponding interval in which the received signal is observed.

3.4.2   Least Squares Estimate

The least squares method finds coefficients $\hat{\boldsymbol{\beta}}$ which minimizes the sum of the squared error of the linear model

$$\sum_{n=0}^{M} \{y(n) - \sum_{p}^{P} \boldsymbol{\beta}_p x_p(n)\}^2 = [y - \mathbf{X}^H \boldsymbol{\beta}]^H [y - \mathbf{X}^H \boldsymbol{\beta}] \tag{3.33}$$

These coefficients $\hat{\boldsymbol{\beta}}$ can then be estimated by a set of simultaneous equations known as the normal equations such that

$$\hat{\beta} = (\mathbf{X}\mathbf{X}^T)^{-1}\mathbf{X}\mathbf{y} \tag{3.34}$$

which is found by taking the derivative of the sum of the squares (3.33) and solving for its stationary point. The least squares estimator is an unbiased estimator when $z(n)$ is white Gaussian noise (WGN). The covariance matrix of $\hat{\beta}$ is such that

$$\mathrm{cov}(\boldsymbol{\beta}) = E[(\boldsymbol{\beta} - \hat{\beta})(\boldsymbol{\beta} - \hat{\boldsymbol{\beta}}^T)] = (\mathbf{X}^H\mathbf{Z}^{-1}\mathbf{X})^{-1} \tag{3.35}$$

If the noise is white then the covariance matrix can be reduced to

$$\mathbf{Z} = \sigma_z^2\mathbf{I} \tag{3.36}$$

where $\mathbf{I}$ is the identity matrix and σ_n are the noise variance values. The covariance of the estimate is then also reduced to

$$\mathrm{cov}(\boldsymbol{\beta}) = \sigma_z^2[\mathbf{X}\mathbf{X}]^{-1} \tag{3.37}$$

Which serves as a goodness of fit metric for the model coefficients $\boldsymbol{\beta}$.

3.5 System Identification for SAR

3.5.1 Time Domain Problem Formulation

The following treatment continues estimation of the radar range profile as a discrete and finite impulse response. As presented initially in Section 3.2.2, the observations at the receiver can be expressed as the convolution of the transmission sequence and the finite impulse response vector $\mathbf{n}$ for a single pulse p as

$$y^p(n) \quad = \quad h^p(k) * x^p(k) + n^p(n) = \sum_{k=0}^{K+N} h^p(k)x^p(k-n) + n(n) \tag{3.38}$$

where the transmitted waveform is

$$\mathbf{x}^p = \left[x^p(0), x^p(1), \cdots, x^p(k), ..., x^p(N-1)\right]^T \quad k = (0, 1, \cdots, N-1)$$

where k is the kth sample of the transmitted waveform. The finite impulse response is

$$\mathbf{h^P} = \left[h^p(0) \quad h^p(1) \quad ... \quad h^P(K-1)\right]^T$$

The linear convolution can also be expressed in matrix form as follows

$$\mathbf{y} = \mathbf{X}\mathbf{h} + \mathbf{n} \tag{3.39}$$

where $\mathbf{X}$ is a $(N + K - 1) \times K$ rectangular and Toeplitz matrix where columns contain time shifted versions of the transmitted signal $\mathbf{x}_p$ and the received signal is of corresponding length $(N + K - 1)$. The terms after the data vector can be zero as they correspond to before or after the transmitted signal.

$$\mathbf{X} = \begin{bmatrix} x(0) & 0 & ... & 0 \\ x(1) & x(0) & ... & 0 \\ \vdots & & & \\ & \vdots & \ddots & \\ x(K-1) & x(K-2) & ... & x(0) \\ x(K) & x(K-1) & ... & x(1) \\ \vdots & & & \\ x(N-1) & x(N-2) & ... & x(N-K) \\ 0 & x(N-1) & ... & x(N-K+1) \\ \vdots & & & \\ 0 & 0 & ... & x(N-1) \end{bmatrix}$$

In order to estimate the impulse response we use the least squares framework described above such that the impulse response of the scene can be expressed as [97]

$$\hat{\mathbf{h}} = (\mathbf{X}^H \mathbf{R}_{nn}^{-1} \mathbf{X})^{-1} \mathbf{X}^H \mathbf{R}_{nn}^{-1} \mathbf{y} \tag{3.40}$$

If the noise and interference source is white (e.g. uncorrelated) , the covariance matrix

is reduced to a diagonal of the variances $\mathbf{R}_{nn} = \sigma_n^2 \mathbf{I}$ giving the simpler ordinary least squares (OLS) estimator:

$$\hat{\mathbf{h}} = (\mathbf{X}^H \mathbf{X})^{-1} \mathbf{X}^H \mathbf{y} \tag{3.41}$$

The expression gives an exact estimate of the impulse response, but is computationally expensive to compute - note that there are several matrix multiplications and an inversion. To proceed with least squares estimation, the properties of square and circulant matrices, as used in OFDM in equation (3.24) are exploited to express the problem more efficiently in the frequency domain.

3.5.2 Cyclic Extension

By describing the problem in the frequency domain we can exploit factorization with the discrete Fourier transform (DFT) to create a computationally efficient least squares expression. Matrices that are square, circulant and Toeplitz factor conveniently with the discrete Fourier transform. Rearranging the $(N + K - 1) \times (K)$ rectangular matrix given in (3.39) into this format allows an efficient implementation using a DFT. The transmitted signal matrix length and the impulse response vectors are manipulated as follows to allow the problem to be represented as a circular convolution

$$\mathbf{y} = \mathbf{X}_c \begin{bmatrix} \mathbf{h} \\ \mathbf{0}_{N-1} \end{bmatrix} + \mathbf{n} \tag{3.42}$$

$$\mathbf{X}_c = \mathbf{F}^H \text{diag} \{ \mathbf{F} \mathbf{x}_{c_1} \} \mathbf{F} \tag{3.43}$$

where $\mathbf{X}_c$ is formed using (3.24) and $\mathbf{x}_{c_1}$ is the first column of a circulant signal matrix such that

$$\mathbf{x_{c_1}} = \left[x(0), x(1), \cdots, x(N-1), \underbrace{x(N), x(N+1), \cdots, x(N+K-1)}_{\text{zero terms}} \right]^T \tag{3.44}$$

The ith column of $\mathbf{X}_c$ is obtained by applying $i - 1$ cyclic shifts downwards to $\mathbf{x}_{c1}$, where $i = 2, ..., M$ and $M = N + K - 1$. This cyclic extension is performed by adding $K - 1$ zero terms. Now the signal matrix is circulant, Toeplitz and square of dimension $M \times M$. Correspondingly, the impulse response vector is extended by $N - 1$ zero samples, the extension shown as a $N - 1$-dimensional vector $\mathbf{0}_{N-1}$, so its vector is now
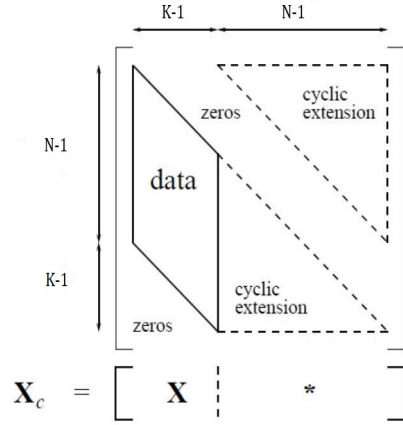
Figure 3.3: *Form of the cyclically extended matrix X_c relative to the original rectangular matrix X where $K - 1$ is length of impulse response and $N - 1$ is signal length*

also of dimension M. The last $K - 1$ columns of $\mathbf{X}_c$ beyond $N - 1$ can contain any value as the corresponding elements in the impulse response vector are zeros. Then these additional samples do not have to be transmitted and this extension is merely an artifact used in this stage of the processing.

3.5.3 Frequency Domain Solution

Applying Fourier transforms to both sides of time-domain circulant matrix equation (3.42) and using the identity property, where $\mathbf{F}$ is the M-point DFT, gives

$$\mathbf{Fy} = \mathbf{F}\mathbf{X}_c\mathbf{F}^H\mathbf{F}\begin{bmatrix} \mathbf{h} \\ \mathbf{0}_{N-1} \end{bmatrix} + \mathbf{Fn} \tag{3.45}$$

Now the expression for circulant-Toeplitz matrices given in (3.43) can replace $\mathbf{X}_c$ and again using the identity property gives

$$\mathbf{Y} = \mathbf{\Omega}\mathbf{H} + \mathbf{N} \tag{3.46}$$

where $\mathbf{\Omega} = \mathbf{F}\mathbf{X}_c\mathbf{F}^H = \mathrm{diag}\left\{\mathbf{Fx}_1\right\}, \mathbf{Y} = \mathbf{Fy}, \mathbf{H} = \mathbf{F}\begin{bmatrix} \mathbf{h} \\ \mathbf{0}_{N-1} \end{bmatrix}$ and $\mathbf{N} = \mathbf{Fn}$. Given an expression of the system model in the frequency domain, a corresponding generalized

least squares estimate for **H**

$$\hat{\mathbf{H}} = (\boldsymbol{\Omega}^H \boldsymbol{\Omega})^{-1} \boldsymbol{\Omega}^H \mathbf{Y} \tag{3.47}$$

Equation (3.47) is an approximation since it does not embody the constraint on the estimate inherent in (3.42), specifically

$$\mathbf{0}_{N-1} = [\ \mathbf{0}_{N-1,K} \quad \mathbf{I}_{N-1}\ ]\mathbf{F}^{-1}\hat{\mathbf{H}} \tag{3.48}$$

where $\mathbf{0}_{N-1}$ is an column vector of $N - 1$ zeros, $\mathbf{0}_{N-1,K}$ is an $(N - 1) \times (K)$ matrix of zeros and $\mathbf{I}_{N-1}$ is an $(N-1) \times (N-1)$ identity matrix. Now that each of the signals are M dimensional in the frequency domain, they can be treated by element-wise division, such that the matrix operations can be simplified as

$$\hat{H}_i = \frac{Y_i}{\Omega_i} \qquad i = (1, ..., M) \tag{3.49}$$

This frequency domain least squares problem has the same number of knowns and unknowns, which was not the case in the time-domain problem of (3.41) which had fewer unknowns. An approximation to the least-squares estimate of (3.40) is obtained by projecting the estimate provided by (3.49) onto the feasible set of solutions defined by the constraint of (3.48).

$$\hat{\mathbf{h}}_c = [\ \mathbf{I}_K \quad \mathbf{0}_{N-1,K}^T\ ]\mathbf{F}^{-1}\hat{\mathbf{H}} \tag{3.50}$$

where $\mathbf{I}_K$ is an $K \times K$ identity matrix. This operation removes the additional $N - 1$ samples that were added to the original time domain problem to allow the problem to be expressed in the frequency domain via representation via circular convolution. The removal of the extra $N - 1$ terms in the time domain also acts as noise-removal. This works best when $N > K$, as noise removal performance is proportional to the number of samples N removed. Here we are also exploiting the assumption that the impulse response is finite and of known length which was invoked in the formation of the time-domain model. This process of obtaining the solution will be referred to as the time-constrained frequency domain estimation (TCFDE) throughout the rest of this work.

3.5.4   Comparison of TCFDE and OFDM

3.5.4.1   Processing Considerations

As the range profile estimation algorithms for both TCFDE and OFDM-SAR have inherent similarities it is pertinent to compare and contrast the two in their application to SAR. Firstly, it is noted that the OFDM-SAR algorithm described above makes use of a physical cyclic prefix in the waveform to discard these samples on receive to allow its impulse response matrix $\mathbf{R}$ to be represented as a circulant matrix, which ultimately allows the receive and transmitted samples to be of the same length, allowing element-wise division in (3.29). This approach is restrictive for larger scene sizes, as it cannot process swath lengths longer than the signal $N < K$ as shown in (3.31) the range-cell elements then overlap resulting in reduced resolution. The frequency domain division resulting from the use of cyclic extension is also applied in the proposed TCFDE method, but crucially, the transmitted signal is not physically altered. Algorithmically, the transmitted signal is extended and the impulse response is also artificially extended in (3.42) to allow the vector to take on the same dimension. This is not assuming that the impulse response is longer than initially assumed, only a processing artifact. These modifications allow benefits that are not seen in the OFDM algorithm such that; 1) the impulse response length may be longer than the signal length $(N < K)$ without reduction is observed range resolution; 2) there is then a noise-suppression stage in-built to the final step where the impulse response is constrained in the time domain.

3.5.4.2   Energy, Waveform and Timing Considerations

For both methods the receiver expects signal returns to arrive from t_i onwards , as depicted in Figure 3.4. The figure highlights that although the received signal is both cases is $K + N - 1$ samples long, and arrive at the same time at the respective receivers, the first K received samples in the OFDM case are removed. For the comparisons here, and as is typical in SAR, it is assumed that the furthest scatterer reflection will have returned before the next pulse is transmitted. Assuming a relatively low pulse repetition rate (PRI), this is a valid assumption to avoid the effects of range-folding. Both systems are ready to transmit the next pulse $N + K - 1$ time samples after the first return begins - after one full returned pulse duration. If the period between transmit and receive is small, this can result the signals overlapping and interfering
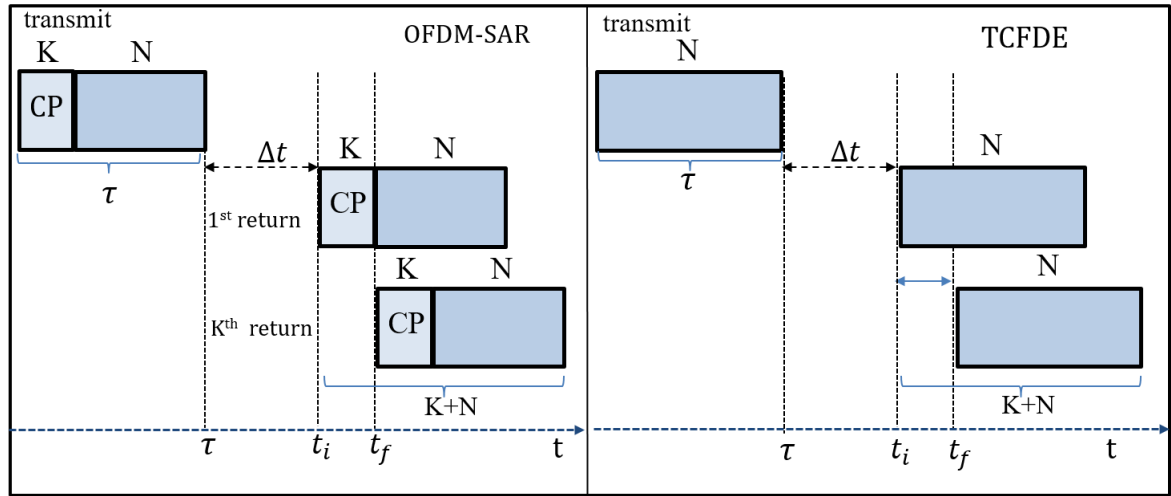
Figure 3.4: *Timing overview for one pulse repetition interval from transmission to receipt for the OFDM (left) and TCFDE (right) estimation schemes.*

(range folding). If this overlap is less than K time samples, the OFDM signal is not affected, as the first K samples will be discarded on receive. Therefore, in this way, the OFDM signal is protected from range-foldover whereas OFDM-SAR uses the full received signal.

Though both algorithms exploit the cyclic extension factorization with the FFT; the OFDM signal does so in the traditional approach by physically transmitting a cyclic prefix at the start of the signal but the TCFDE algorithm adds extra zeros in processing to give efficient factorization. This post-receive processing will not prevent performance degradation for TCFDE if pulse-overlap occurs.

The key difference is energy usage. The OFDM-SAR algorithm requires transmission of unused signal energy as K of the transmitted $N + K - 1$ samples are discarded at receive. For the same scene size, the OFDM algorithm requires K samples more transmit time. Figure 3.5 shows that for a waveform where $N < K$ and K samples are removed, the majority of the waveform energy is discarded. The TCFDE algorithm is waveform independent in the sense that it does not require particular transmit waveform properties such as a cyclic prefix or particular phase or frequency relationship - so it can easily use waveforms that have been designed with constant modulus waveforms that make efficient use of the transmitted by running it in saturation. While OFDM waveforms can also use constant amplitude modulus waveforms, it may be at the cost of losing the initially designed spectral shape which can have strong impact on performance
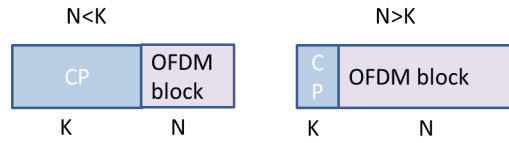
Figure 3.5: *Diagram exemplifying energy loss on receive for OFDM-SAR waveforms, for a large number of range cells, a large proportion of the signal energy is lost. K is number of samples in range profile and N is number of transmitted signal samples.*

for OFDM-SAR [31].

3.6   Simulated Results

In order to exemplify the effects from using different range-profile reconstruction methods, the following section presents a simulation analysis to compare various waveform-estimator pairs. The following simulations demonstrate results for the matched filter, the OFDM-SAR estimator and the proposed TCFDE method. Simulations performed are on reconstruction of a range profile with a single range scatterer, SAR simulation with a number of point targets, tests on the applicability of TCFDE in terms of Doppler tolerance and situations where the impulse response is longer than expected.

3.6.1   Range Profile Example

Each of the range-profile estimators will be assessed according to the resultant base noise-floor level and apparent resolution according to the width of the peak. The base noise level is determined either by the algorithms ability to suppress noise, or in the extent of range sidelobes in high sidelobe cases. This noise-base measurement level is important in SAR imaging as it corresponds to the ability to image low reflectivity scatterers. The resolution, determined by the width of the peak then also determines how finely point scatterers can be resolved. To clearly demonstrate the range-sidelobes from an individual range cell only one range scatterer is used in this demonstration.

LFM, NLFM and OFDM waveforms are used in the following assessment of the range-profile estimators. In the interest of a fair comparison, all waveforms have the same energy-budget, such that the longer OFDM-block plus cyclic extension waveform is

scaled to have the same transmitted power as the LFM and NLFM waveforms. Each of the signals are limited to an energy budget such that total waveform energy $E_T = \mathbf{x}^H \mathbf{x} = 1$. Four simulated examples are shown to demonstrate two distinct cases at low and high noise level where:

1. $N < K$: the scene length creates an impulse response that is longer than the corresponding discrete representation of the signal

2. $N > K$: the scene length impulse response is shorter than the discrete representation of the signal.

The two levels of noise covariance are $\sigma_n^2 = 1e^{-5}$ and $\sigma_n^2 = 0.01$. The respective experiments use a pulse length of $N = 512$ and K range gates, such that in the first experiment $K = 128$ and in the second $K = 2560$ to test TCFDE capability for $K >> N$. Changing the pulse length has implications for the energy content so this demonstration will only change the overall range-profile length. The parameter size for N was chosen based on the corresponding radar bandwidth, pulse length size and sampling rate also used in [31]. Values for K were chosen to represent extremes with respect to N to demonstrate results for when the range profile is smaller or much larger (worst case generally) than the pulse length.

The NLFM waveform is designed over the same frequency-time sweep as shown in Figure 3.6 and has its spectrum designed using SPA with the Hann window as input - as discussed in Chapter 2, a non-rectangular spectral shape reduces the height of the sidelobes due to the relationship with the autocorrelation function. An OFDM waveform is generated as per the algorithmic description in [31] such that the frequency profile is completely flat but with large variations in the time domain. The LFM, NLFM and OFDM waveforms used are shown in Figure 3.6. An additional waveform is generated for OFDM using weights in the frequency domain according to the NLFM to compare OFDM-SAR results using a non-spectrally flat waveform. The instantaneous frequency in Figure 3.6 is not shown here for OFDM-SAR. The OFDM waveforms are spectrally precise owing to their design from the weights in the frequency domain and direct synthesis to the time domain, as shown for the spectrally flat OFDM waveform in Figure 3.6 b. This design approach gives rise to its large variance of values, shown in the real component of the time domain in Figure 3.6 c, not constrained by constant
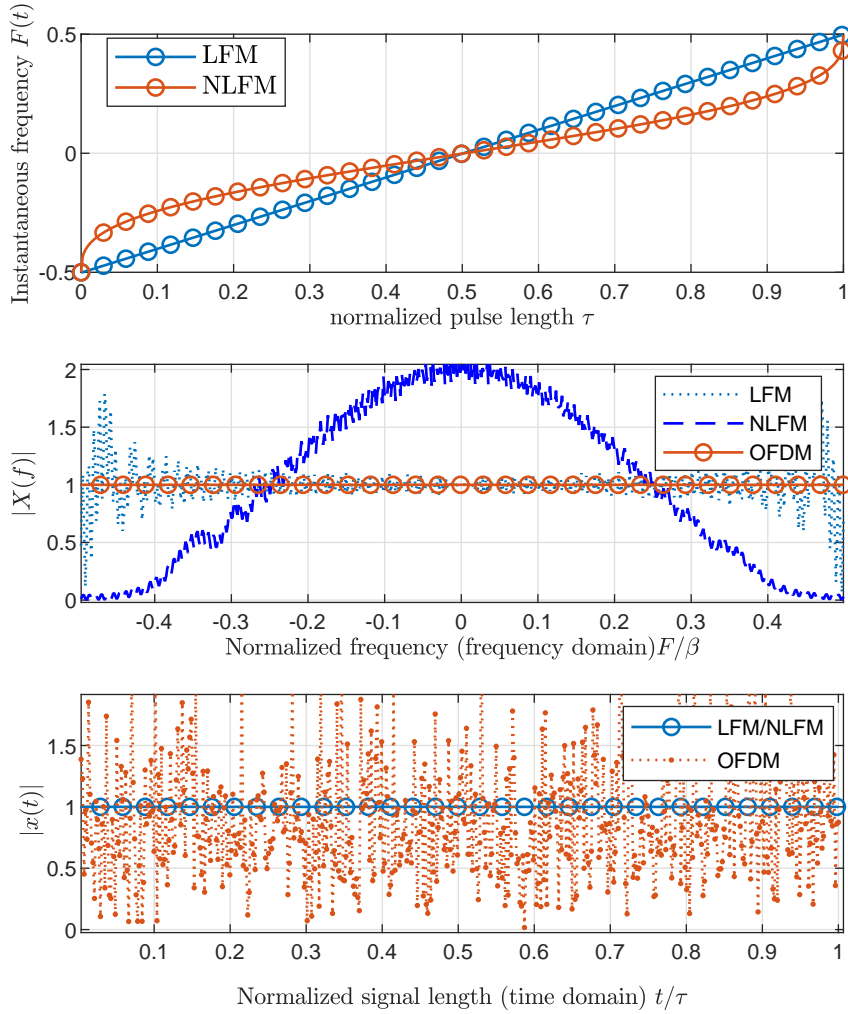
Figure 3.6: *LFM, NLFM and OFDM waveform comparison*

increase in the change of frequency or by constant modulus amplitude.

The waveform-pair estimators under test are: LFM-MF, NLFM-MF, LFM-TCFDE, NLFM - TCFDE, OFDM - OFDM-SAR and NLFM/OFDM - OFDM-SAR. Results are shown for the same bandwidth B_c and pulse length τ_c, but the overall scene length, or range profile swath, R_w is changed. Each of the values obtained in Table 3.1 has been evaluted using a set of 1000 runs to obtain the mean value.

Estimator-Waveform	Scenario A	Scenario B	Scenario C	Scenario D
Set-up:	$N > K, \sigma_n^2 = 1e^{-5}$	$N > K, \sigma_n^2 = 0.01$	$N < K, \sigma_n^2 = 1e^{-5}$	$N < K, \sigma_n^2 = 0.01$
MF-LFM	2.19	2.2	2.25	2.25
MF-NLFM	0.36	0.36	0.71	0.72
OFDM SAR -OFDM	$2.7e^{-8}$	0.02	$9e^{-6}$	8.6
OFDM SAR-NLFM	$2.8e^{-8}$	0.02	$1.1e^{-5}$	16.1
TCFDE-LFM	$2.0e^{-8}$	0.017	$2.7e^{-8}$	0.2
TCFDE-NLFM	$3.1e^{-7}$	0.39	$2.7e^{-8}$	0.68

Table 3.1: *Resultant MSE values for various estimator-waveform pairs*

3.6.1.1 Performance Assessment

The majority of radar metrics are centralized around the matched filter scheme, high-lighted in a study for OFDM radar [98]. For example, the standard radar ambiguity function and "mismatch loss" are inherently based on the nature of matching two signals. As this is highly embedded into radar literature, new metrics are required when using non-traditional receive filters. While MF based algorithms are assessed based on the sidelobe levels for autocorrelation, the TCFDE and OFDM-SAR algorithms do not perform an auto-correlation like operation and as such do not have an analogous metric to the auto-correlation sidelobes. As a linear-least squares algorithm and standard for system identification algorithms [97] the natural approach to error assessment is the overall mean square error in the estimate. Continuing, comparisons are drawn using this metric. To find a single metric which accounts for the structure of the response which includes resolution and sidelobe level itself is a non-trivial task. Therefore this metric [97] does not give specific information about structure or sidelobe level, but an overall representation on how similar the range-profile estimate $\hat{\mathbf{h}}$ is to its true discrete representation $\mathbf{h}$,

$$\rho = \text{tr}(\text{cov}(\mathbf{h} - \hat{\mathbf{h}})) = \mathbf{E}[(\mathbf{h} - \hat{\mathbf{h}})(\mathbf{h} - \hat{\mathbf{h}})^H] \tag{3.51}$$

3.6.1.2 Results

Table 3.1 shows the resultant MSE values for the listed estimator-waveform pairs.

In Table 3.1 is observed that the values for the MSE for the matched filter (MF), both LFM and NLFM, are in general much higher. Although the matched filter is the optimal detector in noise, it is subject to IRCI, whereas the other estimators are not.

The MF results have consistently larger MSE values owing to both the lower resultant resolution and the larger sidelobes as a direct result of IRCI. Also note that the MF-NLFM offers significantly decreased MSE values due to the decreased sidelobes. For the cases where the range profile is increased to $K = 2560$, the MSE is increased for both MF-LFM and MF-NLFM. Again, this effect can be attributed to IRCI. With more range samples, there is more IRCI, worsening the MSE value. The MF estimation method, by design, is robust to increased levels of white noise. Conversely, the OFDM waveform-estimator is the most sensitive and its performance significantly degrades with increased noise, especially when combined with decreased resolution in the insufficient cyclic prefix case, as demonstrated in Scenario D. The TCFDE case provides some noise-reduction, comparing the flat spectral OFDM waveform and TCFDE-LFM in Scenario B, the TCFDE has lower MSE values in both high noise cases (Scenario B & D).The NLFM waveform as input to the TCFDE is subject to increased distortion compared to the LFM which becomes more evident with added noise. This effect is more prominent in Scenario D where $N < K$ as the extent of noise removal is proportional to N. The largest values arise from using an NLFM-OFDM waveform paired with the OFDM-SAR estimator in noise with a longer scene length.

A selection of these estimator-waveform pairs are plotted in Figure 3.7. Firstly, Figure 3.7a shows the low noise case and short scene scenario. As expected, the MF-LFM plot yields the highest sidelobes and the poorest range resolution due to limitation from the autocorrelation function. The MF-NLFM estimation yields much lower sidelobe levels and also finer resolution, owing to the relationship between spectral shape and autocorrelation. While the MF-NLFM pair gives lower sidelobe levels, note that the TCFDE-NLFM pair performs worse than the TCFDE-LFM. This point stresses the importance of the role of the estimator in the waveform-estimator pair.The base level of the waveforms processed by the TCFDE and OFDM-SAR algorithm the similar for the case of very low noise, with very narrow peaks and sidelobes. Comparing Scenario A to C - both of which are in the low noise case - C represents a longer impulse response; most of the sidelobe and base-noise levels are the same across the waveform-estimator pairs, excluding the OFDM result, which now has a much higher noise level and a wider peak. This is as a result of the algorithm reverting to the insufficient cyclic prefix case. Adding noise into the system and comparing A to B and C to D, the estimation methods and their robustness to noise becomes apparent.
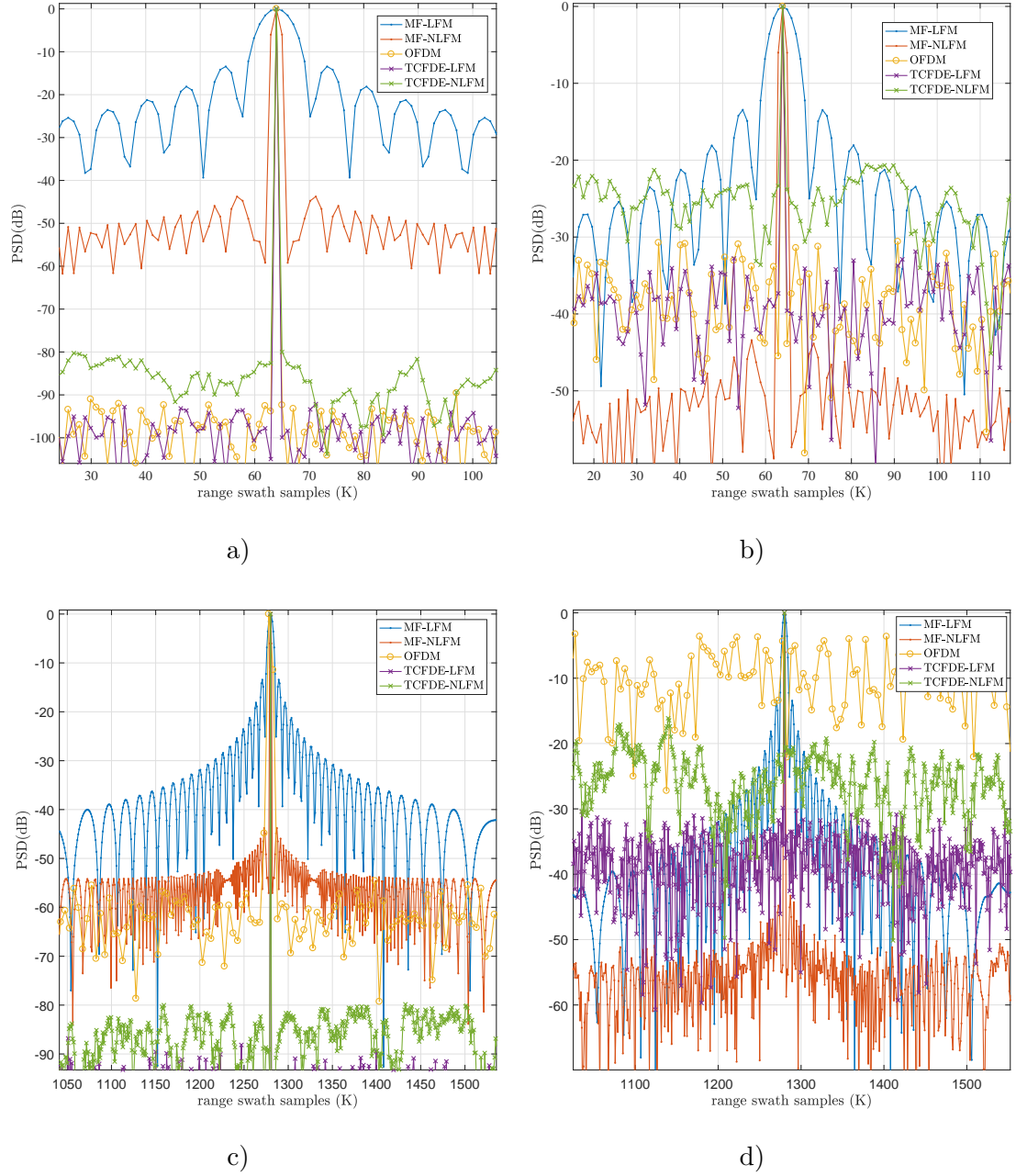
Figure 3.7: *Top left to bottom right: Scenario A: $N > K, \sigma_n^2 = 1e^{-5}$, Scenario B: $N > K, \sigma_n^2 = 0.01$, Scenario C:$N < K, \sigma_n^2 = 1e^{-5}$ Scenario D:$N < K, \sigma_n^2 = 0.01$. The results have been normalized such that the maximum peak value was set to 0dB in the case of each estimator.*

Summary

- Matched Filter: high sidelobes, lower resultant resolution, robust to white noise, invariant to scene length changes, optimized performance for shaped, non-flat waveforms

- OFDM-SAR: low sidelobes, high resolution, poor robustness to noise, heavily dependent on scene size $N > K$, preference to spectrally flat waveforms

- TCFDE: low sidelobes, high resolution, some noise-suppression ability, some dependence on scene size, but operational for $N > K$ with suitable waveform

Both the OFDM-SAR and TCFDE algorithms using a spectrally weighted waveform perform worse compared to their spectrally flat counterparts. Whereas the MF method performs better using NLFM that the approximately spectrally flat LFM. This highlights the necessity of choosing the correct estimator and that waveform design must be tailored according to its receive estimator. Chapter 4 will further discuss the impact of the waveform spectral content on the performance.

3.6.2 SAR Images

To demonstrate the resultant performance each of the range-profile estimation algorithms have on the final SAR image, a series of simulated SAR images have been generated using the MF, TCFDE and OFDM-SAR range-profile estimators combined with the backprojection algorithm. These have been calculated for the same set of scenarios as the single-scatterer case in the previous section. Two sets of images, (a-f) and (g-l), are created with different range swaths to create the correct K:N ratio and therefore both have different range-cell to pixel ratios and image resolutions. For $N > K$ there are minor visible differences in the images between lower and high noise cases. The OFDM and TCFDE images provide finer resolution than the MF examples as also observed in the single scatterer examples. For this short range swath set-up the noise reduction and sidelobe levels perform well for all estimators - there is little noticeable qualitative difference between the higher and lower noise set but the differences are apparent in the image MSE value. The $N < K$ set shows the greatest visible distinction between methods where the OFDM high noise image shows visible rings, distorting the quality of the image. The same effect is apparent to a lesser extent with the TCFDE

in g). Higher resolution is given in the images which used frequency domain division (TCFDE & OFDM), but are subject to increased levels of distortion with increased background white noise.

3.6.3   Doppler-Shift

The TCFDE estimator is set-up in a such a way that it may be more vulnerable to spectral mismatch due to the direct division in the frequency domain. To demonstrate the impact of Doppler shifts due to platform motion, which is inherent in SAR, on the received signal the following simulations demonstrate the resultant impact on range-profile estimation. The effect of a Doppler shift on a waveform is represented as a stretching or a compression of the signal in time and can be represented as follows [98],

$$y_d(t) = \sqrt{\gamma} y(\gamma(t - \tau)) \tag{3.52}$$

such that

$$\gamma = 1 + \beta = 1 + \frac{2}{c} \cdot \langle \hat{\mathbf{u}}, \mathbf{v} \rangle \tag{3.53}$$

where $\hat{\mathbf{u}}$ is a unit direction vector $\frac{|\mathbf{u}|}{\mathbf{u}}$ and $\mathbf{v}$ is the velocity vector of the platform which defines the angle between their inner product θ, shown in Figure 3.9. From a moving platform such as in SAR, the Doppler shift is then dependent on the velocity vector between the platform and a signal reflector, which is then dependent on the angle.

$$\theta_d = \cos^{-1} \frac{|\mathbf{u}||\mathbf{v}|}{\mathbf{u}\mathbf{v}} \tag{3.54}$$

The following simulations calculate the resultant received signal due to a Doppler shift for a spotlight operation where the angle changes across the collection aperture. The smallest angle that occurs on a straight flight path is determined by $\theta_{min} = \tan^{-1} \frac{C_w}{2d_0}$, where C_w is cross-range swath, which gives the maximum shift $\gamma_{\max}$. For the zero shift case, γ_0 is given when the platform is perpendicular to the scatterer $\theta_0 = 90° \Rightarrow \beta = 0 \Rightarrow \gamma = 1$. To test in upper-limit conditions, the background white noise level $\sigma_n^2 = 0.1$. The platform velocity is $200 \mathrm{m}s^{-1}$, the cross range width $C_w = 2.5$km and the slant-range vector $R_0 = 6$km. Two simulations are performed:
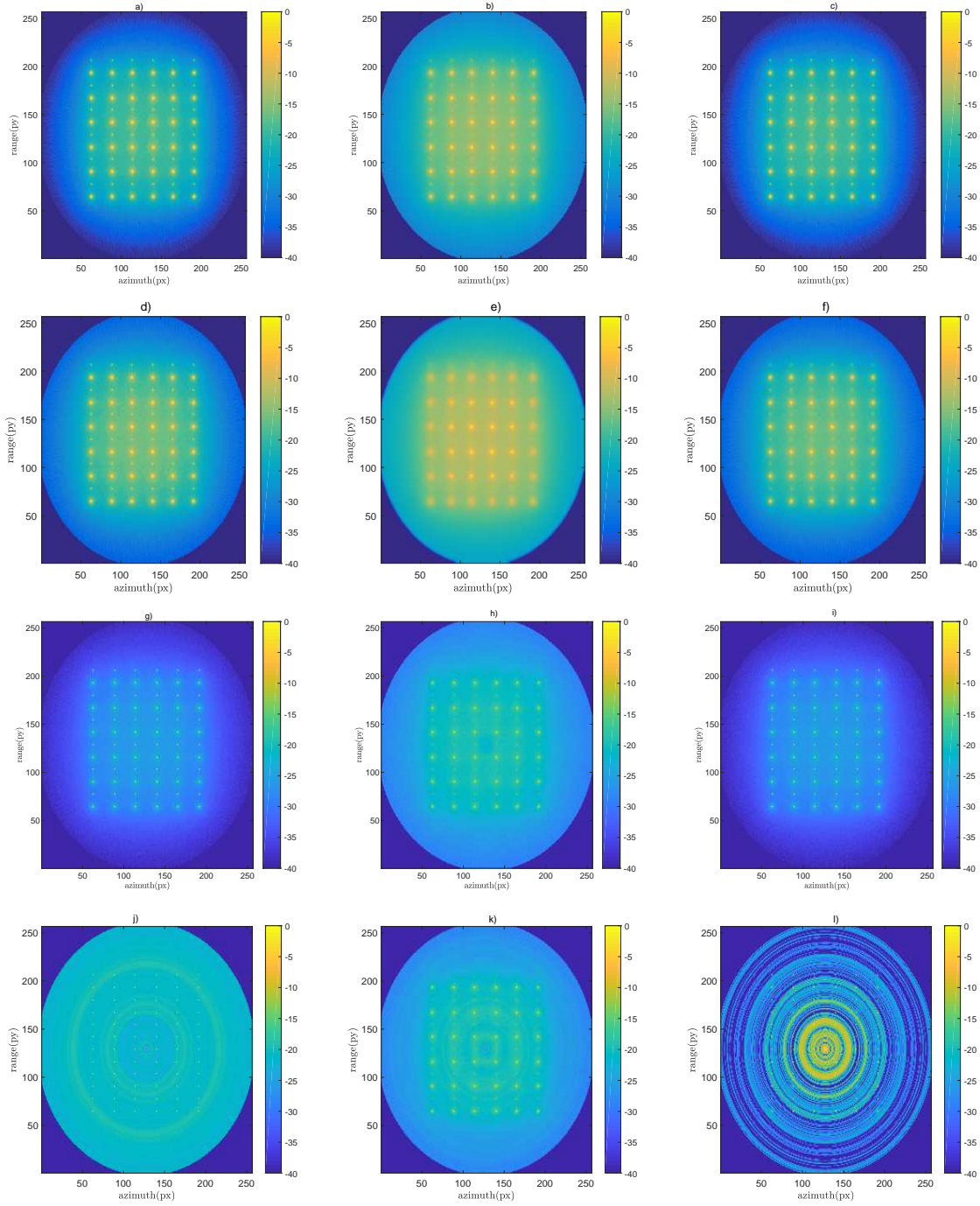
Figure 3.8: *Column 1: LFM-TCFDE, Column 2: MF-LFM, Column 3: LFM-NLFM. Scenario A: a-c, Scenario B: d-e, Scenario C: g-i,Scenario D: j-l. See Table 3.1 for Scenario definitions*
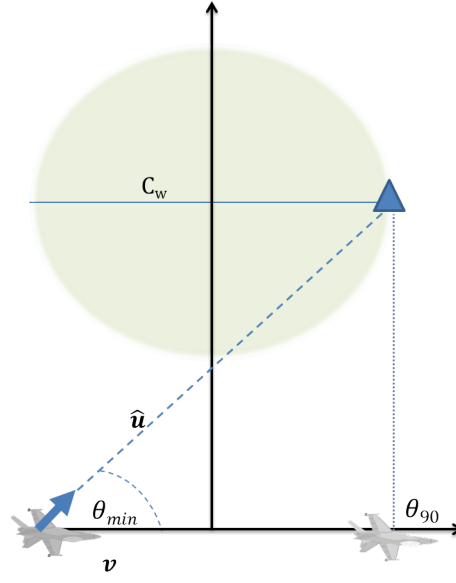
Figure 3.9: *Depiction of relevant vectors and scene scenario for Doppler shift in a SAR scenario*
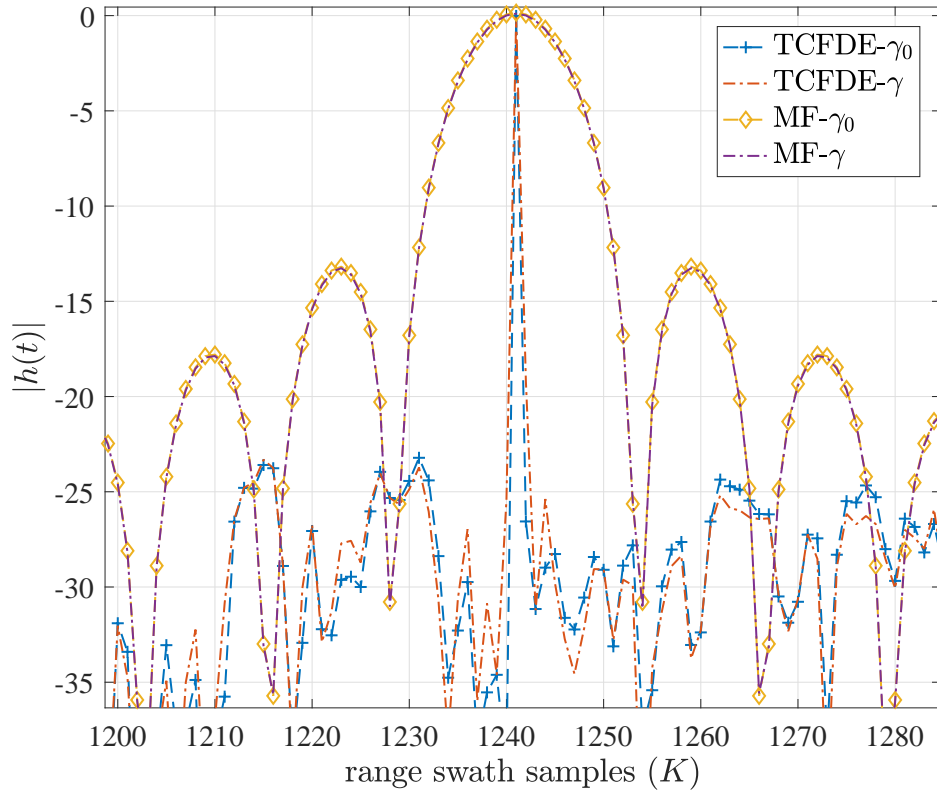
Figure 3.10: *Single point scatter for maximum and minimum Doppler stretch for specified scene, shown for both TCFDE and MF*
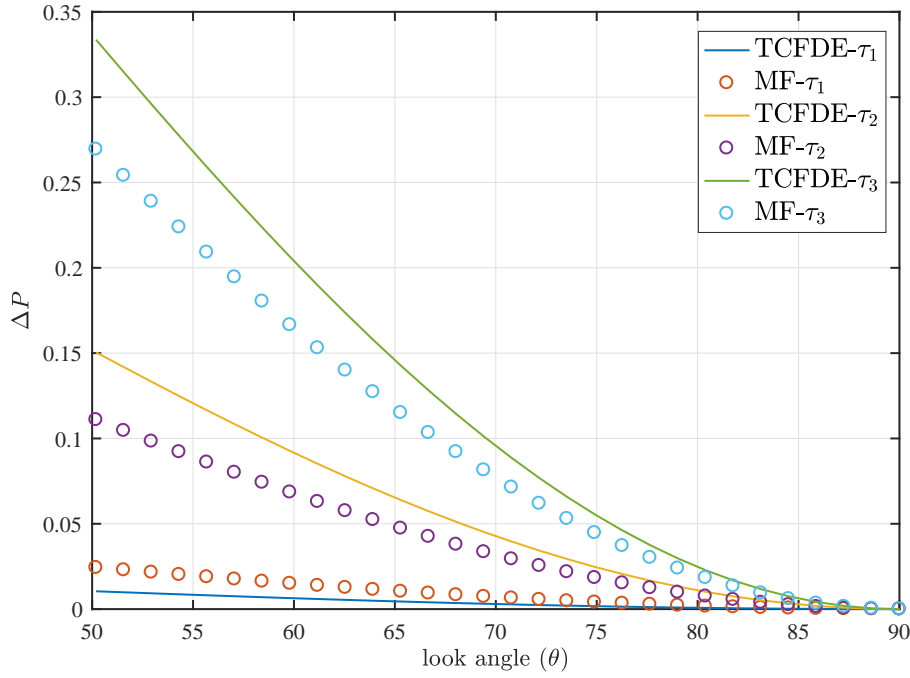
Figure 3.11: *Increasing times such that $\tau_1 = 0.25\tau_c$, $\tau_2 = 0.5\tau_c$, $\tau_3 = \tau_c$*

Simulation 1

The resultant shifted received signal is calculated according to (3.52) for the zero shift and maximum shift case. This is calculated for both MF-LFM and TCFDE-LFM. The received signal is passed to the range profile estimation algorithm and the result for the zero shift and maximum shift case are shown in Figure (3.10). There is a slight but non-significant difference between the maximum and minimum shifted range-profile estimations. This is slightly more prevalent for TCFDE. As a result, it can be concluded that the Doppler shift sensitivity of the TCFDE method for SAR is negliable compared to the MF and therefore will not have an impact on the performance of the technique.

Simulation 2

The performance is assessed here by comparing the zero shift estimate to the estimate at each successive angle, comparing like-for-like estimators to give a measure of the extent which the shift is affecting the MSE. The change in performance is calculated as

$$\Delta\rho = \text{tr}(\text{cov}(\hat{\mathbf{h}}_{\gamma_0} - \hat{\mathbf{h}}_\gamma)) = \mathbf{E}[(\hat{\mathbf{h}}_{\gamma_0} - \hat{\mathbf{h}}_\gamma)(\hat{\mathbf{h}}_{\gamma_0} - \hat{\mathbf{h}}_\gamma)^H] \tag{3.55}$$

where $\mathbf{h}_{\gamma_0}$ is the estimated range profile from the zero shift case and $\mathbf{h}_\gamma$ is range profile at each specific Doppler shift. For longer waveforms, there is a larger duration over which the shift occurs. Three LFM waveform durations were used to analyse the differences caused as a result of Doppler shift. The resulting performance shift over angle is demonstrated in Figure 3.11. For small waveform durations, TCFDE has less performance difference than the MF. For longer waveform durations, it is shown that MF has consistently less difference.

Overall, it can be concluded that for a moving platform in SAR the Doppler shift does not cause significant degradation to the TCFDE approach for range-profile estimation.

3.7 Chapter Conclusions

It has been demonstrated in this chapter that frequency-domain system identification methods are applicable for use in range-profile estimation in SAR. Similar to emerging high-resolution methods in OFDM-SAR it can provide an IRCI-free range profile exemplified in low sidelobes and fine resolution. As the TCFDE approach does not require use of a cyclic-prefix or a particular constraint in time in frequency, it is a suitable candidate to support waveform diversity. However, it is noted then the potential drawback lies in added distortion if a highly-shaped non-flat spectral waveform is used. This can be mitigated to some extent with the inbuilt noise suppression. It is noted that this performance degradation when using a spectrally shaped waveform is less than that seen in OFDM. For a scene size, the IRCI free estimation can offer a reduction in MSE error. MSE is a relative measure, and cannot directly give information alone, it can be compared against the other estimators to contrast the performances. The results from Scenario D suggest by using TCFDE for a large scene size (compared to pulse length) and where the SNR is 20dB, an improvement of 15dB in sidelobes can be made compared with MF, where instead of sidelobes, the restriction is the base noise level. However, an alternative and widely used method in combination with the MF is to apply windowing functions, which can also serve to dramatically reduce the sidelobe level. Comparions made here are for unwindowed MF.

Chapter 4
Spectrum Competitive Waveform Design

4.1 Introduction

Although waveform design has been applied to a range of radar scenarios, there has been little research towards adaptive SAR systems for interference mitigation. Current spectral waveform design methods for interference mitigation are generally aimed at other radar modes, such as detection [29]. As discussed in Chapter 3, waveform design is inexorably linked to the end purpose of the radar and its subsequent signal processing - a waveform optimal for detection will not necessarily be optimal for obtaining the best estimate of the range profile in SAR. As such, these methods do not perform well in SAR due to the creation of gaps in the spectrum which is detrimental to the imaging performance. By shaping the waveform to avoid the source of the interference, large gaps are created in the scene frequency response and raise the range sidelobes, as experienced in the earlier attempts to mitigate interference in SAR [3, 12, 73, 75]. Often neighboring RF signals can leak into the operational bandwidth of the radar or the radar can be affected by transmissions from an unlicensed user attempting to operate in the same bandwidth.

A SAR image is formed by obtaining the range profile of the desired scene from many successive angles, but the presence of RFI disrupts the quality of the range profile estimate. As each successive range-profile is altered due to the angle, it requires re-estimation. Given the ability to modify the spectral content of the waveform via adaptive waveform design, it is then desirable to obtain the best possible estimate of the scene in the presence of interference. This problem is set up as a system identification problem, motivated by modifying the waveform such that it attempts to estimate the range profile with the minimum mean square error criterion.

Particularly in a spectrally-crowded environment, there is no guarantee that external

RFI will be spectrally constant across the entire duration of operation. To address this, the adaptive waveform design solution will re-estimate the RFI spectrum at every received pulse - the smallest timeframe available to carry out this measurement. There is then a pulse-to-pulse dependance on the estimate of the RFI from the previous pulse which gives the most recent measurement. It then must be assumed that the RFI is spectrally constant within the window between estimating the RFI from the most recent returned signal and designing and transmitting the next waveform. In this work, it is also assumed that the RFI is entering the receiver as a direct signal and is not interacting with the terrain. Additionally, it is assumed that the RFI is correlated.In this Chapter a computationally efficient system-identification/waveform-design scheme for mitigating RFI in SAR on a pulse-to-pulse basis is presented. No prior knowledge of the RFI is required. The main contributions of this Chapter are:

- Joint range-profile/interference-spectrum estimation. Range-profile estimation, set up as a classical system identification problem in Chapter 3, is expanded to address interference estimation. Through this formulation, the optimal solution is identified as the generalized least squares (GLS) problem with a well defined Cramer Rao lower bound (CRLB) [99]. By extending concepts from frequency domain adaptive filtering [100], an approximation to the GLS estimator that is based on the fast-Fourier transform (FFT) is developed. This approximation is free from inter-range-cell interference and, significantly, also provides an estimate of the interference spectrum on-the-fly.

- Adaptive waveform design. A similar frequency domain approximation to the CRLB is developed. This approximate CRLB is optimized with respect to the spectrum of the transmitted signal given the usual energy constraint on the waveform. This leads to a simple closed form solution that we prove is the global minimum for the approximate CRLB (given the energy constraint).

- Computationally efficient combined estimation/design/synthesis. To illustrate the potential of the above they are combined with a waveform-synthesis technique for nonlinear linear frequency modulation (NLFM) based on the stationary phase approximation (SPA) [33]. This synthesis methodology is considered because: i) its computational complexity is similar to what is proposed above; (ii) NLFM meets the constant amplitude waveform constraint required for many practical

systems and only requires phase shifters rather than time delays in electronically steered systems. It is noted however that the techniques mentioned above are not restricted to this form of synthesis or to NLFM. It is shown that the combined system has complexity of $O(M \log_2(M))$ per transmitted pulse, where M is the sum of range extent and transmit signal length in samples.

4.2 System Model & Problem Formulation

The following section presents the adaptive waveform design framework for interference mitigation in SAR. The problem formulation for the time domain is given and is followed by the newly proposed frequency domain system identification modified for added interference.

4.2.1 System Framework

The system block diagram shown in Figure 4.1 operates as per Algorithm 1 where p is the current pulse number in a coherent burst of P consecutive pulses. Steps 2 to 6 of the Algorithm describe the operations in the main blocks of Fig. 2, starting in the top left hand corner and moving clockwise round the diagram.

Algorithm 1 Adaptive Waveform Design Scheme

Initialize: first pulse x_1 as LFM
1: **for** $p = 1 : P$ **do**
2:    Transmit pulse $\mathbf{x}_p$.
3:    System identification: the transmitted pulse and the associated received signal $\mathbf{y}$ are used to estimate the impulse response $\mathbf{h}_p$ of the SAR scene and interference $\hat{\mathbf{N}}$ at the pth position of the radar.
4:    Interference spectrum estimate; formed from the interference estimate.
5:    Transmit waveform optimization: optimize transmit spectrum using estimate of interference spectrum.
6:    Stationary phase waveform design: transmit spectrum is used to synthesize the next NLFM transmit pulse $\mathbf{x}_{p+1}$.
7: **end for**
8: Pass the collection of P impulse responses $\{h_p\}_{p=1}^{P}$ to the SAR image formation algorithm.

In the adaptive system shown in Figure4.1 the first transmitted pulse is used to obtain an estimate of the interference frequency profile $\hat{\mathbf{N}}$ and a scene estimate $\hat{\mathbf{h}}_1$. The first step

on waveform transmission is the waveform interaction with the scene (impulse response) and the interference plus noise - the received signal $\mathbf{y}$ is then a superposition of both of these signals. The least-squares system identification uses both the transmitted signal and the received radar signal (with RFI) as an input. The LS system identification aims to estimate the impulse response $\hat{\mathbf{h}}$. The resultant error from this estimation process is the RFI spectrum $\hat{\mathbf{N}}$. This error is then smoothed to produce an interference spectral estimate which is used to aid the design of the next transmitted waveform. The spectrum of the waveform is then passed to the stationary phase waveform synthesis to produce a time domain signal.

An LFM signal is used to start the process as is it nearly spectrally flat and aids the initial system identification calculation to estimate the interference spectrum by placing energy across the entire band. If there is no correlated noise present, the flat spectrum is optimal for the impulse response estimation. In correlated noise this first LFM pulse is expected to perform sub-optimally as it is not yet shaped according to the interference as this is initially assumed to be unknown. This method simultaneously obtains interference and scene data on the same pulse, which if successful, is an advantage compared to passive approaches that do not collect scene data while collecting interference data. This first LFM pulse then allows an estimate of the RFI spectrum and subsequently enables the design of the next NLFM pulse to obtain an enhanced estimate by shaping the spectrum of the waveform. To allow full use of the synthetic aperture, all pulses are used to form the image.

4.2.2 Time Domain Problem Formulation

Following from the TCFDE framework introduced in Chapter 3, here the estimation of the range profile is again expressed as a discrete time problem, recalling the expression given in 3.39

$$\mathbf{y} = \mathbf{Xh} + \mathbf{n}$$

where $\mathbf{X}$ is a $(N + K - 1) \times K$ rectangular and Toeplitz matrix where columns contain time shifted versions of the transmitted signal $\mathbf{x}_p$. Because it is assumed that the impulse response is finite and all the collected returns from the transmitted signal, equation (3.39) defines $N + K - 1$ equations in K unknowns and is thus an overdetermined system. The noise plus interference $\mathbf{n}$ is an $[N + K - 1]$ dimensional vector
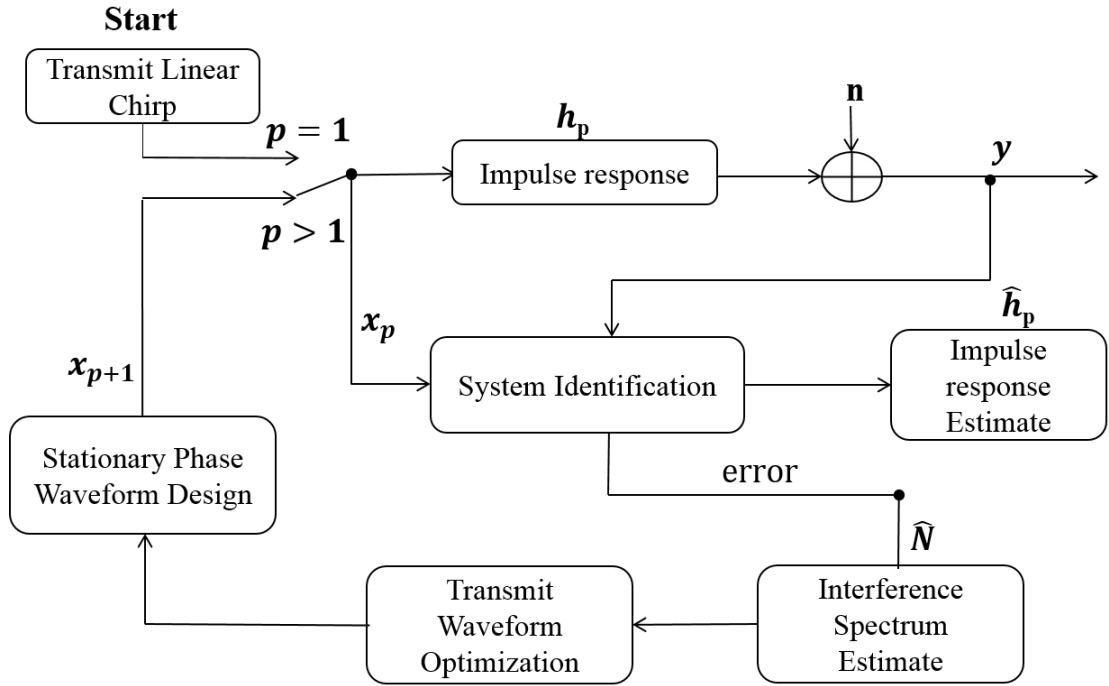
Figure 4.1: *Pulse-to-pulse system flow chart.*

with co-variance matrix $\mathbf{R}_{nn} = E[\mathbf{n}\mathbf{n}^H]$ and the interference is assumed to exist within the same bandwidth as the transmitted signal. Chapter 3 considered the case where there was no interference and the covariance matrix was reduced to a diagonal of the variances $\mathbf{R}_{nn} = \sigma_n^2\mathbf{I}$ giving the ordinary least squares (OLS) estimator, giving the following expression for the impulse response

$$\hat{\mathbf{h}} = (\mathbf{X}^H\mathbf{X})^{-1}\mathbf{X}^H\mathbf{y} \qquad (4.1)$$

The covariance matrix now requires use of the generalized least squares (GLS) expression [97]

$$\hat{\mathbf{h}} = (\mathbf{X}^H\mathbf{R}_{nn}^{-1}\mathbf{X})^{-1}\mathbf{X}^H\mathbf{R}_{nn}^{-1}\mathbf{y} \qquad (4.2)$$

Using the estimator for the GLS problem directly is computationally expensive and furthermore, initially, the interference covariance is unknown. Generalized least squares is equivalent to applying ordinary least squares to a whitened version of the system [97]. It is then possible that if the spectra for the transmit signal is matched to the interference, that the ordinary least squares solution can be used by "whitening" the system. The following work in this Chapter seeks a more formal solution. Waveform

design is employed to achieve the optimal estimation of the scene impulse response in the presence of correlated interference according to the least-squares solution. Waveform design for the optimal least squares solution should try to minimize the error to find the best fit for $\hat{\mathbf{h}}$. The Cramer-Rao lower bound (CRLB) for the generalized least squares estimate of the impulse response vector is given by the spread of the covariances [97]

$$\text{cov}(\mathbf{h} - \hat{\mathbf{h}}) = E[(\mathbf{h} - \hat{\mathbf{h}})(\mathbf{h} - \hat{\mathbf{h}})^H] = (\mathbf{X}^H \mathbf{R}_{nn}^{-1} \mathbf{X})^{-1} \tag{4.3}$$

Using the CRLB as a criteria for optimization, waveform design for SAR system identification in the presence of interference can be formulated as the following constrained optimization problem

$$\begin{aligned} &\min_{\mathbf{x}} \quad \text{tr}(\mathbf{X}^H \mathbf{R}_{nn}^{-1} \mathbf{X})^{-1} \\ &\text{s.t.} \quad \mathbf{x}^H \mathbf{x} = E_T \end{aligned} \tag{4.4}$$

where E_T is the energy in the transmitted signal. There does not appear to be an existing analytical method to solve this expression. A possible numerical optimization procedure is particle swarm optimization (PSO), a global optimization technique [101]. This can be applied to the optimization problem to find the best overall waveform under the constraint of energy. As it is an iterative method PSO potentially requires a large number of computations to find the solution - especially as matrix inversion is required on each iteration. We propose a more computationally efficient approach to estimating the impulse response by factorizing with the DFT and expressing the problem in the frequency domain. The following steps aim to approximate the CRLB of (4.3) to facilitate a tractable analytic solution that is computationally efficient. However we use (4.4) and its solution through PSO, as a benchmark to quantify the performance loss incurred by the approximation.

4.2.3 Frequency Domain Solution

The following frequency domain solution expands on the TCFDE method for estimating the impulse response in order to design the waveform. Applying Fourier transforms to both sides of time-domain circulant matrix equation and using the identity property,

where $\mathbf{F}$ is an $[N + K - 1]$-point discrete Fourier transform gives

$$\mathbf{Fy} = \mathbf{F}\mathbf{X}_c\mathbf{F}^H\mathbf{F}\begin{bmatrix} \mathbf{h} \\ \mathbf{0}_N \end{bmatrix} + \mathbf{Fn} \tag{4.5}$$

Now the expression for circulant-Toeplitz matrices given in (3.43) can replace $\mathbf{X_c}$ and again using the identity property gives

$$\mathbf{Y} = \mathbf{\Omega}\mathbf{H} + \mathbf{N} \tag{4.6}$$

where $\mathbf{\Omega} = \mathbf{F}\mathbf{X_c}\mathbf{F}^H = \mathrm{diag}\{\mathbf{Fx}_1\}$, $\mathbf{Y} = \mathbf{Fy}, \mathbf{H} = \mathbf{F}\begin{bmatrix} \mathbf{h} \\ \mathbf{0}_N \end{bmatrix}$ and $\mathbf{N} = \mathbf{Fn}$, where each of the vectors listed are of dimension $M \times 1$. Given an expression of the system model in the frequency domain, a corresponding generalized least squares estimate for $\mathbf{H}$

$$\hat{\mathbf{H}} = (\mathbf{\Omega}^H\mathbf{D}^{-1}\mathbf{\Omega})^{-1}\mathbf{\Omega}^H\mathbf{D}^{-1}\mathbf{Y} \tag{4.7}$$

where

$$E[\mathbf{N}\mathbf{N}^H] = \mathbf{F}\mathbf{R}_{nn}\mathbf{F}^H = \mathbf{D} \tag{4.8}$$

The noise-covariance matrix $\mathbf{R_{nn}}$ is positive definite as there will always be some level of background white noise due to the presence of thermal noise in the receiver. The eigen-decomposition can be written as

$$\mathbf{R_{nn}} = \mathbf{V}\mathbf{\Lambda}\mathbf{V}^H$$

where Λ is a diagonal matrix of the eigenvalues and $\mathbf{V}$ is the orthonormal matrix such that $\mathbf{V}^H\mathbf{V} = \mathbf{I}$ whose columns are the corresponding eigenvectors. The eigenvectors also define the Karhunen-Loeve transform(KLT) of the noise vector $\mathbf{V^H n}$ .The elements of $\mathbf{V}^H n$ are orthogonal and therefore uncorrelated since

$$E[\mathbf{V}^H\mathbf{n}\mathbf{n}^H\mathbf{V}] = \mathbf{V}^H\mathbf{R}_{nn}\mathbf{V} = \mathbf{V}^H\mathbf{V}\mathbf{\Lambda}\mathbf{V^H}\mathbf{V} = \mathbf{\Lambda}$$

The KLT has history of being approximated by signal-independent transforms such as the DFT and the discrete cosine transforms due to its complexity. This approximation of the DFT to the KLT has lead to the DFT being used to approximately orthogonalize

signals. The justification for this was initially used in Markov-1 processes [102]. Examples can be found in the fields of frequency-domain adaptive filtering [72, 100] and in radar, where the frequency snapshot model uses the orthogonalization assumption [103] and also in [29] to justify use of the frequency domain to avoid a matrix inversion.

Assuming that now, due to the application of the DFT, the frequency domain samples are uncorrelated, the off-diagonal elements of the frequency domain interference covariance matrix $\mathbf{D}$ will be approximately zero and are disregarded allowing a vector expression $\tilde{\mathbf{D}}$ to be formed from the diagonal replacing $\mathbf{D}$ in (4.7).

$$\tilde{\mathbf{D}} = \text{diag}(\mathbf{D})$$

This provides a simple estimate in the frequency domain which is element wise. With this approximation we have what might be called a "doubly-diagonal" system, both the input signal matrix Ω and the noise covariance matrix $\tilde{D}$ are diagonal. The GLS of (4.7) reduces to OLS with the added benefit that we do not require knowledge to $\tilde{D}$ to form the estimate.

$$\hat{H}_i = \frac{Y_i}{\Omega_i} \qquad i = (1, 2, \cdots, M) \tag{4.9}$$

$$\hat{\mathbf{h}}_c = [\ \mathbf{I}_K \quad \mathbf{0}_{N-1,K}^T \ ] \mathbf{F}^{-1} \hat{\mathbf{H}} \tag{4.10}$$

where $\mathbf{I}_K$ is an $K \times K$ identity matrix. This works best when $N > K$, as noise removal performance is proportional to the number of samples N removed. This effect on performance is demonstrated in section 4.5.3. The corresponding estimate of the time-constrained frequency response is then:

$$\hat{\mathbf{H}}_c = \mathbf{F}\left(\begin{bmatrix} \hat{\mathbf{h}}_c \\ \mathbf{0}_{N-1} \end{bmatrix} \right) \tag{4.11}$$

Finally, using the constrained frequency response estimate, an estimate $\hat{\mathbf{N}}$ of the interference $\mathbf{N}$ is provided

$$\hat{\mathbf{N}} = \mathbf{Y} - \Omega \hat{\mathbf{H}}_c \tag{4.12}$$

and from which an estimate of the interference spectrum $\tilde{\mathbf{D}}$ can be formed in a straightforward way, $\tilde{\mathbf{D}} = \mathbf{g}(|\hat{N}_i|^2)$, where $\mathbf{g}$ is a moving average filter which is applied to

smooth the spectral estimate.The unfiltered spectral estimate $\mathbf{D} = |N_i|^2|$ may exhibit large sample to sample fluctuations as this estimate results from a single realization of the spectrum. Thus, directly using this spectral estimate would also yield a waveform that is high in sample-to-sample fluctuation and may not provide a good representation of the true spectral distribution.

The TCFDE of (4.9),(4.10) and (4.11) provide an approximation to the GLS of (4.2) that is DFT based. This approach is more computationally efficient than the direct GLS estimator. Using the TCFDE is thus better suited to the relatively long impulse responses that are typical in SAR, as larger DFT dimensions scale better computationally than matrix inversions. In addition the TCFDE does not require explicit knowledge of the interference covariance matrix $\mathbf{R}_{nn}$ and provides a mechanism through (4.11) to estimate the spectrum of that interference "on-the-fly". The latter capability facilitates adaptive waveform design.

4.3 Waveform Optimization

We now have three possible estimators for the impulse/frequency response. Equation (4.2) provides the optimal solution if the interference covariance matrix is known. Its performance is given by (4.3). The unconstrained frequency domain estimate of (4.9) is the simplest computationally but it is liable to give poor performance as it has no capacity for noise reduction and it approximates linear convolution with circular convolution. The constrained frequency domain estimate of (4.9),(4.10), and (4.11) is an improvement on (4.9) because it enforces linear convolution and reduces noise through (4.10) and (4.11). The performance of this constrained frequency domain estimate are explored further in [104]. Central to many adaptive waveform design (AWD) methods is the judicious choice of a cost function. Ideally we would like to use a cost function that accurately reflects the performance of the radar, e.g. (4.3). However, if we chose to implement (4.2), the optimization of (4.4) is a still a major challenge. Often a cost function is chosen that is an approximation to or a bound on the actual performance metric because no convenient closed form solution for the metric exists. For example, in AWD for detection [36], the asymptotic performance is used as a cost function because no closed form solution for the detector performance on finite data sets exists. Similarly, in bearing estimation [105], the CRLB is used even

through the estimator does not achieve that bound. Again no closed form expression for the performance of the estimator exists. Thus while we advocate the use of the constrained estimate of (4.9) ,(4.10), & ((4.11)) for estimating the impulse response, we use the unconstrained estimate of (4.9) to provide a simple cost function for the waveform design that leads to a closed form expression for the transmitted spectrum in terms of the spectrum of the interference. As argued earlier the performance of the unconstrained estimate is poorer than the constrained one and thus we are optimizing an upper bound on the performance of the constrained estimate. Start by assuming that (4.6)-(4.8) are an accurate representation of the estimation problem. If this was the case the performance ρ of the estimate (4.11) would be given by:

$$\text{cov}(\mathbf{H} - \hat{\mathbf{H}}) = E[(\mathbf{H} - \hat{\mathbf{H}})(\mathbf{H} - \hat{\mathbf{H}})] = (\mathbf{\Omega}^H \mathbf{D}^{-1} \mathbf{\Omega})^{-1} \tag{4.13}$$

This can be reduced into a single value to quantify the performance by using the trace of the covariance matrix.

$$\rho \triangleq \text{tr}((\mathbf{\Omega}^H \mathbf{D}^{-1} \mathbf{\Omega})^{-1}) = \sum_{i=0}^{M-1} \frac{D_i}{|\Omega_i|^2} \tag{4.14}$$

As in (4.4), the performance of the estimation is limited by the total energy in the transmitted signal such that in discrete time, using Parseval's theorem is given as follows.

$$E_T = \sum_{i=0}^{M} |\Omega_i|^2 = \sum_{k=0}^{N-1} |x_i|^2 \tag{4.15}$$

We seek to minimize the performance metric ρ and hence optimize the performance of the system identification subject to the energy constraint of (4.15). The optimization problem for the frequency domain estimator can be expressed as follows

$$\min_{\mathbf{\Omega}} \quad \sum_{i=0}^{M-1} \frac{D_i}{|\Omega_i|^2}$$
$$\text{s.t.} \quad \mathbf{\Omega}^H \mathbf{\Omega} = E_T \tag{4.16}$$

For ease of notation we define the energy at each frequency sample as

$$E_i = |\Omega_i|^2 \tag{4.17}$$

In a similar manner to [29] we incorporate the constraint by defining a Lagrangian, where we define $f(\mathbf{E}) = \sum_i \frac{D_i}{E_i}$, $g(\mathbf{E}) = \sum_i E_i$

$$
\begin{aligned}
\min_{\mathbf{E}} \quad & f(\mathbf{E}) \\
\text{s.t.} \quad & g(\mathbf{E}) - C = 0 \quad (E_i > 0, \forall i)
\end{aligned}
\tag{4.18}
$$

Due to the energy being a non-negative value, this necessitates the presence of inequality constraints which would normally require application of Karush-Kuhn-Tucker(KKT) conditions. In this case, the inequality is a simple example. In its place, therefore, the problem is approached here by first solving the optimization problem without the inequality constraints using the Lagrangian, then proceeding to identify all possible solutions and show that only one of these solutions satisfies the inequality constraints and that it is a minimum. Proceeding without the inequality restraint, a Lagrangian solution is feasible because there is a single equality constraint and the gradient of $\mathbf{g}(E)$ is a non-zero constant, such that the constraint will always be enforced. Defining the Lagrangian function as

$$
L(\mathbf{E}, \lambda) = f(\mathbf{E}) + \lambda(g(\mathbf{E}) - C)
\tag{4.19}
$$

Necessary conditions for a solution are obtained by setting the partial derivatives of $L(\mathbf{E}, \lambda)$ with respect to each of the elements of $\mathbf{E}$ to zero

$$
\nabla_E f(\mathbf{E}) + \lambda \nabla_E g(\mathbf{E}) = \mathbf{0}_N
\tag{4.20}
$$

$$
\frac{\partial L}{\partial E_i} = -\frac{D_i}{E_i^2} + \lambda = 0
\tag{4.21}
$$

$$
\lambda = \frac{D_i}{E_i^2}, \quad \forall i
\tag{4.22}
$$

Since both $D_i > 0$ and $E_i > 0 \quad \forall i$, then $\lambda > 0$

$$
E_i = \pm\sqrt{\frac{D_i}{\lambda}} = \frac{\pm\sqrt{D_i}}{\sqrt{\lambda}}
\tag{4.23}
$$

Now applying the energy equality, where $C = E_T$

$$
E_i = E_T \frac{\pm\sqrt{D_i}}{\sum_i \pm\sqrt{D_i}}
\tag{4.24}
$$
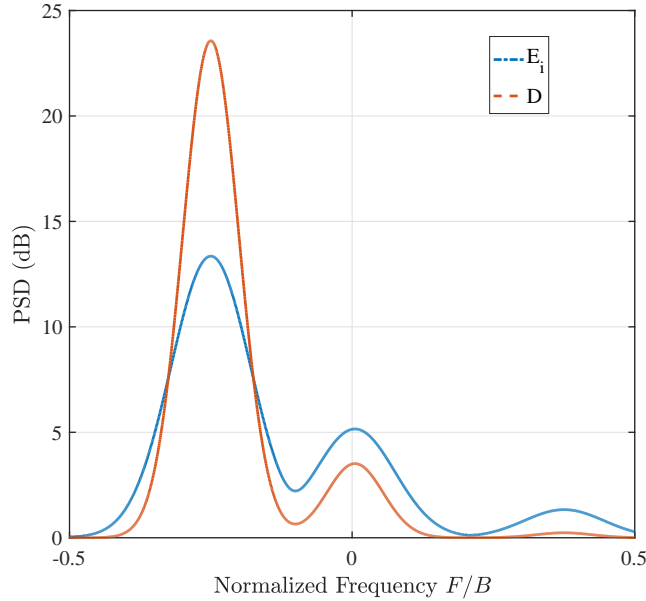
Figure 4.2: *Illustrative example demonstrating signal energy outcome from (4.25) is proportional to the interference energy.*

There is then 2^N possible solutions dependent on the choice of sign on the square root of each D_i. Consistently choosing either all positive or all negative roots, the solutions are then, in both cases

$$E_i = E_T \frac{\sqrt{D_i}}{\sum_i \sqrt{D_i}} \tag{4.25}$$

This solution then satisfies the non-negative energy constraint and the remaining solutions all contain both positive and negative choices for the square roots of each D_i. Which finally gives an expression for the transmitted signal energy distribution which optimizes the frequency domain least-squares problem. The sufficiency conditions are shown in Appendix A. For brevity we will call (4.25) frequency domain waveform optimization (FDWO).While the development here is similar to [29], the result is distinctly different. In [29] a detection problem is addressed whereas here we address system identification problem. Thus it is not surprising that the results might be different and it is interesting to note that there is no sense of "water-filling" here or conclusion that signal energy should be directed to areas of the spectrum where the interference density is relatively low as in [29]. Rather (4.25) suggests a more competitive approach. An example signal outcome **E** for a given interference energy **D** is shown in Figure 4.2.

4.4   Waveform Synthesis

The previous section has determined the energy distribution across the frequency band. The following describes a possible method of synthesizing a time domain signal according to the spectrum described in (4.25). We desire a chirp based signal with constant amplitude modulus and spectrum distribution. The stationary phase approximation (SPA), a standard technique used for synthesis of nonlinear FM waveforms [1], provides synthesis according to these criteria. The synthesis technique detailed here is independent from the TCFDE scheme. If desired alternative waveform synthesis techniques can be used in conjunction with the TCFDE scheme, provided that they synthesize a signal with the desired frequency spectrum e.g. using OFDM techniques or non-chirp based methods.

4.4.1   SPA Background

SPA relies on the assumption that amplitude variations are very slow compared to phase variations, which results in most of the energy becoming concentrated around stationary points. Applying a Fourier Transform to a general chirp signal with amplitude and phase variation creates the following intractable integral

$$X(f) = \int_{-\infty}^{\infty} a(t)e^{j\phi(t)}e^{-j2\pi ft}dt = \int_{-\infty}^{\infty} a(t)e^{j\psi(t)}dt \tag{4.26}$$

where $\phi(t)$ is waveform phase, $\psi(t)$ is a phasor term and $a(t)$ is amplitude. A large majority of the contribution to the Fourier spectrum occurs where the change of oscillation of the function is at its lowest, a stationary point, this can be exploited to calculate an approximation to the integral. SPA requires the frequency to be monotonic which allows there to be only 1 stationary point and the solution is then

$$\dot{\psi}(t) = \dot{\phi}(t) - 2\pi f = 0 \tag{4.27}$$

and thereby a relationship between t and f is given simply as

$$\dot{\phi}(t) = 2\pi f \tag{4.28}$$

This occurs when the frequency is monotonically increasing and the amplitude variations are much slower than the phasor variations, such that

$$\frac{|\dot{a}(t)|}{a(t)} \ll |\dot{\psi}(t)| \tag{4.29}$$

When the amplitude variations are very slow compared to the phase variations, integrating over the majority of the time axis will represent integrating a constant amplitude phasor. The integral of one period of a phasor is zero if the instantaneous phasor frequency $\dot{\psi}$ is not zero. This is applicable to the chirp waveform as across the time axis of the waveform, the amplitude is constant except from switch-on and switch-off. Provided that the signal has constant amplitude, the following expression can be used to relate the phase and the spectrum [1],

$$\ddot{\phi}(t) = \frac{a^2(t)}{\mathbf{E}(f)} = \frac{C}{\mathbf{E}(f)} \tag{4.30}$$

where C is a constant. For a given signal the energy is automatically constrained under the time integration limits and across the bandwidth in frequency. The average chirp rate is $\gamma = \frac{B_n}{t_1 - t_0}$, where B_n is nominal bandwidth and t_0 and t_1 are times at the start and end of the sweep respectively.For ease of notation we describe the process in continuous time. The energy of the transmitted chirp waveform is defined as

$$E_T = \int_{-\infty}^{\infty} |x(t)|^2 dt = \int_{t_0}^{t_1} |\exp\{j\phi(t)\}|^2 dt \tag{4.31}$$

Then using Parseval's theorem the total energy expression can be related to the chirp spectrum:

$$E_T = \int_{-\infty}^{\infty} \mathbf{E}(f) dF = t_1 - t_0 = \frac{B_n}{\gamma} \tag{4.32}$$

Which satisfies that the signal has finite energy for a fixed time duration $t_1 - t_0$ which is the area under $\mathbf{E}(f)$.
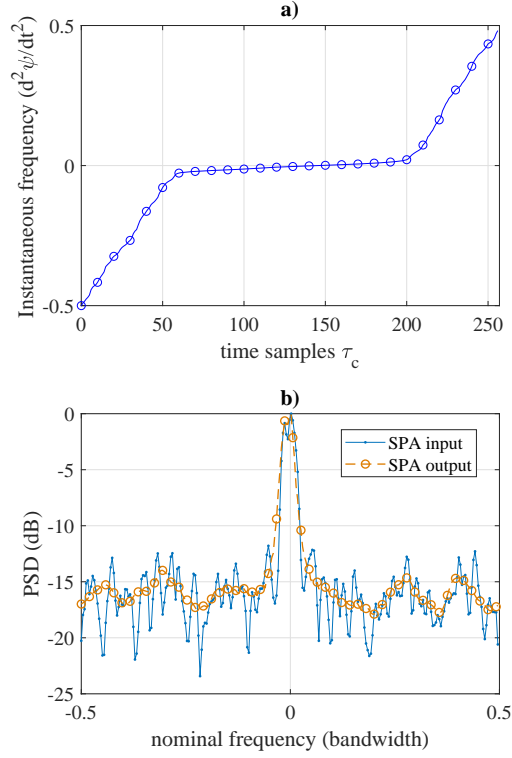
Figure 4.3: *a): Input spectrum given by* $\mathbf{E}(f)$ *(blue) and resultant transmit spectrum given by SPA. b): Synthesized transmit signal. Non-linear upward sweep in instantaneous frequency gives non-linear "chirp" waveform.*

4.4.2 Implementation

The following steps demonstrate how to synthesize a discrete time waveform given a desired spectrum while constraining the finite waveform energy over the radar waveform bandwidth using the SPA. The energy of the transmitted chirp waveform as defined in the time domain was given in (4.15). Now using total energy expression in 4.32 can be re-expressed in discrete format as:

$$E_T = \sum_i^M \mathbf{E}(i) = \{t_1 - t_0\} = \frac{B_n}{\gamma} \tag{4.33}$$

which again satisfies that the signal has finite energy for a fixed time duration $t_1 - t_0$, the area under $\mathbf{E}(f)$. Using this relationship, the total energy in the time domain can

be mapped onto the frequency domain using the following steps, allowing a desired spectrum to be synthesized with continually increasing phase and constant modulus amplitude as given by (4.30).

The algorithm table below and the corresponding Figure 4.4 describe the discrete SPA implemenation steps.

These expressions allow synthesis of a NLFM waveform according to a desired spectrum $E(f)$ by continually increasing the phase. As demonstrated in Figure 4.3 the output spectrum is an approximation to the input spectrum as provided by $E(f)$. While this method is not exact, it is a computationally simple approach for waveform synthesis compared to more precise but computationally complex methods demonstrated in the literature. Furthermore, a precise replication of the input spectrum may not be required as $E(f)$ is calculated based on an estimate of the interference $D(f)$ provided by the system identification on the prior pulse. By approximating to the spectrum of the interference, small errors in the interference estimate are not further propagated into the performance of the system identification of the current pulse. The spectral estimate is likely noise after a single realization, therefore the input spectrum to the SPA $E(f)$ is passed through a moving average filter to smooth out the spectrum so as not to force the SPA to follow the sharp sample-to-sample deviations.

Algorithm 2 SPA Implementation

1: Perform discrete integration of the desired spectrum $E(f)$ shown in Figure 4.4 a using a cumulative sum to generate corresponding energy values in the time domain, which are represented by time vector $t_f(i)$:

$$t_f(1) = E(1)$$

$$t_f(2) = E(1) + E(2)$$

$$t_f(i) = E(1) + \cdots + E(i-1) + E(i) \tag{4.34}$$

These values are irregularly spaced across the time domain, as they are dictated by $E(i)$, and span $t_f(i) = (1, \cdots, N)$. Parseval's rule is now applied to normalize the total energy to maintain equal energy in the time and frequency domains. The resultant values are shown in Figure 4.4 b.

2: Generate a regularly spaced frequency axis to represent the frequency domain points of interest across the desired bandwidth B_n such that

$$f_F = (1, \cdots, M) \tag{4.35}$$

where $f_F(1) = -\frac{B_n}{2}$ and $f_f(M) = \frac{B_n}{2}$. Using the SPA relationship given in (4.30), f_F can be mapped to t_F, such that the instantaneous frequency at time $t_F(i)$ is given by $f_F(i)$. f_F forms the y-axis values shown in Figure 4.4 c and t_F are the x-axis values.

3: Generate a regularly spaced time axis corresponding to the desired points in time for waveform synthesis

$$t_T = (1, \cdots, N) \tag{4.36}$$

4: Using the mapping between the irregularly spaced time-energy vector t_f and the regularly spaced vector in frequency, f_f, interpolate to obtain the desired frequency values f_T at the desired waveform synthesis time-domain points given by t_T. This forms the desired interpolation points and the x-axis point shown for the interpolated data in Figure 4.4 d.

5: The phase of the desired waveform can now be calculated from the interpolated frequencies f_T

$$\psi(i) = 2\pi \sum_i^N f_T(i) \tag{4.37}$$

6: Finally use the phase to synthesize the desired waveform via

$$x(i) = \exp\{j\phi(i)\} \tag{4.38}$$

The real component of the synthesized waveform is shown in Figure 4.4 e and the resultant output spectrum in Figure 4.4 f.
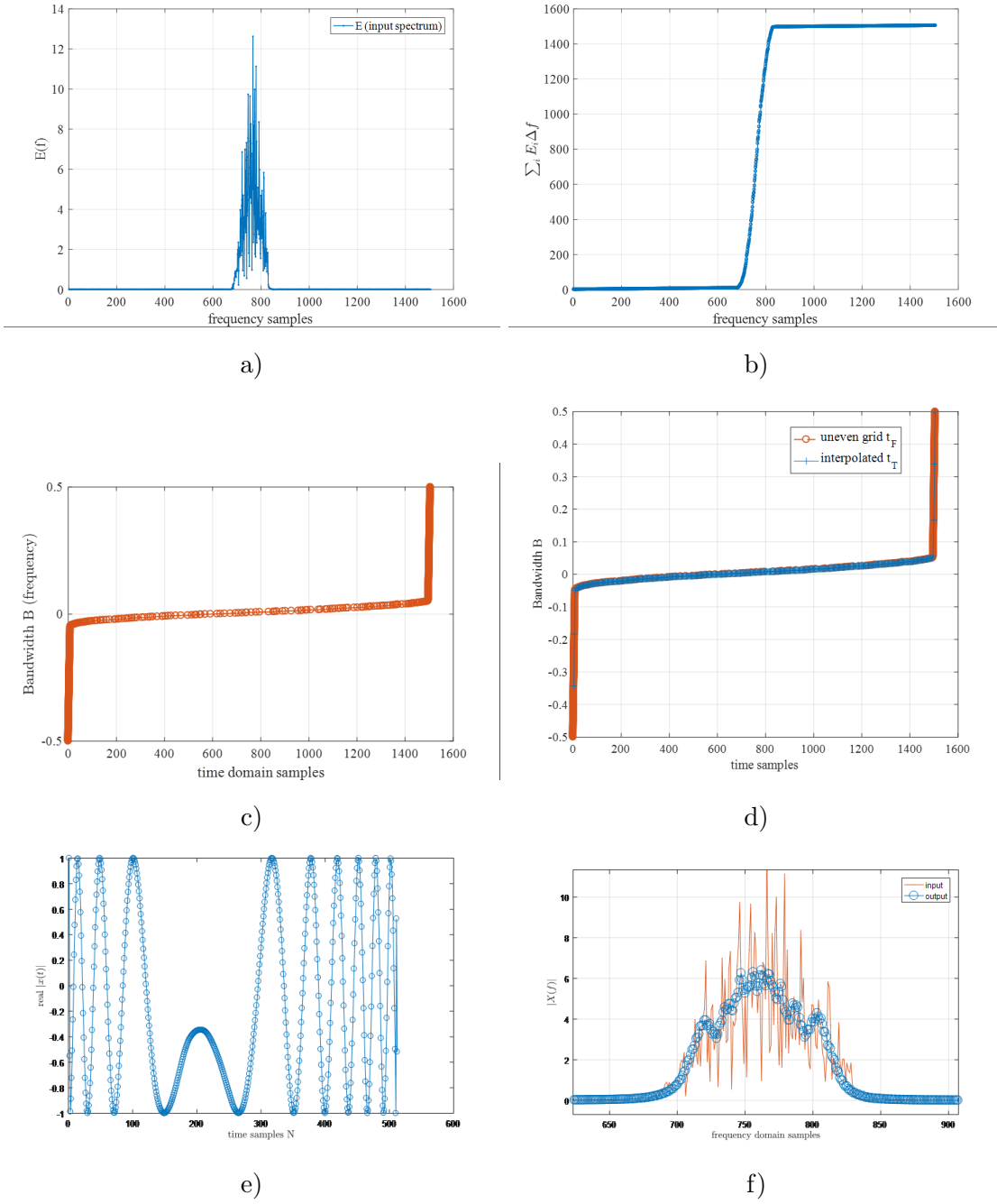
Figure 4.4: *SPA Implementation process: a)Input spectrum b) Cumulative sum of spectral energy c) Energy projected onto time domain d) Interpolation to obtain values of frequency at desired time samples e) Real component of new synthesized waveform f) Input(desired) and output (synthesized) SPA spectrum*

4.5 Performance Evaluation

4.5.1 Simulation Experiment Set-Up

The following section demonstrates the performance of the TCFDE technique combined with the waveform optimization and design method in terms of the error in the impulse response estimate. This method has been tested using random complex impulse response values so as to demonstrate that the results are not dependent on a particular scattering distribution. Additionally this section aims to evaluate the associated loss in performance that is introduced in the development of the alternative frequency domain estimate, the TCFDE, which approximates the direct estimator (4.3). The assumed knowledge to perform the simulations is as follows; the transmitted signal and its spectral representation, the received signal and the length of the range-swath, which corresponds to the impulse response length K. The known frequency domain representations of the received and transmitted signal, $\mathbf{Y}$ and $\mathbf{\Omega}$ are processed according to steps (4.11)-(4.10), to provide an estimate of the impulse response $\hat{\mathbf{h}}$. The norm of the simulated impulse response vector $\mathbf{h}$ is normalised to unity such that $\sum_{k=0}^{K-1} |h_p(k)|^2 = 1$. Narrowband interference is generated by constructing uncorrelated complex normal samples of length M then passed through a band-pass filter to create correlated interference samples so that the interference lies within 10% of the overall signal bandwidth. The impulse response estimate $\hat{\mathbf{h}}$ is evaluated and 1000 trials are executed at each configuration. The energy in each transmit signal and the total nominal bandwidth is constant across generated waveforms.

To quantify the performance of the following waveform design and estimator pairs under test, and as is usual with the assessment of system identification algorithms, we calculate the norm of the error vector (trace of the error covariance matrix) between the actual complex impulse response value $\mathbf{h}$ and the estimated value $\hat{\mathbf{h}}$.

$$\rho \triangleq \operatorname{tr}(\operatorname{cov}(\mathbf{h} - \hat{\mathbf{h}})) = E[(\mathbf{h} - \hat{\mathbf{h}})^H (\mathbf{h} - \hat{\mathbf{h}})] \tag{4.39}$$

This metric is calculated for the ensemble of pseudo-randomly generated scene impulse responses and interferences as described above. The interference estimate ρ_N is calculated in the same manner as (4.39), replacing $\hat{\mathbf{h}}$ for $\hat{\mathbf{N}}$. TCFDE is a discrete time

technique which can be used for any corresponding transmit signal bandwidth, time and sampling frequency - the important metric for performance being the relationship between K the number of samples corresponding to the scene length and N the transmitted signal length. For the following section , the relationship is shown for a ratio of $K/N = 0.25$. This is incrementally altered in section 4.5.3 by increasing the scene length and keeping transmit signal length constant.

4.5.2 Performance Relative to Interference Power

As the radar system is limited by an upper bound of energy, there will exist a critical interference level where the placement of energy into the same band as the interferer will no longer provide a useful estimate of the impulse response as high sidelobes and noise override the signal. To demonstrate the performances relative to interferer strength, the following simulations increase the interference power to lower the overall signal to interference and noise ratio (SINR) The base SNR (background noise only) is kept constant at 40dB.The SINR is measured at the front end of the radar after the analogue to digital conversion and prior to additional signal processing.

$$\text{SINR} = \frac{\sum_{m=0}^{M} |\Omega_m|^2}{\sum_{m=0}^{M} E[|D_m|^2]} \tag{4.40}$$

where the power of the interferer is a finite value. The total power in the interference is increased at each simulation to demonstrate the result on performance with increasing interference as demonstrated in Figure 4.5. The RFI is 10 % of the total signal bandwidth.The dependency on the interference spectrum relative to the transmitted signal is demonstrated in (4.25). As this necessitates that performance for the FDWO-NLFM-TCDFE method is limited by the level of interference power, the performance with increasing RFI strength is demonstrated here via simulation. The SINR ranges between 35dB and 0dB were chosen as 35dB is just above the level of background noise (40dB), up to 0dB, at which point the transmitted signal and interference signal strength are the same. Typical operational values in a scenario of energy leakage from a neighbouring RFI transmitter may be expected to be around 15dB through to 5dB average SINR, but this greatly depends on the distance of the RFI source from the radar - due to the $\frac{1}{R^4}$ power drop off rule, distance is an important factor [10]. Deliberate jamming systems may have significantly more power available. There are assumed

to be regions of the spectrum which are interference free, which on average lowers the SINR over the bandwidth. If there are a few frequency samples of high strength SINR e.g. -20dB, this is treatable and the overall SINR will lower signficantly depending on the remaining areas of the radar bandwidth which have no RFI present. In UHF/VHF radar which has a very congested spectrum, the average SINR values will be much higher as there are few spectral regions within the radar bandwidth that have no RFI energy present. Chapter 5 deals with scenarios that are more similar to UHF/VHF region interference.

Simulated examples demonstrate how performance error varies with interference power for the following waveform and impulse response estimation techniques;

1. LFM with stretch processing

2. Initial LFM- Time Constrained Frequency Domain Estimate

3. Frequency Domain Waveform Optimization-NLFM-Time Constrained Frequency Domain Estimate

4. Generalized Least Squares optimized with Particle Swarm Optimization with known interference covariance $\mathbf{R}_{nn}$

Where (1) is the standard SAR configuration, (2) is the first step of the system identification process as shown in 4.1,(3) is the second and following pulses designed waveforms using the suboptimal estimator and (4) is the global optimal solution constrained under energy, but without amplitude or phase constraints. For a comparison to TCFDE, the PSO method is used to solve the original optimization problem given in (4.4). The PSO optimization is only under the constraint of energy and finds the optimal time-domain waveform solution $\mathbf{x}_{pso}(t)$ based on the interference co-variance matrix $\mathbf{R}_{nn}$. The PSO waveform is generated by using the estimated NLFM waveform for the initial conditions and numerically searching for the optimal waveform to minimize the error in the impulse response estimate (4.4).

4.5.2.1 LFM- Time Constrained Frequency Domain Estimate

This approach to initializing the system is not the optimal solution, but it provides performance as least as good as LFM-stretch (Figure 4.5) until much higher interference

regions. If the interference spectrum is already known, this step can be omitted and the FDWO-NLFM-TCFDE process can be used.

4.5.2.2 Frequency Domain Waveform Optimization-NLFM- Time Constrained Frequency Domain Estimate

Leading from the initial interference spectral estimate given by the LFM-TCFDE the performance of the FDWO-NLFM-TCDFE is indicative of the best system performance. Note that its performance is also dependent on the quality of the interference estimate from the prior pulse. In this way, it serves as an indicator of the overall system performance. It is shown in Figure 4.5 that using this scheme consistently improves performance compared with transmitting the LFM signal- both compared to evaluation via stretch processing and TCFDE.

4.5.2.3 Cramer Rao Lower Bound

The CRLB is a waveform-dependent measure of the best possible performance attainable by a specific designed waveform in an interference characterized by covariance matrix $\mathbf{R}_{nn}$ as shown in (4.3). The true known simulated R_{nn} is used along with the time-domain SPA synthesized waveform to provide the CRLB value. Therefore, it is a useful tool to evaluate any performance losses in the adaptive system. These losses account for both: i) the estimation of the interference to design the waveform and ii) those incurred via the TCFDE impulse response approximation to the direct GLS estimate approach in 4.3. These include the diagonalization assumption used to form the expression in (4.7) and the approximation of linear-to circular convolution and re-constraining this value in the time domain in (4.10) back to linear convolution. The CRLB has been calculated for both the LFM waveform and the NLFM waveform used in the FDWO-NLFM-TCDFE combination and are labeled CRLB-LFM and CRLB-NLFM respectively in Figure 4.5. The larger performance gap between in LFM-TCFDE and CRLB-LFM compared to FDWO-NLFM-TCFDE and CRLB-NLFM can be attributed to the larger error in interference estimate, shown in Figure4.5

4.5.2.4 Particle Swarm Optimiztion-Generalized Least Sqaures

This result serves as an indicator of an absolute lower bound of performance for a given interference. Using the simulated interference covariance matrix, the PSO algorithm searches for the global optimal time-domain waveform solution constrained only by energy (4.3). In the absence of structure constraints in the form of phase or amplitude, while this waveform offers the best performance, this is a both a computationally expensive and not amenable to physical implementation. However, in comparison to the FDWO-NLFM-TCFDE, it demonstrates the performance losses incurred by; (i) using the alternative frequency-domain estimator TCFDE (ii) using SPA to constrain the time-domain waveform to be constant amplitude and increasing in phase over time (iii)

Further, if the CRLB-NLFM estimate (given from the FDWO-NLFM-TCFDE) is compared to the PSO-GLS, the difference shows the performance lost by forcing the amplitude and phase structure via the SPA. For moderate levels of interference there is minimal performance impact of constraining the waveform The difference between the FDWO-NLFM-TDFDE and PSO show the costs of using an alternative estimator and enforcing a chirp.
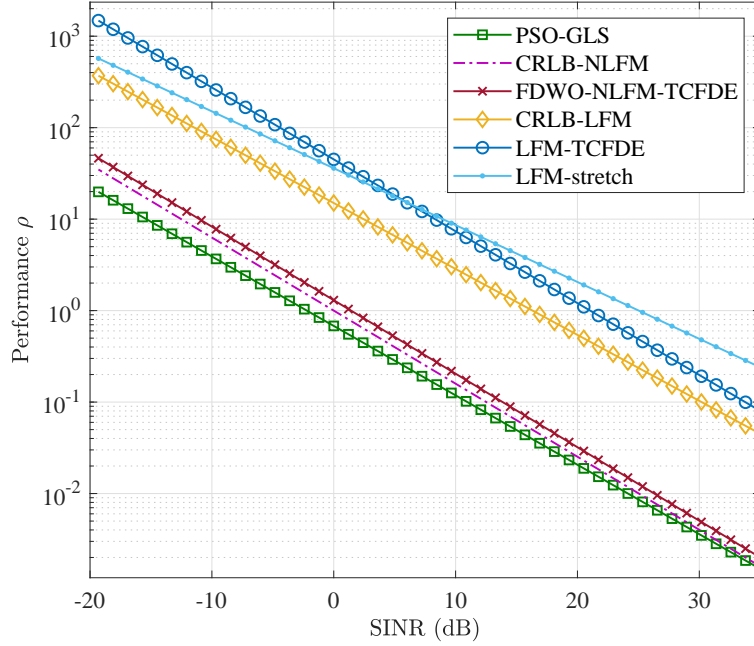
Figure 4.5: *Performance error norm results from 35dB to -20dB at K/N=0.25 on a semi-log plot*

4.5.2.5 Interference Estimate

The performance error of the interference spectrum estimate $\hat{\mathbf{D}}$ is shown for comparison between the initial (LFM) ($p = 1$) and adapted FDWO-NLFM-TCFDE pulse ($p = 2$) and finally a subsequent third pulse ($p = 3$) using the interference estimate from the prior pulse in Fig. 6. There is minimal performance gap between ($p = 2$) and subsequent estimation demonstrating that for static interference further pulses are not required to improve the interference estimate.

4.5.3 Performance for Relative Scene Size

Shown in (4.10), the TCFDE method constrains the frequency-response estimate in the time-domain to re-express the estimate without assuming circular convolution. This step removes $N - 1$ samples to provide the original $K - 1$ range cells, which as a by-product removes noise that was present in the additional $N - 1$ samples. The ability
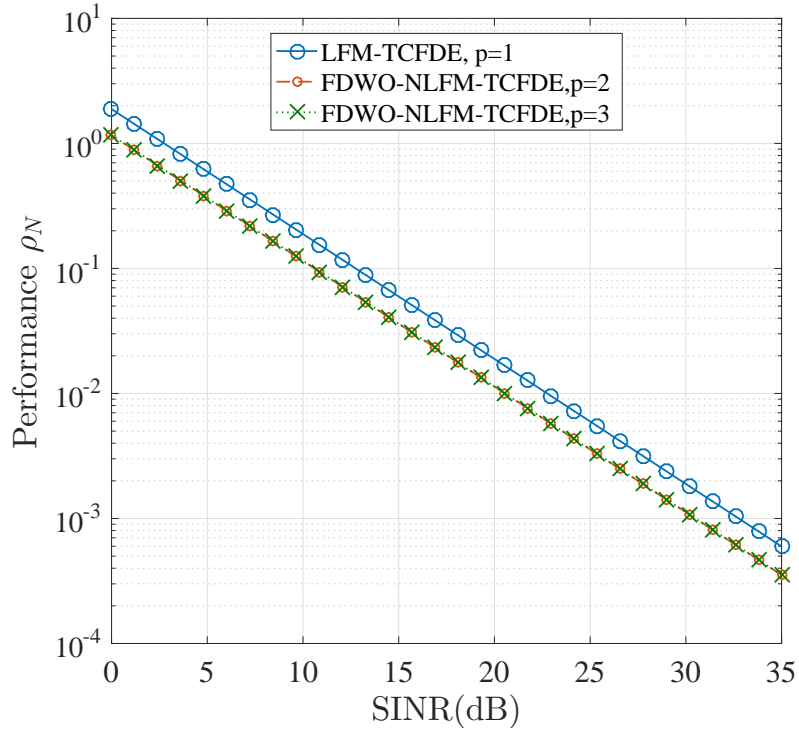
Figure 4.6: *Mean squared error for interference spectrum estimate for initial pulse p=1, adapted pulse p=2, and the subsequent pulse p=3*
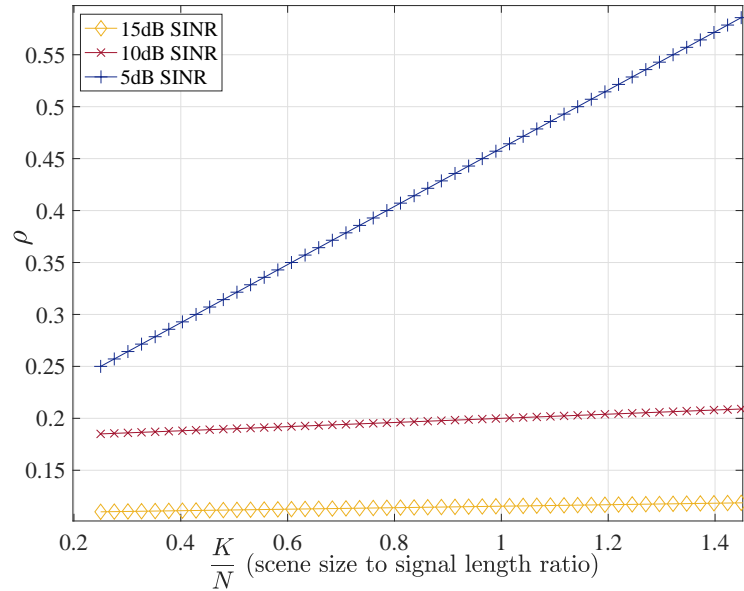
Figure 4.7: *Performance impact for increasing impulse response lengths at varying levels of SINR*

to remove noise/error originating from the estimation process is therefore dependent on the ratio between the discrete representation of the scene impulse response $K - 1$ and the transmitted pulse length $N - 1$. It can be demonstrated (see Appendix B.1 for proof) that the constrained solution is proportional to the unconstrained solution by a factor γ,

$$\text{cov}(\hat{\mathbf{h}}_{\mathbf{c}} - \mathbf{h}_{\mathbf{c}}) = \gamma\text{cov}(\hat{\mathbf{H}}_u - \mathbf{H}_u) = \gamma\rho \tag{4.41}$$

Where $\gamma = \frac{K}{N+K}$, such that $\gamma < 1$, thus constraining the solution will always decrease the error in the solution. When $N > K$ (for small scene sizes) the reduction factor γ is comparatively large but when $K > N$, there is a less error removal through γ.

The following simulated experiment demonstrates different scene lengths relative to the same pulse length and its effect on the TCFDE performance. The longer the pulse-length relative to the scene size, the larger the performance gain. The performance error improves linearly with the removal of samples. This effect is shown in Figure 4.7 for increasing scene sizes while keeping the pulse length N constant. This is demonstrated for interference levels of 5dB, 10dB and 15dB SINR. The higher the interference level, the higher the gradient at which the performance drops off due to additional noise suppression. While the method is operational for larger scene sizes it is at reduced performance as additional noise suppression is greater for smaller scenes.

4.5.4   Performance for Relative RFI Bandwidth

The FDWO solution of (4.25) is dependent on the interference spectrum and the total energy of transmitted signal. The experiment in Section demonstrated the change in performance by changing the overall interference power. The interference spectrum D_i can also occupy varying spans of the radar bandwidth. This experiment demonstrates the impact in performance through increased bandwidth. The overall power-budget is the same, but the spread across the radar bandwidth is increased. While it is uncommon to encounter interference spectra that exceeds 10% of the radar bandwidth, results are demonstrated from the range of 1% to 30% in Figure (4.8) for 5 different overall interference strengths in SINR. The results demonstrate that the FDWO approach provides best performance for lower bandwidths and performance is lost for increasing bandwidths.
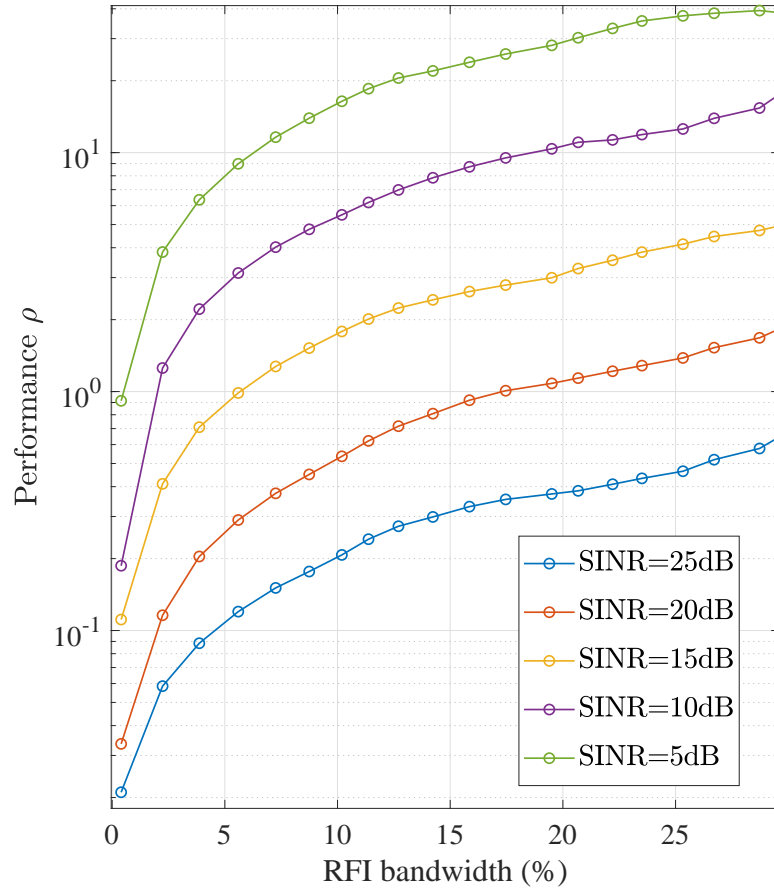
Figure 4.8: *Performance Error varying with increasing RFI bandwidth from 0.5% of the total operational radar bandwidth to 30%.*

4.5.5   Computational Complexity of FDWO-NLFM-TCDFE

An overview of the scaling of the processing required for one pulse is presented in this section. The larger the input scene length K and pulse length N, the higher the number of operations required for the signal processing for the TCDFE scheme per pulse. This method initially appears to be low-computational complexity as this is a non-iterative process. The computational complexity of the full adaptive cycle can be broken down into the following stages : 1) system identification and interference estimation, 2)waveform design, 3)waveform synthesis.

1. System Identification and Interference Estimation:
   The system identification process complexity is given by the number of operations between calculating $\hat{\mathbf{h}}$ and $\hat{\mathbf{N}}$. The upper limit on the computational complexity can be given by considering the computations required each iteration for; element-wise division in (4.9) which increases linearly with the vector size M so there are M divisions, the DFT and inverse DFT in (5.10) $\mathcal{O}(M \log_2 M)$ [106] and finally the element-wise multiplication used in calculating $\hat{\mathbf{N}}$. Calculating $\hat{\mathbf{h}}$ and $\hat{\mathbf{N}}$ requires M-point DFTs as given in (14) and (4.10)

$$\mathcal{C}_1 = \mathcal{O}(M) + \mathcal{O}(M \log_2 M)$$

2. Waveform Optimization and Design:
   The waveform design can be carried out via the expression in (4.25). This requires calculation of the total energy E_T which is a summation over M points and scales linearly.Calculating $E_i(F)$ then requires $\mathcal{O}(M)$ for division of M.

$$\mathcal{C}_2 = \mathcal{O}(M)$$

3. Waveform Synthesis:
   The implementation of SPA requires a cumulative summation of the estimated optimized waveform spectrum $\mathbf{E}_i(F)$ in order to use relationship between change in frequency and time as shown in (4.28). This uses the addition and multiplication operator. Linear interpolation is also required for obtaining frequency values for the set of time samples corresponding to $\ddot{\psi}(t)$. Linear interpolation computational complexity depends both on the number of existing data points M and

the number of data points to be interpolated. For this case, the number of points to be interpolated is the same as the original number of data points. The largest operation performed by an interpolation algorithm is sorting the each data point into the relevant interval between two existing points given as $(2M)\log_2(2M)$. After this, the linear interpolation is simple and performs two additions and one multiplication so scales linearly.

$$\mathcal{C}_3 = \mathcal{O}(M) + \mathcal{O}(M\log_2(M))$$

Overall the FDWO-NLFM-TCDFE based adaptive cycle computational complexity scales with $\mathcal{O}(M\log_2 M)$ as the dominant complexity term per waveform design-transmission or azimuth point.

4.6 SAR Scenario Example

4.6.1 Simulation Set-Up

We consider a spotlight SAR system and assume an approximately circular antenna pattern. In addition, the following simulation assumes a circular flight path to allow the range swath to be the same length at all azimuth points. A representation of the circular flight path is shown in Figure 4.9 and the associated simulation parameters are displayed in the following table. Waveform values based on those used in [31] and platform values based on those representative for operational use of X-band SAR systems.

SAR scene parameters	Value
Platform height: h	1500 m
Range-to-scene centre: R_0	6000 m
Range swath: R_w	512 m
Range resolution: Δ_R	1 m
Range profile samples: K	512
Platform velocity:	200 ms^{-1}
Azimuth flight path length: L	1178m
Flight path angle: θ_c	5.62°
Pixel values	256×256
Pulse length: τ_c	$3.41\mu s$
Bandwidth: B_c	150MHz
Wavelength: λ	0.03m
Sampling rate: f_s	150MHz
Waveform samples N:	512

Table 4.1: *SAR platform and scene values used in simulation*
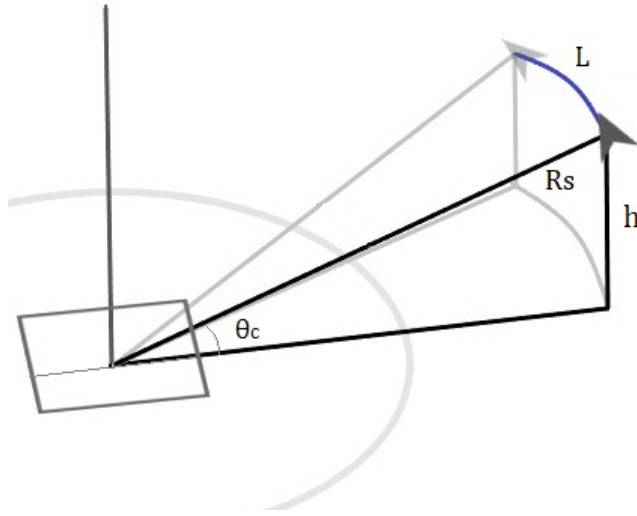
Figure 4.9: *Illustrative figure of radial flight path used in simuations and associated parameters.*

The parameters used for the scene and relative platform positions are as shown in the table:

The estimated impulse response vectors collected at each azimuth point is then processed using the back-projection image formation algorithm. The test scene image is

shown in Figure (4.10) which represents the back-projection image created from the actual impulse responses of the scene without added interference. The test SAR scene represents a static aircraft on the ground and is used to exemplify the effects of interference on the final SAR image.
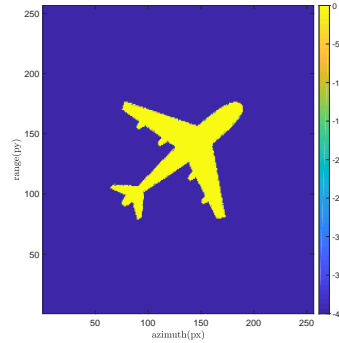
Figure 4.10: *Test SAR image representing a stationary ground-based aircraft created using back-projection with no interference*

4.6.2   Constant Interference Source

In this example the interference source does not change its spectral content $\mathbf{N}$ across the SAR data collection for all azimuth points. After a two-pulse cycle, the waveform does not need to adapt further and continues to transmit the designed pulse $\mathbf{x}_2$. The initial pulse identifies an approximate estimate of the interference spectrum $\mathbf{N}_1$ and the adapted waveform provides an improved estimate of the interference $\mathbf{N}_2$ as demonstrated previously. We compare the SAR images created from the LFM-stretch method, the FDWO-NLFM-TCFDE approach and additionally LFM-TCFDE to demonstrate the imaging result if the waveform was not updated at all.

Figure 4.11 shows images for FDWO-NLFM-TCFDE, LFM-TCFDE and LFM-stretch across each row. Each row representing SINR strengths of 10dB, 5dB and 0dB. With increasing interference strength, the images show increased blurriness of features and some artifacts on the outskirts of the image for the LFM-stretch in column 3. The LFM-TCFDE shows increased "graininess" as a result of increased distortion in each impulse response estimate. The FDWO-NLFM-TCFDE method produces images which degrade to a much lesser extent qualitatively compared with the other approaches.
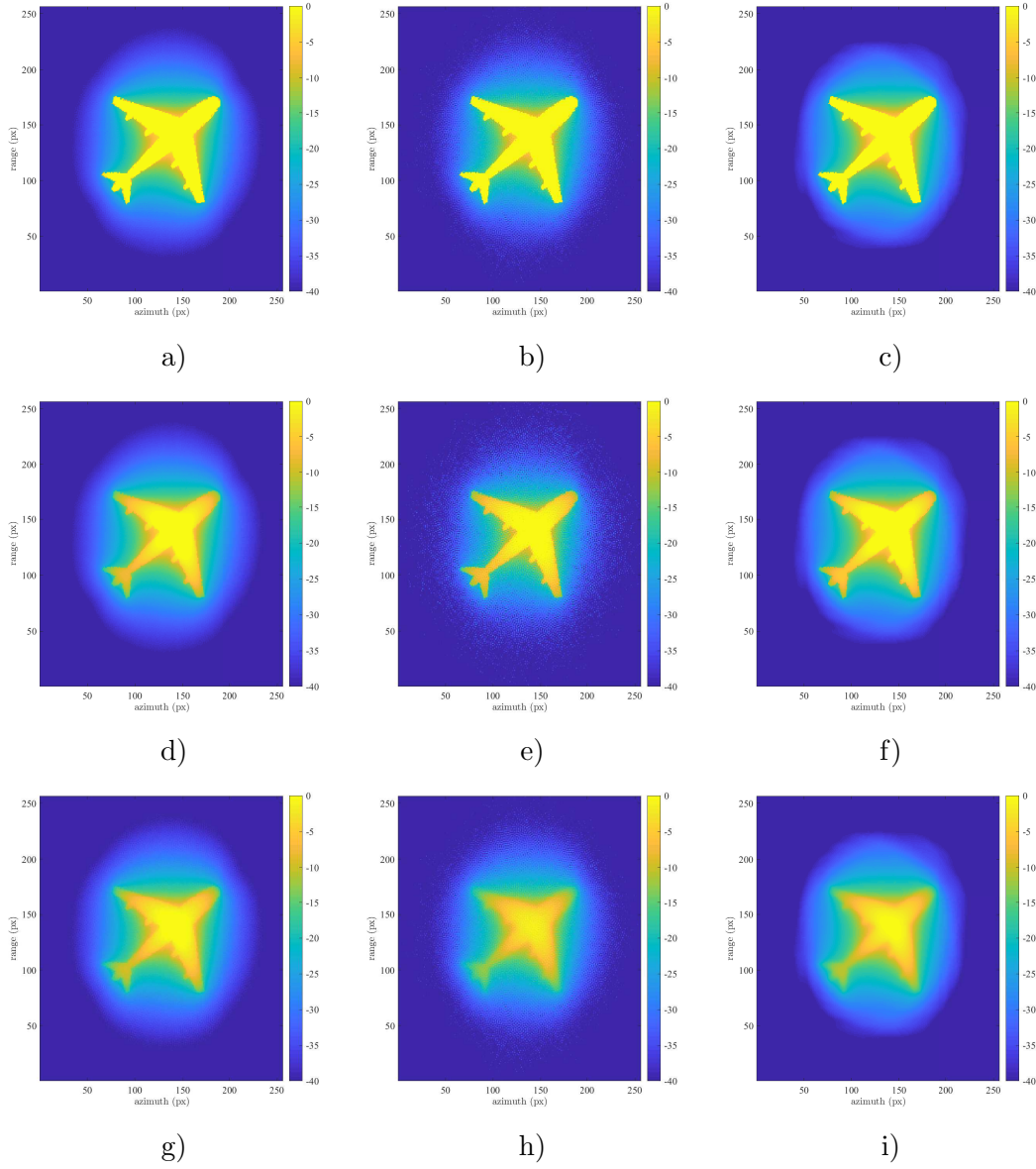
Figure 4.11: *Row 1: 10dB, Row 2: 5dB,Row 3: 0dB. FDWO-NLFM-TCFDE images: a),d) & g). LFM-TCFDE images: b),e) & h). LFM-stretch images: c),f),i).*

4.6.3 Dynamic Interference Source

In the following example the interference spectrum is changing pulse-to-pulse by an upwards sweep in frequency across the radar bandwidth frequency which the radar signal is using and the total width of the narrowband interference is kept constant at 5%. The total SINR is kept constant at 5dB. This scenario demonstrates a need to employ waveform design regularly enough to compensate for interference changing pulse-to-pulse. Figure 4.12 shows images created for an azimuth collection where the waveform design is employed every 5th, 50th, 100th and only once at the beginning of the data collection. The image heavily degrades if the pulse is not adapted at all after the initial interference estimate is obtained introducing severe image artifacts. If the pulse collection is reduced to only once every 5 pulses, the image is not optimal, but still maintains a clear outline of features. If the radar system is not capable of readapting the waveform at every pulse, this reduced rate may then still produce images of an acceptable standard if the interference spectrum is changing at every pulse. The higher the rate of update, the better the image quality.

a)   b)

c)   d)
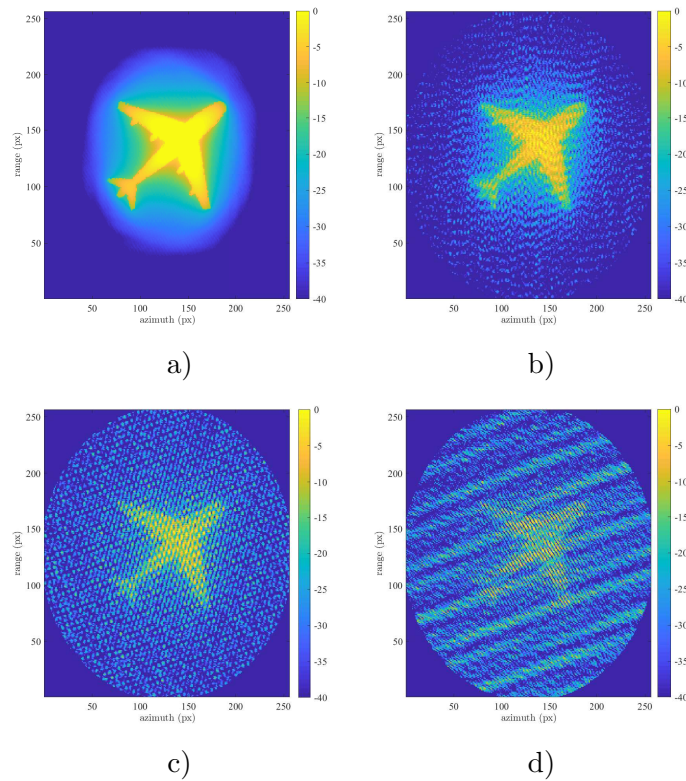
Figure 4.12: *Waveform design updated at every: a)5th pulse b) 50th pulse c) 100th pulse d) once across whole azimuth collection*

4.7   Conclusion

This Chapter has presented a combined system identification and waveform design scheme for mitigating RFI in SAR on a pulse-to-pulse basis. It has been demonstrated that under the TCFDE scheme, to minimize the error in the scene impulse response, the waveform spectral content should be directly proportional to the energy of the RF interference. Using cyclic extension as an artifact in the processing and using diagonalization properties of the DFT allowed formulation of an unconstrained frequency domain estimate. This estimate was then constrained back in the time domain to provide a solution for the impulse response. This interference estimate is then used in the FDWO which shows that the optimal solution is directly proportional the spectrum of the interfernce. Combining this with SPA waveform synthesis has provided a physically feasible means for implementation and is of low computational complexity. Performance is decreased for larger SINR and wider RFI bandwidths, but is able to address larger RFI bandwidths without any additional computational cost. Results have demonstrated that this scheme can be used for cases where the signal length is either greater than or less than the ground patch propagation time, but at the expense of loss of performance due to less noise-removal. This scheme is most suitable for the scenarios where the bandwidth availability is compromised from leakage from neighboring transmitters or other unwanted in-band interference returning usage of the entire spectrum to the radar. Compared to spectrum friendly approaches where areas of the spectrum are avoided due to interference, this scheme competes and aims to return usage of the entire spectrum to the SAR system.

Chapter 5
Waveform Design: Fight or Flight

In the crowded spectral environment, waveform transmission with spectral gaps across its bandwidth is likely to become standard operational practice for wideband radar modes such as SAR. However, this has to be implemented with caution as removing frequency samples from the received signal causes degradation of the final SAR image [71, 107, 108]. This loss of performance is manifested in reduction of resolution and the appearance of large sidelobes which spill across the image masking neighbouring cells with weaker reflectors - a similar set of problems initially caused by the interference. The competitive waveform design scheme for SAR introduced in Chapter 4 demonstrated that placing energy across the entire spectrum the waveform "fights" with an interferer at particular spectral bins, rather than avoid transmission, thereby reducing the extent of reduced resolution caused by omitting samples. The current optimization method focuses on minimising the performance based on the unconstrained frequency response estimate $\mathbf{H}$ according to

$$\text{tr}(\text{cov}(\mathbf{H} - \hat{\mathbf{H}})) = \sum_{i=0}^{M} \frac{D_i}{|\Omega_i|^2}$$

as derived in Chapter 4. The trace is the sum of all elements on the diagonal of the covariance matrix; this is the sum of the squares of the errors across the whole frequency domain specified by the radar bandwidth. The solution to this optimization from the FDWO in the previous chapter suggested that if the power of a finite-power interferer was concentrated increasingly at one bin, all of the energy in the transmitted waveform would be concentrated there, decreasing the energy distributed among the remaining frequencies. This mode of operation is valid as concentrating energy on one bin still acts to reduce the resultant interference at the other frequencies so less energy is required at the other bins. However, if the interferer continues to increase power in one bin, there will come a limit at which competing at that bin no longer "wins" the energy fight, and, on the way to addressing it we have reduced our energy in the remaining bins and so cant estimate the rest of the frequency response in the

other bins with any reliability. Thus, we may have to consider flight, abandon the bins where there is simply too much interference and concentrate our resources, the energy in the transmitted waveform, in the areas of the spectrum where the interference is not too competitive. In order to continue, we revisit the error covariance matrix and the elements along the diagonal. This Chapter continues to only consider the elements of this vector in where we can compete with the interference and modify the waveform optimization process and system identification accordingly.

A cost function is built to minimize the MSE by separating the transmit waveform into spectral regions to either place signal energy or avoid. The method provides a decision on which areas of the spectrum to avoid and transmit - this is particularly useful in the case where the interference is spanning multiple frequency samples or for a band with multiple interferences.This modified cost function requires inclusion of knowledge of the frequency response, which poses a challenge as this is also the desired outcome of the waveform measurement. Possible options to address this are discussed. The waveform design process is computationally efficient, and performed on-the-fly on a pulse-to-pulse basis. As post processing, an attempt is made to recover missing spectral data caused as a result of a gapped transmit spectrum. This process is aided by the resultant decrease error in the present frequency domain data via waveform design. Comparisons are made to well-known spectral interpolation algorithms for SAR phase history recovery (GAPES and AR-Burg).After missing data recovery, standard image formation algorithms are applied to produce a SAR image. These images are improved in terms of reduced artifacts caused by interference and overall image MSE, compared with the standard LFM and linear notched filter interference mitigation approach.

5.1   System Identification

As before, the system identification process provides a pulse-to-pulse estimate of the range impulse response and an interference estimate based on the most recent measurement. Following from the time-domain development in the previous chapter, the system is unchanged until the frequency domain manipulation. The adaptive system structure is largely the same at a high level, as shown in Figure 5.1, the modification is that the impulse response estimate is now altered as the frequency response has admitted gaps in the spectrum, denoted as $\hat{\mathbf{h}}_g$ for the impulse response. The addition in the full
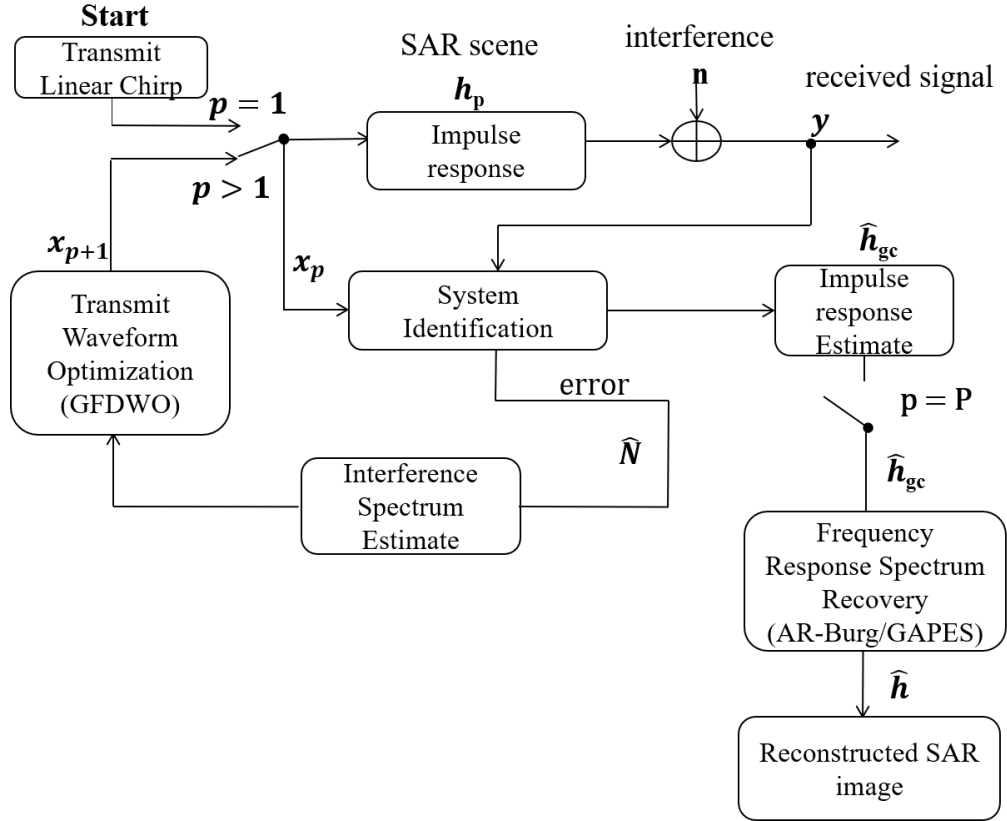
Figure 5.1: *Pulse-to-pulse system flow chart for gapped waveform design*

processing from the previous system is the inclusion of post-processing to attempt to recover the gaps in the spectrum. The following section will describe the modifications made to the system identification block to admit gaps in the spectrum.

To facilitate waveform design with gaps in the spectrum, the interference spectral power defines two sets in the frequency domain for the waveform design process to determine whether to transmit or omit frequency samples. Allow a threshold value τ to be defined according to the maximum interference power D across the frequency samples labeled by index $i = 0 \ldots M - 1$,

$$\tau = \tau_d \times \max(D_i), \quad 0 < \tau_d < 1 \tag{5.1}$$

where $\tau_d = 1$ is analogous to transmitting with the full spectrum. Allow this threshold to define a set $\mathcal{S}$ and its complement $\mathcal{S}^{\complement}$ over the frequency domain samples of the radar
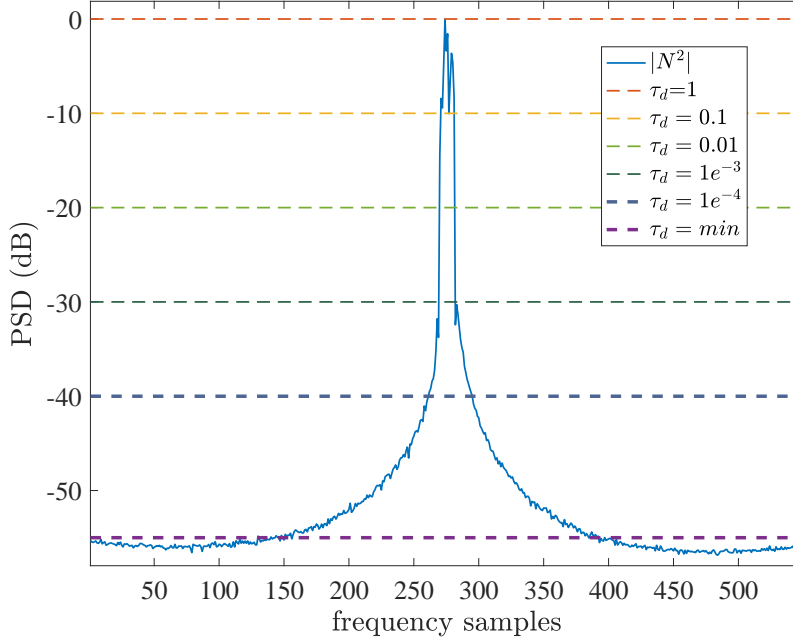
Figure 5.2: *A single realization of interference* **D** *PSD shown in dB with various threshold levels corresponding to the threshold factor τ_d.*

bandwidth,

$$\begin{aligned}
\mathcal{S}(\tau) &= \{i : D_i < \tau\} \\
\mathcal{S}^{\complement}(\tau) &= \{i : D_i \geq \tau\}
\end{aligned} \tag{5.2}$$

These sets will correspond to allowing the transmission of energy in $\mathcal{S}$ and restrict transmission in $\mathcal{S}^{\complement}$. An illustrative example of the threshold applied to a single realization of interference is shown in Figure 5.2. With this distinction between sets defined, the frequency domain system identification can be re-expressed accordingly,

$$\mathbf{Y} = \boldsymbol{\Omega}_{\mathcal{S}} \mathbf{H} + \mathbf{N} \tag{5.3}$$

such that the transmitted signal samples

$$\Omega_i = \begin{cases} \Omega_i & \text{if } i \in \mathcal{S} \\ 0 & \text{if } i \in \mathcal{S}^{\complement} \end{cases}$$

Where $\boldsymbol{\Omega}_{\mathcal{S}}$ denotes the waveform in the frequency domain across the set of "allowed" transmission samples and therefore any samples for $\boldsymbol{\Omega}_{\mathcal{S}}^{\complement} = 0$. The interference plus noise

term $\mathbf{N}$, is unchanged, as is the true frequency response $\mathbf{H}$. Note that the received signal can be written according to separable sets where

$$\mathbf{Y}_{\mathcal{S}}^{\complement} = \mathbf{\Omega}_{\mathcal{S}}^{\complement}\mathbf{H} + \mathbf{N}_{\mathcal{S}} = (\mathbf{0})\mathbf{H} + \mathbf{N}_{\mathcal{S}} = \mathbf{N}_{\mathcal{S}} \tag{5.4}$$

$$\mathbf{Y}_{\mathcal{S}} = \mathbf{\Omega}_{\mathcal{S}}\mathbf{H} + \mathbf{N}_{S} \tag{5.5}$$

The expression in (5.4) implies thats a direct measurement of the interference can be obtained in the spectral region where the signal has not been transmitted. This is a potential advantage of allowing gaps in the spectrum. However, the remainder of the interference in $\mathbf{N}_{\mathcal{S}}$ is still unknown. An illustration of this effect is shown in Figure 5.3c.

$$\mathbf{N} = \mathbf{N}_{\mathcal{S}} + \mathbf{N}_{\mathcal{S}^{\complement}} \tag{5.6}$$

Continuing the frequency domain system identification under the same framework developed previously by estimating the frequency response,

$$\hat{H}_i = \begin{cases} 0 & \text{if } i \in \mathcal{S}^{\complement} \\[2mm] \frac{Y_i}{\Omega_i} & \text{if } i \in \mathcal{S} \end{cases}$$

For samples with no corresponding transmitted energy, there will be no measurement of the frequency response, so is set to zero to avoid division by the zero terms in the waveform $\mathbf{\Omega}_{\mathcal{S}}$. Furthermore, as shown in (5.4) any received energy in this band is interference, which should be removed from the calculation of the frequency response. Else, the standard result applies. Where $\mathbf{H_G}$ is the full frequency response vector with gaps included of length M,

$$\hat{\mathbf{H}}_G = \mathbf{H}_{\mathcal{S}}^{\complement} + \mathbf{H}_{\mathcal{S}} \tag{5.7}$$

As before, constrain the impulse response estimate in the time domain

$$\hat{\mathbf{h}}_{g_c} = \begin{bmatrix} \mathbf{I}_K & \mathbf{0}_{N-1,K}^T \end{bmatrix} \mathbf{F}^{-1}\hat{\mathbf{H}}_{g_c} \tag{5.8}$$

Defining $\hat{\mathbf{h}}_{g_c}$ as the constrained impulse response estimated obtained with gaps in the spectrum.

$$\hat{\mathbf{H}}_{\mathbf{g}_c} = \mathbf{F}(\begin{bmatrix} \hat{\mathbf{h}}_g \\ \mathbf{0}_N \end{bmatrix}) \tag{5.9}$$
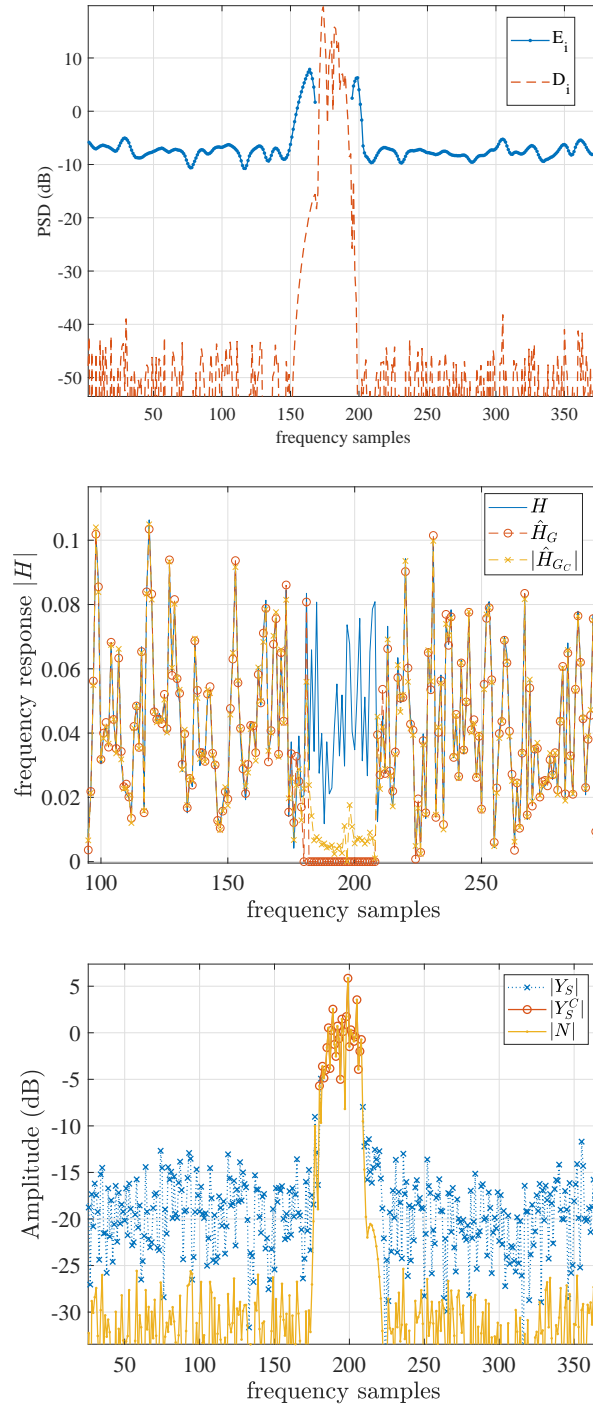
Figure 5.3: *Various stages of the system ID process:top-to-bottom: a) input gapped spectrum waveform and the RFI PSD to be identified b)The true frequency response of the ground, the gapped frequency response and the constrained frequency response c)the interference amplitude and the separated sets of the receive signal $Y_{\mathcal{S}}$ and $Y\mathcal{S}^{\complement}$*

118

This provides an error reduced estimate of the spectrum. Which finally, provides a full estimate $\hat{\mathbf{N}}$ of the interference, where the remainder of the interference $N_{\mathcal{S}}$ can be identified from

$$\hat{\mathbf{N}} = \mathbf{Y} - \mathbf{\Omega}\hat{\mathbf{H}} \tag{5.10}$$

5.2 Waveform Design

The waveform design is based on the FDWO framework developed in the previous chapter. To allow non-competitive operation, the capability to avoid areas of the spectrum in the interest of minimizing the overall MSE is developed. The previous format required knowledge of the interference alone, while this Section demonstrates that the extension also requires partial knowledge of the scene frequency response.

5.2.1 Missing Samples

Continuing to work with the metric of minimizing the MSE of the estimated frequency response from the true frequency response, the following Section discusses development of this cost function. To construct the cost function, the effect of removing samples of the frequency response on the performance in terms of the MSE must be considered. The unconstrained performance according to the MSE criterion was previously defined as the trace of the covariance of the frequency response.

$$\rho = \text{tr}(\text{cov}(\mathbf{H} - \hat{\mathbf{H}})) = \text{tr}(\mathbf{E}|(\mathbf{H} - \hat{\mathbf{H}})(\mathbf{H} - \hat{\mathbf{H}})|) = \sum_{i=0}^{M-1} \frac{D_i}{|\Omega_i|} \tag{5.11}$$

In an ideal case with no noise/interference, the total covariance is zero. Adding noise to the system, the estimate of the performance is degraded as the covariance is now non-zero. In the case that the waveform does not transmit energy in $\Omega_{\mathcal{S}^\complement}$ it is assumed that the frequency samples received in this region only contain background noise, interference or unwanted energy leakage, as shown in (5.4), the measured frequency response is therefore zero. So the resultant performance error added by omitting samples can be written as

$$\rho_{\mathcal{S}(\tau)^\complement} = \text{tr}(\text{cov}(H_i - \hat{H}_i)) = \sum_{i \in \mathcal{S}(\tau)^\complement} |H_i - 0|^2 = \sum_{i \in \mathcal{S}(\tau)^\complement} |H_i|^2, \quad i \in \mathcal{S}(\tau)^\complement \tag{5.12}$$

This term then effectively represents a penalty for removing samples, and its value is added to the covariance term for the transmitted waveform samples. By assuming that each frequency sample is independent, the performance of each set can be calculated separately. Therefore, the total covariance with missing spectral components can be written as follows, substituting back in the covariance for the non-zero frequency samples.

$$\rho(\tau) = \rho_{\mathcal{S}(\tau)} + \rho_{\mathcal{S}(\tau)^{\complement}} = \sum_{i \in \mathcal{S}(\tau)} \frac{D_i}{|\Omega_i|^2} + \sum_{i \in \mathcal{S}(\tau)^{\complement}} |H_i|^2 \tag{5.13}$$

This creates a trade off between the reduction in error caused by omitting frequency samples with high levels of interference and the increase in error caused by the penalty term by omitting samples. To minimize the performance error ρ, the sets need to be defined according to τ such that a balance between the resultant performance of omitting samples and the performance penalty this incurs is obtained. An example of this effect is demonstrated in Figure 5.4 where the values for $\rho_{\mathcal{S}}$ and $\rho_{\mathcal{S}^{\complement}}$ are plotted separately against changing threshold. Here it is demonstrated that increasing SINRs cause varying levels of performance $\rho_{\mathcal{S}}$ with changing threshold. Only a single frequency response plot for different thresholds is shown as $\rho_{\mathcal{S}^{\complement}}$ does not depend on the interference. The performance error for $\rho_{\mathcal{S}}$ increases as the threshold increases, as more interference is included in the covariance estimate (5.13). However, the performance error for $\rho_{\mathcal{S}^{\complement}}$ will then decrease with increasing threshold as less samples are being removed from the frequency response estimate.

5.2.2 Waveform Optimization

With the cost function in terms of the MSE of the frequency response defined, this Section proceeds to demonstrate an approach to solve for the energy distribution of the waveform and the areas to avoid transmission according to the threshold τ. As before in Chapter 4, there is limited energy available for transmission so constrained optimization provides an expression for the waveform spectrum with respect to this criteria. The optimization is carried out in two steps; firstly the energy distribution that minimizes ρ is found by enforcing the energy constraint for a fixed arbitrary threshold, then secondly the threshold that minimizes ρ is found by using the expression for the
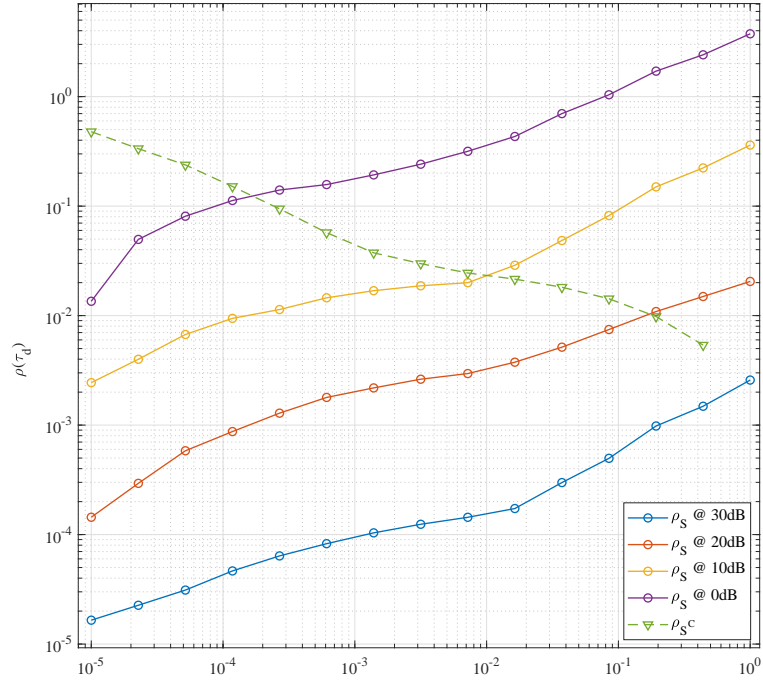
Figure 5.4: *Example shows how the independent components $\rho_{\mathcal{S}^{\complement}}$ and $P_{\mathcal{S}}$ for the performances change according to threshold factor for four different levels of interference.*

energy distribution. This section begins by performing the constrained optimization and follows with a method to evaluate the optimal threshold using the constrained optimization expression.

5.2.2.1 Constrained Optimization

The constrained optimization problem can be expressed as follows under the constraint of the total energy available, where $E_i = |\Omega_i|^2$

$$
\begin{aligned}
\min_{\mathbf{E}} \quad & \rho(\mathbf{E}, \tau) = \sum_{i \in \mathcal{S}(\tau)} \frac{D_i}{E_i} + \sum_{i \in \mathcal{S}(\tau)^{\complement}}^{M} |H_i|^2 \\
\text{s.t.} \quad & \sum_{i \in \mathcal{S}(\tau)} E_i = E_T
\end{aligned}
\tag{5.14}
$$

Proceeding to solve (5.14) under the energy constraint by using the following Lagrangian

$$L(\mathbf{E}, \tau) = \sum_{i \in \mathcal{S}(\tau)} \frac{D_i}{E_i} + \sum_{i \in \mathcal{S}(\tau)^\complement} |H_i|^2 + \lambda(\sum_{i \in \mathcal{S}(\tau)} E_i - E_T) \tag{5.15}$$

Now determine the minimum value of the Lagrangian L by setting the first derivative equal to zero. For this case, the derivative is calculated with respect to values $i \in \mathcal{S}$ and τ is fixed in the following partial derivative, such that for a chosen threshold the resultant waveform energy distribution is then the solution of the Lagrangian optimization.

$$\frac{\partial L}{\partial E_i} = -\frac{D_i}{E_i^2} + \lambda = 0, \qquad i \in \mathcal{S} \tag{5.16}$$

$$\lambda = \frac{D_i}{E_i^2}, \qquad i \in \mathcal{S} \tag{5.17}$$

$$E_i = \frac{E_T \sqrt{D_i}}{\sum_i \sqrt{D_i}}, \qquad i \in \mathcal{S} \tag{5.18}$$

Which provides the waveform energy distribution over the set defined by a chosen threshold τ subject to an energy constraint. The optimal waveform is then obtained by choosing a value of τ and designing a waveform according to the defined sets. As an extension of the previous FDWO but with gaps allowed in the spectrum, this approach is named Gapped Frequency Domain Waveform Optimization (GFDWO). Given a means to obtain the waveform spectrum $E_\mathcal{S}$ for a chosen threshold τ, an optimization procedure is now needed to solve for the optimal threshold value τ.

5.2.2.2 Numerical Search

Substituting in the expression for the waveform energy distribution (5.18), the cost function with implicit energy constraint can now be expressed as:

$$\rho(\tau) = \frac{1}{E_T} (\sum_{i \in \mathcal{S}(\tau)} \sqrt{D_i})^2 + \sum_{i \in \mathcal{S}(\tau)^\complement} |H_i|^2 \tag{5.19}$$

As the cost function is only implicitly dependent on τ via the set definition in (5.2) there is no apparent means to solve this via gradient based methods. Alternatively, 1-dimensional numerical optimization methods which do not use the gradient but instead iteratively step towards the extreme value of the cost function can be used for relatively low computational expense. To find the waveform spectral distribution $E_{S(\tau)}$ and the threshold τ which minimises the performance, carry out the following steps where the stopping tolerance $\Delta\rho_0 = 1e^{-4}$

Algorithm 3 Waveform Optimization: GFDWO

Initialize: Obtain estimate of $\mathbf{D}$, choose initial τ, according to optimization method
1: **while** $\Delta\rho > : \Delta\rho_0$ **do**
2:     Define sets $\mathcal{S}^{\complement}$ and $\mathcal{S}$
3:     Obtain estimate of $\sum_{i \in \mathcal{S}(\tau)^{\complement}} |H_i|^2$
4:     Calculate performance (5.19)
5:     Find next value for τ, based on $\rho(\tau)$
6: **end while**

5.2.2.3   Cost Function Analysis

To gain an understanding of the form of the cost function to choose an appropriate optimization method, the resultant performances according to varying thresholds are demonstrated in Figure 5.5. Varying strengths of interference were generated for both narrow-band interference occupying 1% of the radar bandwidth and wider interference occupying 10% of the radar bandwidth. The performance results are plotted against the relative threshold factor term τ_d which can take on values between $0 < \tau_d < 1$, representing a continuous range of thresholds from: no transmission across the spectrum ($\tau_d = 0$) to reduction to the competitive transmission mode ($\tau_d = 1$) respectively. The threshold value τ_d is relative to the strength of the interference; if the noise floor PSD value of the interference was -60dB from the peak PSD value, -60dB then represents the $\tau_d = 0$ scenario. In this way, it is representative of the dynamic range of the interference. The following results demonstrate the variation of the threshold factor from its maximum PSD value labeled at 0dB to -70dB below the maximum value.

5.2.2.4 Cost Function Results

For lower SINR and narrower bandwidth interferences (shown in Figure 5.5a for cases > 15dB SINR), it is apparent that the competitive case is the optimal transmission mode. For higher interference values the optimal threshold tends towards smaller values, corresponding to larger spectral gaps. The cost function realizations appear to be smooth and convex - so are likely to have a single minimum. The minina represents the threshold factor where the balance between omitting samples and competing with interference has been acheived and finds the lowest MSE. The true position of the minimum may be more difficult to obtain in cases where the gradient changes very slowly. In the case where there is a slowly changing gradient, multiple thresholds yield very little change in performance. This does not impact the final result as it is the minimum performance value of most concern.

The general trend shown in Figure 5.5a & b that for increasing interference SINR, the minimum performance value is obtained with a decreasing threshold factor value. This is an intuitive result, as the lower the interference, the lower the total contributing value for $\rho_{\mathcal{S}}^{\mathsf{C}}$, compared with the cost of missing samples. The cost function results demonstrate that generally better overall performances can be obtained from narrower RFI bandwidths - Figure 5.5a. As the SINR increases, wider bandwidths result in more samples requiring removal from the available samples to transmit, resulting in a greater penalty. For wider band interferences, it can be observed that the best possible performance achievable is worse (higher MSE) compared to narrower interferences. In the competitive mode, the energy has to spread across more bins, reducing the achievable SINR at each sample. Allowing spectral gaps then results in a larger loss of samples for wider-band interferences to compensate for the additional large contributing $\rho_{\mathcal{S}}$ terms.

Plotting the cost functions has determined that the performance cost functions can informally be treated as convex one-dimensional optimization problem.
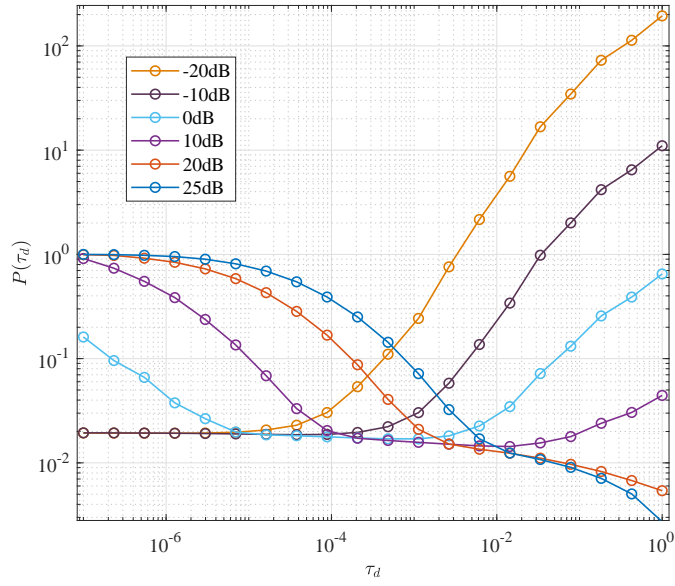
(a) *1% of total radar bandwidth*
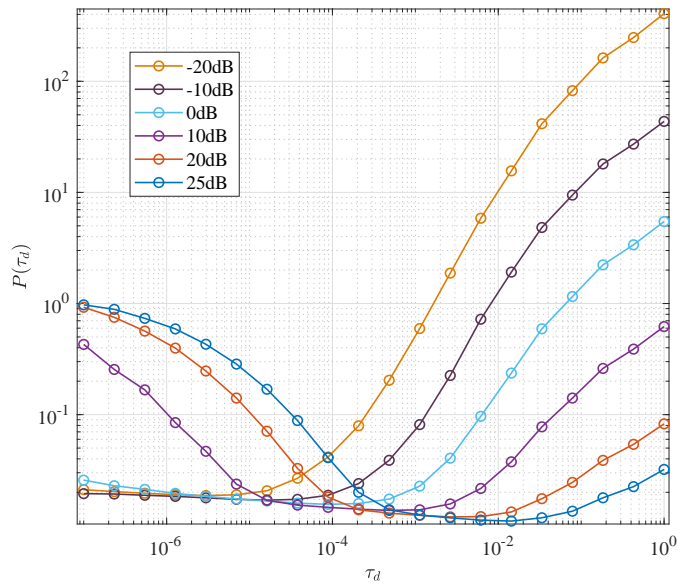
(b) *10% of total radar bandwidth*

Figure 5.5: *MSE performance plotted as a function against relative threshold value τ_d on a semi-log scale. $\tau_d = 1$ (e.g. 10^0)is representative of the competitive case where transmission is across the entire radar bandwidth and no gaps are admitted into the spectrum. $\tau_d = 0$ is representative of no transmission. These results are representative of stepping through from full to no transmission.*

125

5.2.3 Optimization Procedure

While any numerical 1D optimization procedure could be applied, the proposed method for optimization is the "golden section" method which uses two points to begin an iterative search for the value which minimizes a cost function. This is especially useful in this scenario where the result is bounded between $0 < \tau_d < 1$. The golden section is dependent on the objective function being univariate in nature (a single extreme point) which is well suited to convex problems. It is not proven that the performance function has a single minima and it is possible that more than one minimum may exist. However, as shown in Figure 5.5, it is implied that the resultanting performance difference would be very small as the function is both smooth and has a slowly varying gradient around the minimum resulting in many threshold values having similar performance values. Furthermore both of the input functions $\rho_{\mathcal{S}}$ and $\rho_{\mathcal{S}\complement}$ are linearly decreasing and increasing respectively with decreasing threshold factor, the resultanting optimization function will then be well-behaved.

While this method does not guarantee to find the global minimum, choosing a sensible initial input parameter improves the route which the optimization procedure takes, improving the chances of finding the global minimum. As the total energy in the transmitted signal is known, the SINR can be used as an indicative parameter to select a range of thresholds to search. By initializing the optimization with a value closer to the global minimum, the overall result and computational time for the golden section method will be improved. By exploiting the linearly decreasing correlation between the SINR and the threshold factor τ_d, and allowing the search to take on this value $+/- 10\%$ of the estimated value of τ_d the search criteria can be narrowed, reducing the likelihood of becoming stuck in local minima. The SINR metric does not factor into account the spectral shape and interference bandwidth, but provides a rough indicator of performance suitable for initializing the golden search. While the actual results are dependent on the nature of the interference and scene content, this approach provide a search margin for the golden section method. The values do not need to be exact as they are merely providing a starting point for the optimization procedure.

Using the global optimization procedure particle swarm, the true minimum can be found. There is a general trend between the threshold factor and the SINR. As shown in Figure 5.6, by initializing the golden section method with the values indicted by the
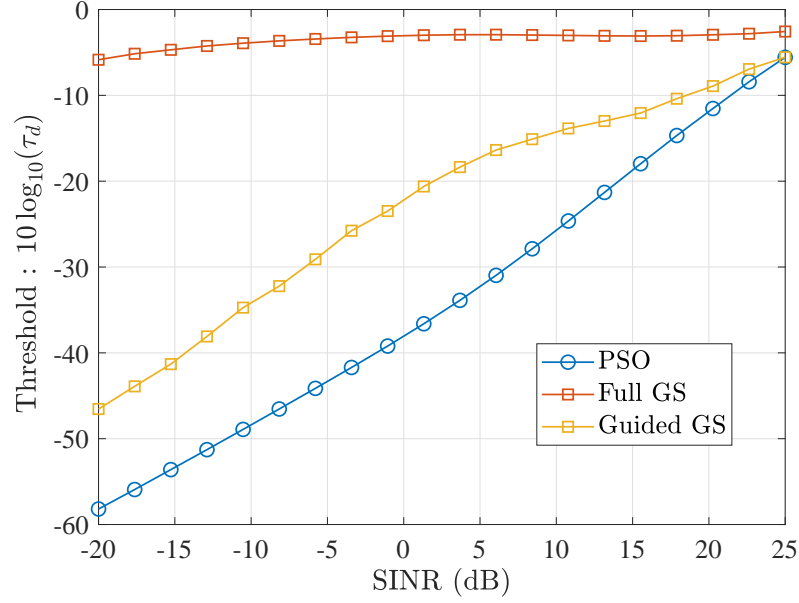
Figure 5.6: *Numerical search for optimal threshold across different time domain SINR interferences at 1% RFI bandwidth for a distributed scene. The algorithms used are the golden search across the full range of τ_d, particle swarm optimization and golden search with specifically chosen search ranges*

SINR, the accuracy of the result, compared with the particle swarm algorithm which is assumed to be the true minimum, has improved. It is shown that the global optimization procedure tends to find lower optimal threshold values. The cost function tends to have slowing gradient near the minimum in which the golden section method converges as the performance difference is less than $1e^{-4}\Delta\rho_0$, the global method continues to iterate until a much smaller convergence criteria is met as it will not become stuck in local minima. These differences in optimal threshold however do not greatly impact the performance due to the slower gradients that can be observed around the minima relating to little change in performance.

5.2.4 Cost Function Estimation

On designing the waveform, the performance cost function must be evaluated by obtaining; a recent estimate of the interference D_i, the frequency response values H_i that will be omitted, and the total waveform energy E_T. Obtaining the current estimate of the penalty parameter of the cost function is problematic in two ways. Firstly, an estimate of the overall energy loss in the return of the next frequency response is required.

Clearly this cannot be known a-priori as this is the desired outcome of the radar data acquisition process. The interference may not change pulse to pulse, but by the nature of SAR data collection, there will almost certainly be a change in frequency response pulse-to-pulse to some extent. Secondly, by not transmitting energy within a given band $\mathcal{S}$, there is a lack of historical information on the frequency response to then make an estimate of the next measurement. Under the waveform design scheme where holes are being placed in the spectrum, this data may not ever be collected. Both problems are missing data problems. As in many applications for missing data, the existing data must be exploited in some manner to predict or assume something about the missing content. Proceeding, it is worth noting that it is not each sample of the frequency response required but the summation over all samples squared.

$$\sum_{i \in \mathcal{S}^{\complement}} |H_i|^2 \tag{5.20}$$

It is postulated that the requirement of a summation, and not the individual values, then gives the problem the freedom such that only an estimate within the correct magnitude will be sufficient. Possible approaches to providing an estimate are as follows:

- Use the frequency response for the immediately prior pulse - while the nature of the synthetic aperture means that the ground frequency response is changing due to changed position and angle, overall the change between pulses is small. In terms of energy, there is the same total response from the scene, but the sample to sample magnitudes are subject to a change within this limit at each pulse. The summed value over a number of pulses may then gives more leeway - the changes sample to sample may be high with respect to the value of the measurement (depending on platform motion), but the change in summed average will not be significant in terms of order of magnitude.

- If the prior pulse frequency response has gaps in the spectrum due to waveform design or is corrupted with a high level of interference, there are two options; 1) take a crude estimate of the frequency response using the mean value across the existing data, assuming that the ground can be represented as wide sense stationary. 2) interpolate using a fast AR method to obtain an estimate of (5.20).

- Use autoregressive methods along the slow-time data collection to extrapolate

the data to predict the total energy loss. This is likely to be a computationally inefficient approach due to the possibly low information gain with respect to high computational cost

The waveform design has to adapt to both the possible change in interference, and the certain change in frequency response over the azimuth run. While changes in frequency response may be slow on a pulse-to-pulse basis, they are guaranteed to change over the course of the azimuth data collection at a rate proportional to the pulse-repetition interval(PRI). The longer the PRI, the more change that will be observed from a moving platform.

There are two key cases to consider when using the previous frequency response measurement. Firstly, the most common case in this scheme, in which the previous frequency response has a gap in the spectrum. The second case is where a new interference source has appeared in the previous pulse and has corrupted the frequency response in a region that was previously unexpected. In this scenario, the system identification is able to locate the frequency bins with the highest interference so that these samples are not used for estimating the next frequency response. Both of these cases then lead a gap in the frequency response of the scene.

To carry out waveform design, methods to estimate the penalty function with missing information are explored.

Method 1: Basic Averaging

To design the next waveform, the frequency response from the previous pulse H^{P-1} is used which is assumed to have spectral gaps. The assumption is made that the average of absolute value of the frequency response squared of the known samples is approximately equal to the value across the unknown samples

$$\frac{\sum_{i\in\mathcal{S}}|H_i^{P-1}|^2}{N_a^{P-1}(\tau)} \approx \frac{\sum_{i\in\mathcal{S}^{\complement}}|H_i^{P-1}|^2}{N_m^{P-1}(\tau)} \tag{5.21}$$

where N_a is the number of available samples and N_m is the number of missing samples. For scenes where the frequency response is wide sense stationary, this assumption should hold well.The penalty function is then calculated so for each threshold estima-

tion carried out in the optimization procedure, only the corresponding new number of missing samples requires updating.

$$\rho_{\mathcal{S}^{\complement}}(\tau) = \frac{N_m(\tau)}{N_a^{P-1}(\tau)} \sum_{i=1}^{N_a^{P-1}} |H_i^{P-1}|^2 \tag{5.22}$$

Method 2: Autoregressive Interpolation

Again, using the previous gapped frequency response, the individual values aim to be filled in using autoregressive interpolation. This method is detailed in full in Section 5.4. Using the existing values in the previous frequency response $H_{\mathcal{S}}^{P-1}$, forward and backwards linear prediction aims to fill in the missing samples. These samples can then be inserted into the usual equation for the penalty value (5.20). This method comes at a much higher computational expense than averaging, for each missing sample AR coefficients must be calculated according to the input data, before performing the actual estimation of the missing sample.

Figure 5.7 demonstrates an example of these methods applied to a single realization of the absolute value of the frequency response. As shown the averaging method appears to taper over the gap in a simplistic manner whereas the AR approach shows sample to sample variation.
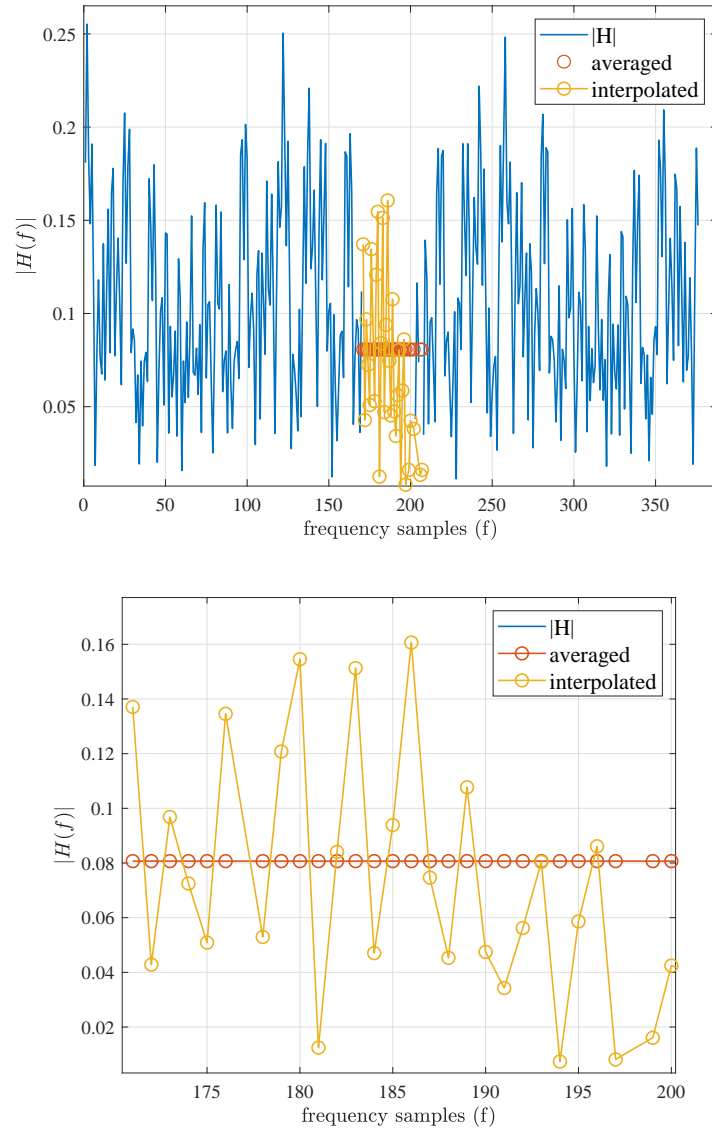
Figure 5.7: *Assumed values of |H| used for estimating the penalty value - both the averaged and interpolated values are shown for a sparse scene frequency response. Zoomed in plot of gap shown below*

Spectral Gap Estimation Impact on Performance

The following simulations were carried out with the intention of demonstrating the impact of frequency response estimation over the gap using previous information, compared to the optimal outcome using the true frequency response of the current pulse of

interest. The simulations are based on those described previously, values can be found in Chapter 4 or Appendix A. The pulses are based on pulse 2-4 of the SAR collection to allow initialization of a gapped waveform.

The example considers two consecutive pulses (pulse 3 & 4), the first of which has already been designed to have a gap in the spectrum $\mathbf{X}_{S(\tau)^{\complement}}^{P-1}$ according the chosen threshold τ^{P-1} based on the known measurement of the interference two pulses ago $\mathbf{D}^{P-2}$ and the predicted frequency response loss calculated based on $\mathbf{H}^{P-2}$. The second pulse in the experiment is the current pulse which is under design. Using the most recent interference estimate obtained from the prior pulse $\mathbf{D}^{P-1}$, and the gapped frequency estimate $\mathbf{H}_{S}^{P-1}$, results for the different proposed methods of estimating (5.20) are compared. To demonstrate how the performance changes with increasing interference levels, and therefore differing threshold levels, the same experiment is conducted at different SINR levels.
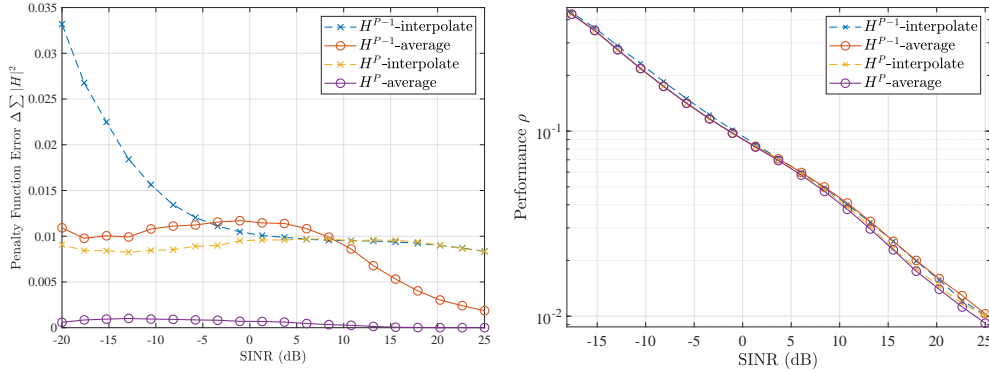
(a) *Differences between the estimated penalty and actual penalty value* **(b)** *Final performance value for distributed scene*

Figure 5.8: *Results using different methods to approximate missing frequency response show for both the penalty value and overall performance. The previous pulse with a gap is used to predict the next transmitted waveform.*

Figure 5.8a shows the direct difference in penalty value between what the true frequency response in the gap is, and the estimated gap for the averaging and interpolation method. This is demonstrated here for a distributed scene where the frequency response exhibits high levels of sample to sample variation - exemplifying a worst case scenario (sparse scenes with fewer strong target returns have less sample to sample variance).

High sample to sample variation referring to the variation being on the same scale as the value of the measurement itself. AR methods struggle to model the rapid changes and a small gap may not represent the average value for the averaging method. While it is not possible to obtain the current frequency response method before waveform design, it is shown here for comparison purposes - this has been obtained in simulation by firstly calculating the optimal gapped waveform using the true penalty value (known to the simulation by design), then using the return to estimate the frequency response. The best performance shown is the result for the difference in penalty value (5.20) between the estimate and true value and applying the averaging method to the current pulse frequency response result. All method's performances are related to the quality of the frequency response estimate they are based on which decreases with SINR. The interpolated approach has a larger performance error than the averaging method, for both versions. Overall, the scale of error compared with the frequency response value is small. This then results in a very small impact on the performance difference as shown in Figure 5.8b. As the SINR decreases, this error in penalty estimate is smaller in comparison with the additional error due to interference and more missing data in the system. Then, it is concluded that estimation using the summation across the penalty value is a reasonable substitute for the lack of the known frequency response estimate.

5.2.5 Waveform Synthesis

The previous Chapter demonstrated that for a continuous spectrum, the SPA provided a suitable fit to an input spectrum. As an approximate method, the SPA struggles to replicate the deep nulls under the constant modulus amplitude constraint. While the waveform synthesis is a secondary consideration to the FDWO method, it is a considerable factor in the final perfomance. Ideally to produce deep notches, a more computationally expensive but precise synthesis method would be used such as [64], however this does not support functionality for the adaptive element of the system. Instead, the proceeding results are shown for direct synthesis, assuming this has been achieved via some means such as OFDM waveform synthesis. For a more practically realistic comparison, the results obtained using SPA are also shown. This problem in itself is a research topic in its own right, and it outside the scope of the research here.

5.3 Performance Evaluation

5.3.1 Simulation Set-Up

The estimated optimal waveform for varying levels of interference are shown in terms of their resultant constrained frequency response MSE and the resulting interference estimate MSE. When the threshold is at the maximum, the penalty term disappears, so is plotted to compare the results against the competitive case. The case where the threshold is chosen to fully remove interference at any value above the noise floor is shown as τ_{min}. This result is then combined with the waveform design and system identification approach as before, but with the pre-selected threshold. The result with the same noise-floor threshold is also shown for a standard LFM and matched filter where all frequency samples with interference present are notched out on receive. As the SINR increases, the performance decreases linearly with SINR for the full competitive case, while the gapped spectrum case decays at a slower rate - shown in Figure 5.9a. The competitive performance is entirely dependent on the increasing level of error in the frequency response according to the ρ_S term. The gapped spectrum case has slower decaying performance as it removes the highest interference contributions but then adds to the error by removing more samples as the interference strength increases (and the optimal threshold also decreases). The minimum threshold case does not change as the interference increases as all the contributing interference above the noise floor are removed at all cases. This comparative result then demonstrates the performance gain that can be made using this optimal threshold waveform design method, as opposed to standard operation where all interference is removed.
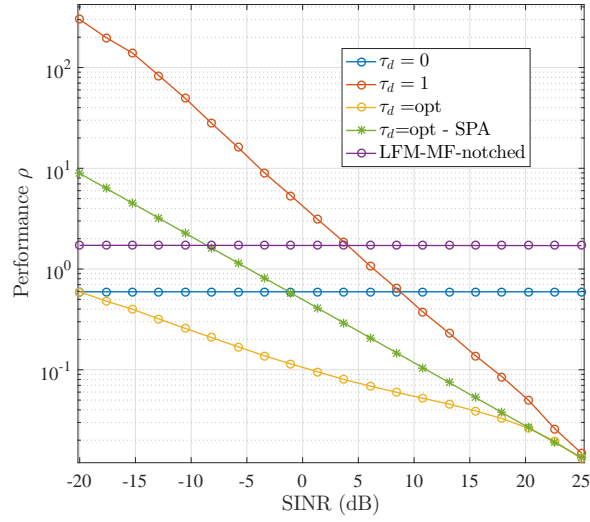
(a) *Frequency response MSE*
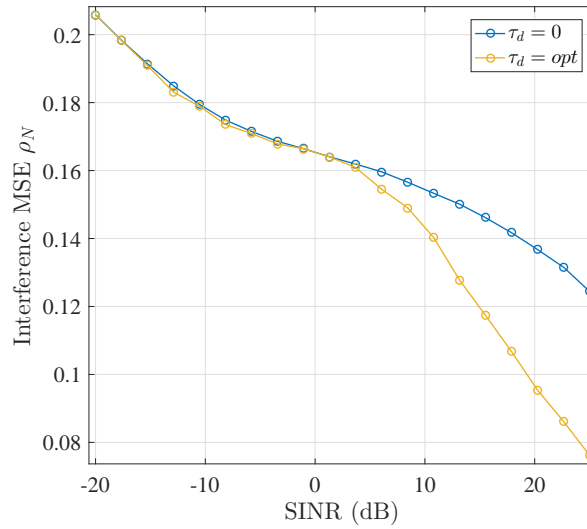
(b) *Interference estimate MSE*

Figure 5.9: *MSE performance results with 5% RFI bandwidth present for varying SINRs*

For the interference estimate, the competitive case performance degrades linearly with the SINR in dB, as demonstrated in the previous chapter, but is not shown here due to its effect on the scale of the graph. The differences between the interference estimate error from the optimal and the minimum threshold case are small. This is as a result of the direct measurement of the interference where the waveform does not transmit

- as shown in (5.4). The low threshold case performs similarly to the optimal case as the interference is measured directly in the gapped spectral region, the additional performance gain available in the optimal case is due to the improved interference estimate obtained from $\rho_{\mathcal{S}^{\complement}}$ - the overall MSE is improved here in the optimal case.

An example interference spectrum and the resultant waveform is demonstrated for four different interference levels in Figure 5.10. Three waveforms are shown; the resultant optimal threshold waveform, the competitive case, and the minimum threshold case. In the first example at 20dB SINR, the threshold creates a small gap where the strongest interferer lies. Increasing the interference to 10dB SINR, the threshold lowers further and a larger waveform gap is created. At -5dB SINR, for this case the minimum threshold waveform and the optimal waveform are very similar. There is very little change between the threshold here and for the following result at -20dB SINR. This is a good example of the effect where the performance function does not see much change in performance for relative threshold value. The total relative threshold factor value has changed as interference dynamic range is 65dB in example c) but 85dB in example d). Although the optimal threshold factor has changed, the resultant waveform and performance has only differed slightly.

This waveform design method finds particular use for a spectrum with multiple interferers as shown in this case. The transmitted energy below the threshold operates in a spectrum competitive way to maintain the minimal MSE. For example, if across the radar bandwidth there are stronger and a weaker interference sources, the waveform optimization will choose the appropriate threshold to compete where possible, and place spectral holes otherwise. Also for wider-band interference signals that spill energy across multiple neighbouring bins, this technique will find the optimal level to compete or avoid at no additional computational cost.
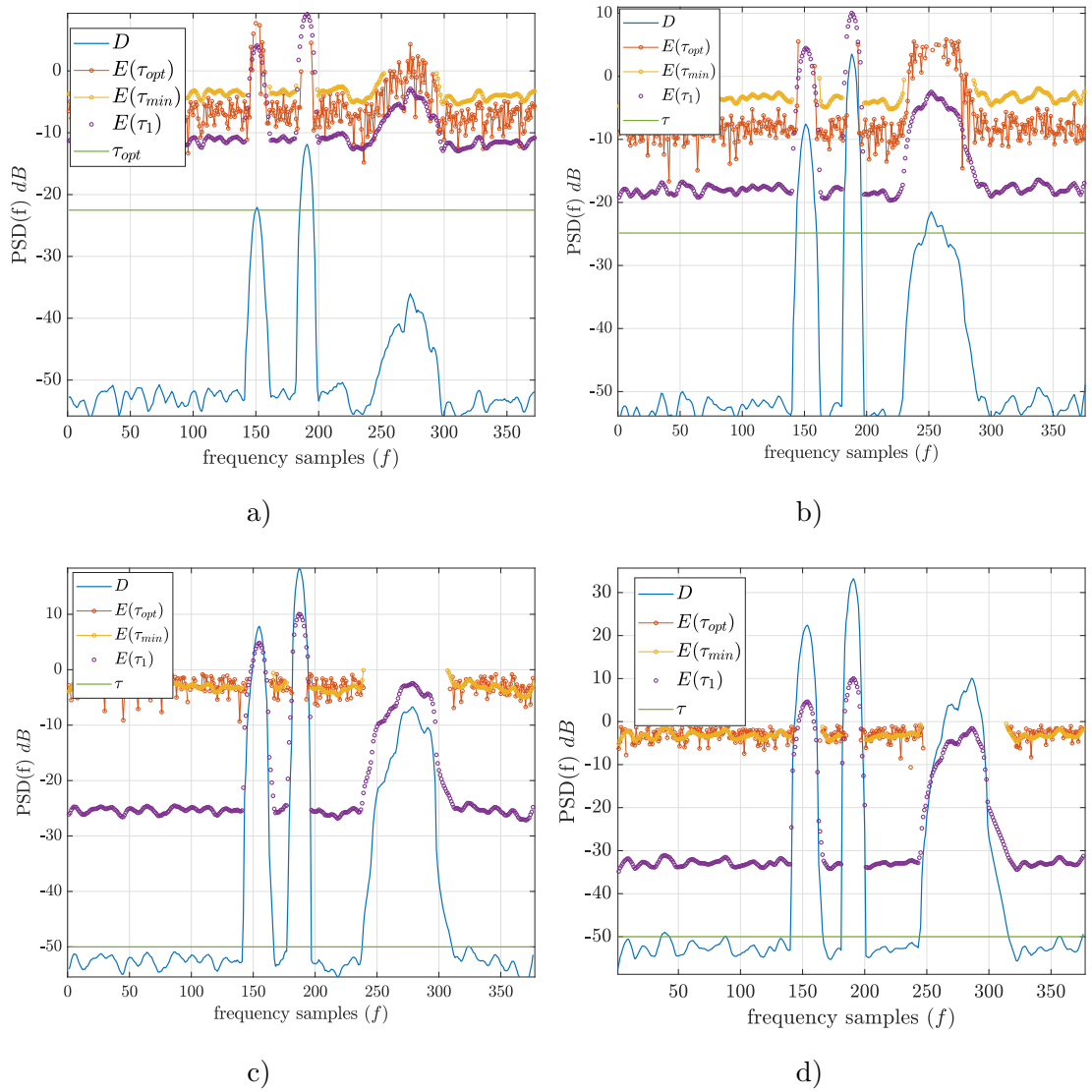
Figure 5.10: *Waveform design plots in frequency domain at respective SINR: a)20dB b)10db c)-5dB d)-20dB*

5.3.2 SAR Image Result

To demonstrate the performance impact of correctly designing the threshold according to the interference level and using the developed waveform design criteria, a series of example SAR images are shown. The interference has been kept constant across the collection and averaged according to the exponential smoothing criteria also used in the previous chapter. At each pulse, the prior pulse is used to predict the gap using

137

the averaging method detailed in Section 5.2.4. The interference estimate is updated at each pulse according to an exponential smoothing window, where the averaging window is 10 pulses long. The constrained impulse response vectors for each pulse are then formulated from the constrained frequency response vectors by application of the IFFT. Each of the impulse response vectors are then used in the back-projection image formation. Two contrasting sets of images are shown, one at 5dB SINR where the competitive case is still applicable as demonstrated previously, the other at -20dB SINR at which point the competitive case has significantly degraded. Also shown is the case where any interference above the noise-floor is notched out ($\tau_d = min$). This is also applied to a LFM-notched matched filter, where any interference above the noise floor has a null placed at the relevant receive frequency.

a)   b)   c)   d)

e)   f)   g)   h)
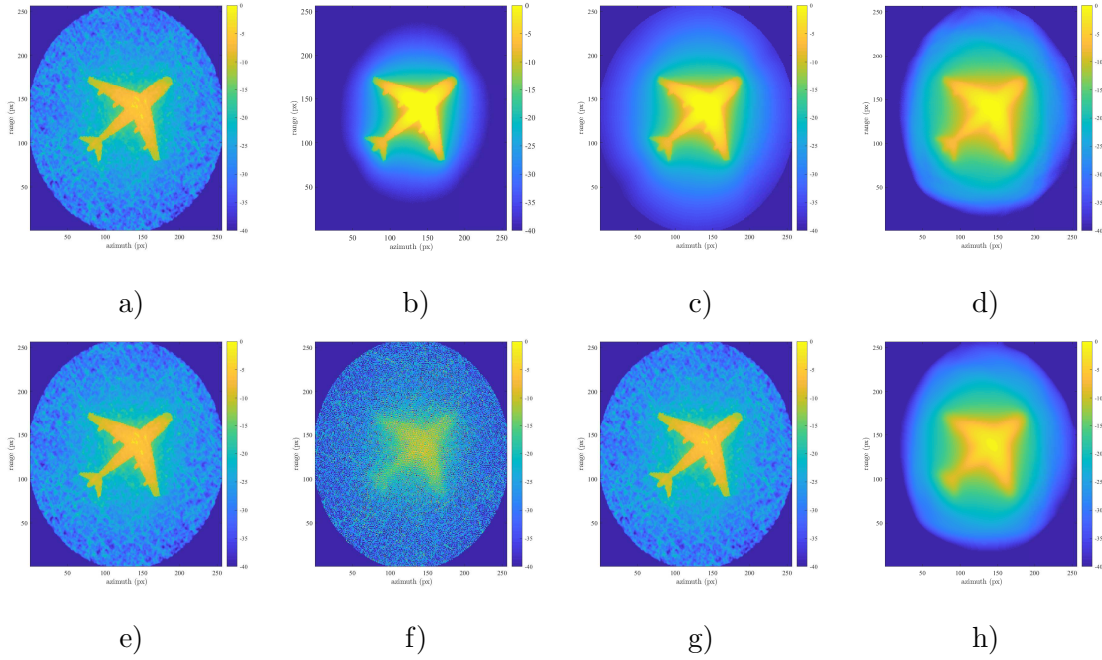
Figure 5.11: *Figures a - d represent images formed at 5dB SINR, figures e - h represent images formed at -20dB SINR. Images a & e are formed with $\tau_d = min$ threshold, b & f formed with $\tau_d = 1$, c & g τ_{opt} and d & h are formed using a matched filter where frequencies with interference are notched out on receive*

The images at 5dB appear to be of similar quality for $\tau_d = opt$ and $\tau_d = 1$, whereas the fully notched cases show additional artifacts and some further blurring - particularly for

the notched matched filter. Increasing to -20dB, the competitive case is by far the worst image result. The results for the minimal and optimal threshold are similar, as artifacts have been introduced due to the missing spectral components in the optimal case as more samples have been removed due to higher interference. The result for the notched matched filter appears to be unchanged, as the processing is the same regardless of SINR.

5.4   Spectrum Recovery

It has been discussed that creating gaps in the spectrum causes a decrease in the performance in terms of the frequency response MSE due to raised sidelobes throughout the range profile. There are a class of methods which attempt to refill the spectrum based on the available data. As the waveform design creates gaps in the spectrum, it is then appropriate to consider these interpolation algorithms as a post-processing step to produce an enhanced estimate of the frequency response. This allows the formation of images without holes in the spectrum, improving the final image MSE. Additionally, by improving the estimate of the existing estimate of $\mathbf{H} \in \mathcal{S}$ through minimising the MSE by waveform design, it is proposed that an enhanced estimate of $\mathbf{H} \in \mathcal{S}^{\complement}$ can be made by refilling the spectrum, compared with a transmitted LFM signal, notch-on receive and then re-fill. Reconstructing missing phase history has previously been demonstrated by a collection of algorithms [88], [89]. The most successful application in terms of result for computational cost are generally accepted to be gapped APES [90] and the autoregressive method AR-Burg [89]. Below the basic operation of the algorithms and any assumptions made are briefly noted.

5.4.1   Gapped Spectral Estimation

The amplitude and phase estimation (APES) algorithm is a matched filterbank approach to amplitude spectrum estimation. GAPES is the extension of the algorithm to include gapped data and has previously been successfully applied to missing phase history problems where the image range profile is set up as a spectral estimation problem [90]. The filterbank that is used by APES and its resulting estimated spectrum can be used to minimise a least squares criterion which can also be applied to the missing

data. The least squares criterion then iteratively restores the missing samples, based initially on the APES filterbank and spectral data that is constructed from the known data. The only assumption this algorithm makes about the unknown data is that the missing samples have the same spectral content as the known data. In this context, the spectral data is the impulse response of the scene, and the time-series data is the phase history. (In SAR it is common in across areas to interchange the labeling of the impulse response of the scene as time series data or frequency data, depending on how the phase history (or frequency response) data is then delimited. It has no bearing on the end result and is merely a notational preference.) This assumption that the spectral data from the missing samples is the same as the known samples has previously been shown to hold well for a small number of spectral peaks, which in this context corresponds to a scene with few strong reflectors. This assumption then does not hold well for a homogeneous scene with many targets of similar strength, corresponding to a high density of spectral data to be recovered.

The creation of the filterbank depends on the construction of full-rank covariance matrices. The length of the filters then need to avoid including the "edges" of the data (start and end), to avoid including zeros representing discontinuities that do not correctly model the data. This must be taken into account again when introducing the gaps in the data, enforcing lower filter lengths. It has previously been shown that longer filter lengths increases the resolution of the estimate, but at the cost of less statistical stability. Higher spectral resolution can be obtained by defining a higher resolution grid to estimate the spectrum. Choosing a suitably low length filter to avoid discontinuities in the data and pairing this with a grid that is finer than the original Fourier samples to yield a result with a high resolution, that is also numerically stable. GAPES has a disadvantage in that its computational expense is high. The original filterbank estimation requires a covariance matrix inversion for every spectral point to be estimated. The covariance matrix is of dimension $L \times L$, where $L = N - M + 1$ and N is the total length of the time-series, and M is the chosen filter length. So by decreasing the size of the filter the cost of the matrix inversion is increased, in addition to the expense incurred by introducing a finer spectral grid to increase the resolution. However, as each pulse is processed independently, this does not need to be performed on the fly and can be applied to the data after collection. As the waveform design at each pulse optimizes the scene based on the interference to improve the estimator input data, there is no benefit

to processing the spectrum-refilled data on a pulse-to-pulse method on the fly.

5.4.2 Linear Prediction

Auto-regressive (AR) models represent a stochastic signal by expressing each output variable as a linear summation of its own previous values. The current value of an AR sequence is calculated as a linear combination of the past p values, determined by the order of the model p, plus input white noise

$$y(n) = -\sum_{k=1}^{p} a(k)y(n-k) + \epsilon(n) \tag{5.23}$$

where $y(n)$ is a stationary stochastic signal and ϵ is white noise. The estimation of the autoregressive parameters $a(k)$ can be performed by a variety of methods, namely the Yule-Walker, Levinson-Durbin algorithm (LDA) and the Burg algorithm (which itself uses the LDA). The estimation algorithms are driven by recursively minimising the sum of the squares of the error between the original and approximated values. The Burg algorithm uses the LDA but with different inputs to obtain a more numerically stable result. The LDA approach directly estimates the autoregressive coefficients, while the Burg algorithm estimates the reflection coefficients which represent the time dependence between $y(n)$ and $y(n-k)$ after filtering out the prediction from the previous $k-1$ samples. Comparisons between various AR estimators show the Burg algorithm to have lower bias and better numerical stability [109]. Moreover, this particular AR-estimator method has been previously implemented for a missing phase history.

5.4.2.1 Implementation

The missing frequency response data from the scene is assumed to be an autoregressive stationary process, such that its AR coefficients can then be estimated using the Burg algorithm. With the exception of the missing samples, the data is uniformly sampled, which allows application of the Burg method. Using both forward and linear prediction, the existing data allows interpolation into the gap from either side. The Burg algorithm has a modified version specifically for segmented data, which readily fits into the context of the missing data problem, allocating the segments into the region before and after the gap [110]. The implications of segmenting the data are that the maximum possible

model order is reduced; the larger the spectral gap, the lower the maximum model order can be. However it is worth noting a higher model order does not correspond to a better fitting AR model - higher order models can lead to overfitting of the data. The optimal model order can be calculated by minimising Akaike's information criteria [111]

$$AIC(p) = \ln(\text{RES}(p)) + \frac{2p}{N} \tag{5.24}$$

Where RES is the residual variance of the model calculated for a model order p, N is the number of samples in the data set - in this case $N = k + M$.

5.4.3   Comparison of spectrum recovery techniques

A series of experiments were carried out to demonstrate how the algorithms perform in the context of this work. For increasing interference SINR, the difference between the algorithm MSE and the raw data MSE is demonstrated - both for a sparse scene with just 1% of the overall range profile is populated, and for a distributed scene with every cell in the range profile populated with a complex value. A distributed scene is homogeneous with no significantly strong point targets and exhibits a frequency response with higher levels of covariance. A sparse scene represents the opposite scenario with only a very small number of targets and a relatively flat frequency response. Results in Figure 5.12 are averaged over 100 Monte-Carlo runs, where the impulse response and interference are non-deterministic. Shown in Figure 5.13 is a realization of the frequency response recovery and in Figure 5.14 the resultant range profile for the gapped, the AR-Burg and GAPES recovered data.
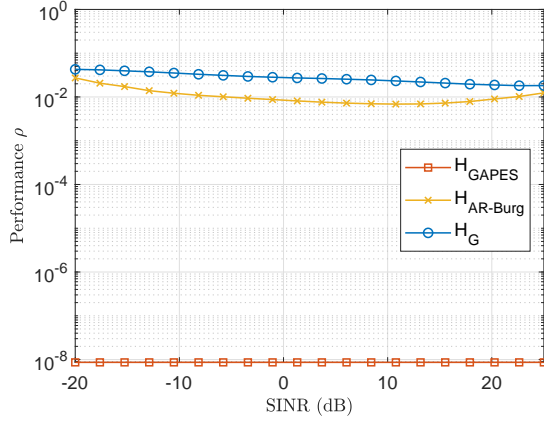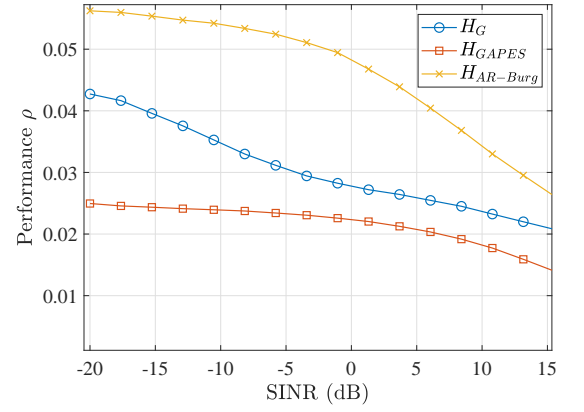
(a) *Sparse scene frequency response recovery*   (b) *Distributed scene frequency response recovery*

Figure 5.12: *Spectrum recovery results in terms of MSE for varying SINR*
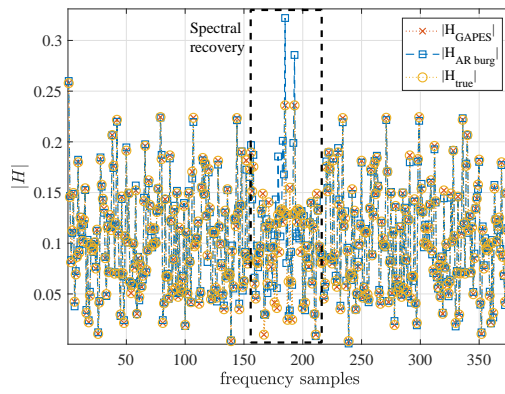
(a) *Sparse frequency response*   (b) *Distributed frequency response*
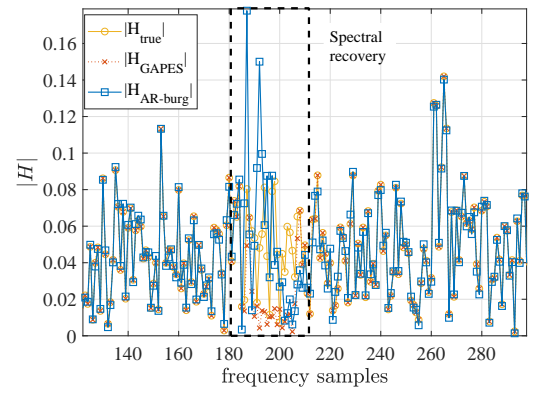
Figure 5.13: *Example realizations of frequency response recovery*

143

(a) *Sparse scene*

(b) *Distributed scene*
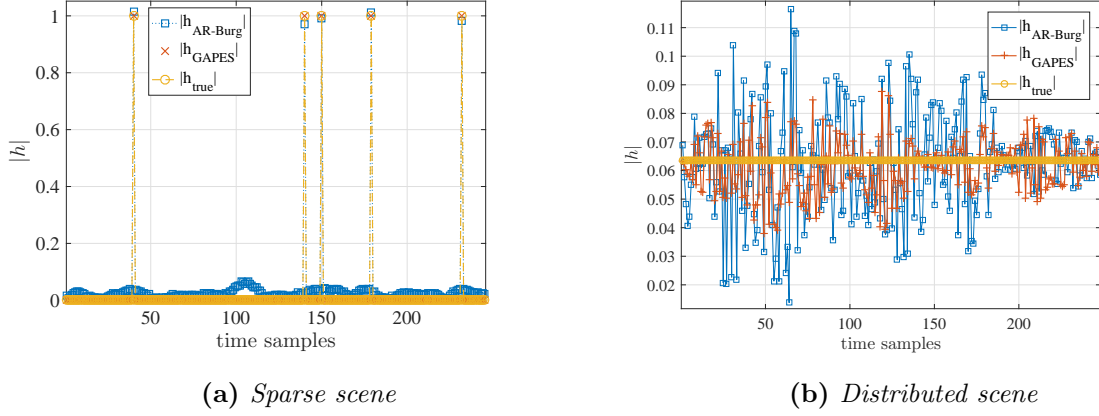
Figure 5.14: *Example realization of final impulse response after spectral recovery*

The sparse scene recovery using the GAPES algorithm is very accurate, recovering the original frequency response to the level of numerical precision of the data. For a sparse scene, the small number of targets corresponds to a small number of superimposed frequencies for the GAPES algorithm to recover, which is easily recoverable from the existing data. The performance degrades for a distributed scene, which represents a large number of frequencies to recover - the missing frequency samples are then not easily obtainable from the present data. The GAPES algorithm is very computationally expensive, but outperforms the AR-Burg algorithm for all observed data points. For the sparse scene, AR-Burg improves the gapped data, but worsens the estimate of the gapped data for a distributed scene. For scenes with fewer targets, the recommended algorithm would be AR-Burg to save on computation time, but for homogeneous scenes with no or little distinctive targets, the GAPES algorithm must be used to yield improved results. For many SAR scenes, the AR-Burg algorithm should be applicable, as many images have targets with larger reflectivity and particular reflectors of interest, particularly in military applications.

5.5 Simulated SAR Images

To demonstrate the final result of the adaptive process and spectrum re-filling the following Section details a series of SAR image examples.

5.5.1 Example 1: Constant Interference Source

For a constant interference source, exponential averaging provides an increasingly accurate statistical estimate of the interference. The waveform design is updated at each pulse according to the most recent estimate of the interference and the previous frequency response estimate. The interference estimate is updated with an exponential smoothing window of length 10 pulses, and the frequency response gap penalty is estimated via averaging described in Section 5.2.4. With few other parameters changing, this example can clearly demonstrate the final results between the different interpolation algorithms. It is observed that compared to the gapped spectrum image, using
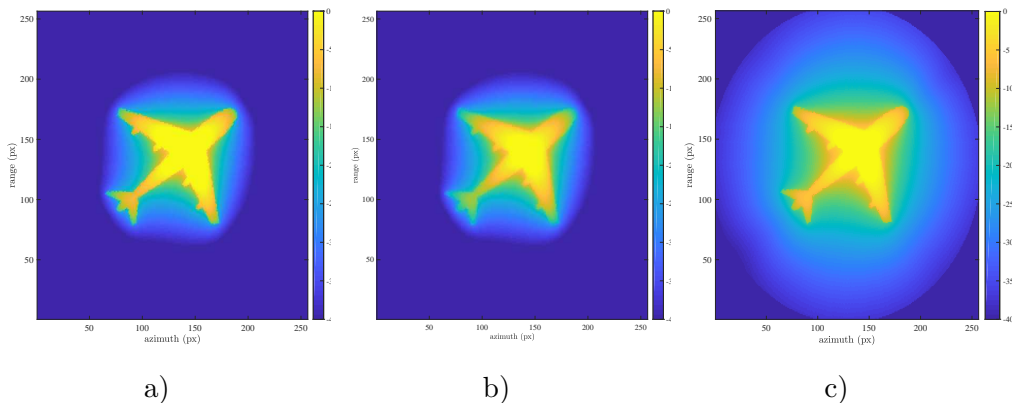
Figure 5.15: *Waveform design and spectrum recovery at 0dB SINR: a) GAPES-recovered image b) AR-Burg recovered image c)Image with holes in spectrum*

spectral recovery lowers the sidelobe levels which then increases the possible dynamic range of the SAR image. The example shown in Figure 5.15 shows that GAPES provides the best quality image in terms of blurriness. Both images offer similar levels of dynamic range.

5.5.2 Example 2: Changing Interference Source- Sweep

In parallel to the example in the previous chapter, an interferer which has a sweeping centre frequency across the radar bandwidth during the azimuth run is simulated. The example in 5.15 shows the resulting impact on image formation when the image is updated at every pulse, every 10th pulse and every 50 pulses out of a total of 500 azimuth collection points. Due to the interference changing between pulses and the

145

most recent possible update being the one prior, this exemplifies the best effort in the worst case scenario, as the update scheme cannot obtain interference updates spectra on an intra-pulse basis. Comparing the image in Figure 5.16a to the prior example, Figure 5.16, shows the level of degradation caused from changing interference pulse-to-pulse. Some additional blurriness is caused, but the image quality is still reasonable. As expected, the images show increasing levels of distortion with lessening waveform update rates. At higher interference levels which changes pulse-to-pulse as shown, the waveform must be updated more regularly to avoid corrupting the frequency response estimate.

a)   b)   c)
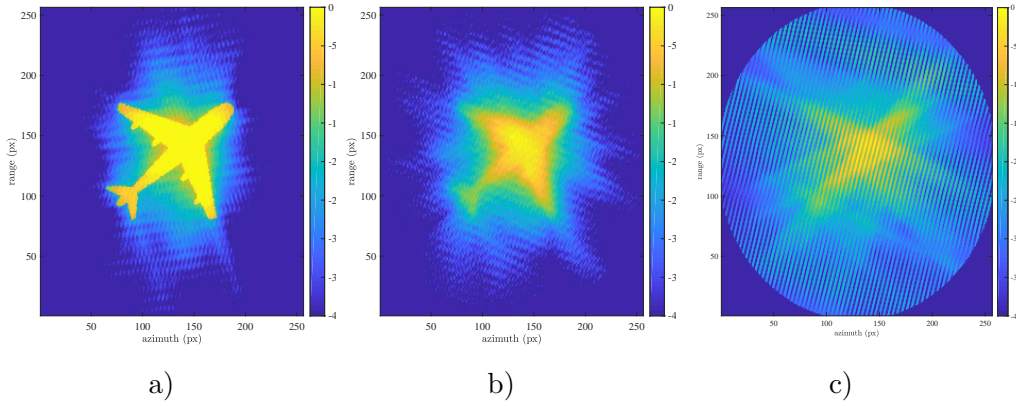
Figure 5.16: *Waveform design and spectrum recovery using GAPES at 0dB SINR with interference changing pulse-to-pulse: a) Update at every pulse b) update at every 10th pulse c)update at every 50th pulse*

5.6   Adaptive System Overview

This Chapter has proposed an extension to the adaptive waveform design technique based on the initial system identification and FDWO concept with added spectral avoidance. The waveform design and system identification process depend on applying a threshold to the interference estimate to separate the frequency-domain data into two regions; firstly a set where the interference is deemed too disruptive to compete and waveform transmission should avoid transmission and secondly, a set where the waveform should transmit its energy optimally to minimise the impulse response MSE. In the case where the interference is too high, the system identification process has high levels of interference in the frequency response and the interference estimate is very low

- neither result is then useful for the adaptive system without additional processing, for example using computationally expensive methods that are infeasible on the fly to estimate and subtract interference. The key difference from the competitive approach is the requirement of partial information on the scene frequency response, as demonstrated in Section 5.2.4.

Now the full system has been discussed, a possible outline of the system logistics are discussed here, including: the initialization of the system, the adaptive scheme with waveform design and the system identification receive filter and additional post-processing leading to image formation.

5.6.1 System Initialization

As the radar system is switched on, it is beneficial to have a measurement only period before transmission, sometimes known as a "sniff", to obtain initial information on background noise and interference levels at the receiver. If there is interference present, this measurement will be used in the waveform design. However, an estimate of the scene frequency response will also be required if the interference is suitably high and therefore it is likely that the waveform design criteria chooses to place gaps in the spectrum. An appropriate course of action could be to initially estimate a threshold according to the overall SINR, as was done to refine the optimization search in Section 5.2.3. In low SINR levels an LFM signal can be transmitted in order to obtain a rough estimate of the full frequency response and the interference profile. This cannot be used if the interference is very high on receive as the estimate of the frequency response can be significantly degraded.

5.6.2 Scene Data Acquisition

After the initial measurements of the frequency response and interference have been obtained, the waveform can be redesigned at every pulse according to the most recent gathered interference data or a decision can be made at each pulse based on whether the interference has changed more than a user defined parameter to the interference when the waveform was last designed. This is also run alongside a check with the change in frequency response. As the previous competitive system only needed information

on whether the interference had changed - if the background interference source did not change, the waveform could remain the same throughout the entire data collection. In this scheme, with the added dependence on the ground frequency response, the waveform may require more redesign as the frequency response will change across the aperture. The frequency response changes slowly pulse - to - pulse, depending on the PRI and the change in look angle and if there has been any change in scene content. If the radar platform is moving rapidly, this will cause a larger change in angle and require a higher rate of waveform re-design.

5.6.3   Data Recovery

After the adaptive data-acquisition period is complete, any missing frequency data samples can be recovered offline as the waveform design has gathered the optimal impulse response MSE at each pulse. SAR images can be created with these missing gaps, but for optimal image performance, an attempt was made to refill these in the interest of reducing sidelobes, MSE and any artifacts caused by the missing data.

5.7   Chapter Summary

This chapter has expanded on the competitive waveform design framework by using information on the scene frequency response to alter the optimization process to allow creation of a gapped waveform spectrum where it improves the frequency/impulse response MSE. It has been demonstrated that the results will either be equal in performance or better than that possible for the competitive framework. The waveform design continues to act in a partially-competitive manner by placing spectrum energy where interference lies to obtain a better estimate of the frequency response, but now additionally allows the gaps at the spectral locations where the interference is too disruptive to the estimate of the frequency response. Placing a threshold on the interference makes a binary decision on which samples to compete with, and which to avoid. By allowing gaps, a penalty term is introduced which causes some degradation of performance, manifested as a rise in sidelobes, reduction in resolution, and therefore a reduction in the dynamic range in the SAR images, reducing the ability to image low reflectivity scatterers. As is standard in the missing phase-history problem, spectrum recovery has

been achieved by using the GAPES algorithm for both sparse and distributed scenes. This method is slightly more computationally expensive than the prior due to the requirement for 1D numerical optimization at each pulse. However, relative to alternative waveform design optimization methods such as those described in [27], this 1D approach requires far less computation and is still expected to be a feasible method for on the fly waveform adaptivity.

There are several complexities that are included when considering a waveform with spectral gaps. Firstly an appropriate method to recover the lost spectral data and also consideration of whether it is necessary to invest the required compute time to attempt to recover the omitted spectral data. While using the SPA method does not yield the necessary nulls in the spectrum as dictated by the GFDWO, it produces an approximation which still provides improved results to the FDWO for high interferences. Applying the SPA to the GFDWO may not produce deep nulls, but the improved performance is owed to the removal of putting all the energy resources into competing with a small number of large interference bins.

Chapter 6
Chapter 6: Conclusions

This thesis has proposed a solution for RFI SAR mitigation via an adaptive waveform design scheme. The aims and solutions proposed in this thesis are as follows:

1. **Reducing impact of of RFI on resultant image**: The system identification method proposed, the time constrained frequency domain estimate (TCFDE), provided an improved estimate of the impulse response and the interference spectra via spectral waveform design (this result also meets aim 4- to be capable of estimating interference).The methods discussed in Chapter 4 are more suited to narrowband RFI, whereas Chapter 5 methods are more capable of treating RFI with $< 1\%$ of the radar bandwidth. The impulse response estimate is provided on a pulse-to-pulse basis providing a resultant test SAR image which is improved in terms of image clarity (enhanced sharpness of features) and increased dynamic range. Applied in a real system, this would likely correspond to reduction of image blurring, removal of any added lines in the image and the ability to image terrain and other weaker reflectivity targets.

2. **Adaptive solution via low cost computational algorithms**: The adaptive cycle discussed in Chapter 4 consists of: system identification (via TCFDE), waveform design and waveform synthesis (via stationary phase approximation SPA). The newly designed waveform is adapting to the most recent estimate of the interference provided by the system identification, therein lies the adaptivity. The frequency domain waveform optimization (FDWO) method provided a closed-form solution which was developed by allowing an approximation in the frequency domain. As a non-iterative method, this provides a reduction in computation required. Additionally, it scales in complexity with the length of the received signal length M. Depending on the compute power of the radar system, this algorithm is likely capable of running within the span of 1 pulse repetition interval(PRI). This algorithm is of the same complexity as the discrete Fourier transform(DFT).

DFT based algorithms are already run on legacy radar systems so it is plausible that the proposed adaptive method would too. The methods described in Chapter 5 are based on the same adaptive cycle elements of system identification, waveform optimization and waveform synthesis, with modifications. The gapped frequency domain waveform optimization (GFWDO), is not closed-form but uses a 1-D optimization. However, this typically requires only a small number (around 10) of computationally cheap iterations to provide a solution. These iterations do not require the DFT but just vector summation. Therefore the overall combined complexity of the adaptive cycle in Chapter 5 is still $O(M \log_2(M))$.

3. **Is feasibly implementable to current electronically scanned radars**: It was laid out in Chapter 2 that for a waveform to be physically viable, it should have a constant amplitude waveform to allow synthesis via class-C amplifiers and be continually increasing in phase to assist beam-steering. By using the stationary phase approximation, both of these waveform synthesis criteria are met. However, as discussed, in Chapter 5 a more difficult synthesis problem is introduced. While the GFDWO solution dictates that the wavefom sythesizes large gaps in the spectum, these are not obtainable under the constraints of constant amplitude and increasing phase via SPA. There is then some reduction in performance between the desired waveform and the output. It is possible that SPA in conjunction with another method that places notches across the NLFM synthesized waveform may result in an improved waveform synthesis.

6.1 Recommendations and Future work

This thesis has provided a first-look at the necessary theory and demonstrated possible results that could be obtained using adaptive waveform design for interference mitigation in SAR via simulation. The results show that there is a significant improvement in the impact of RFI possible using these methods. However, it is important to take note that these results will be restricted to at some limit by the saturation point of the receiver. After a radar hardware-defined limit, the combined strength of the interference and the return signal will drive the receiver into the non-linear region corrupting the signal. Due to the adaptive nature of the techniques used in this thesis, it has not been possible to use real SAR data sets that mimic the behavior of adaptation in this study.

In the near future, experimental radar systems which employ waveform agility and are software driven facilitated by FPGAs may allow small scale tests of this system. With a controlled interference source, this could more realistically test the upper limit of the radar system for saturation.

To improve the waveform synthesis result in Chapter 5, a study into possible methods for introducing notches alongside SPA in a computationally efficient manner is recommended. There are many existing methods discussed in Chapter 2 i.e. [2, 64], but few that are computationally cheap and that offer good performance. Modifications to the existing SPA method could yield slightly better performance, if a "stop" and "go" method was used - i.e. seperate the synthesis process into bands where transmission is allowed; over time allocating energy for transmission at wanted frequencies and having small periods of no transmission for times corresponding to unwanted frequencies.

It is well-known that high sidelobes pose a significant problem in detection modes - the TCFDE method may be applicable in LPRF modes with a long signal duration and no range ambiguities to provide a sidelobe free range profile. However, the higher Doppler shifts typically found in airborne detection modes are significantly higher than those demonstrated in Chapter 3 for SAR platform motion relative to the ground, which would require further investigation.

As highlighted by [17, 47], the target recognition problem requires a different spectral waveform design solution to the detection problem and also requires a high bandwidth to discern features. The RFI mitigation methods discussed in this thesis may be directly applicable to a target recognition problem which, due to its high bandwidth, is likely to meet the same problems as SAR in the crowded spectrum in its vulnerability to RFI.

The solutions in this thesis were devised using the basis of system identification and optimizing the CRLB to provide the best estimate of the impulse response. Alternatively, this problem could be approached by forming an optimization problem based on the information theory route, similar to the techniques in [17, 47]

Another possible future route of investigation is to use compressive sensing methods [91, 112] to reconstruct the missing spectrum that is removed instead of GAPES or AR-Burg.

Appendix A
Simulations

A.1   Simulation Parameter Values

The basic radar waveform properties used throughout this thesis are as given in table A.1 and are unchanged unless explicitly stated otherwise.

As highlighted in the text, the standard backprojection algorithm [113, 114] was used to form the image with the evaluation of the impulse response at each azimuth position. This process is carried out by initially calculating the range to every bin in the range profile. A matrix representing the number of pixels in the range and azimuth directions is initialized and used to form the image. Once this is defined, the distance between the platform and and each pixel representation of the surface is calculated at each azimuth point. Interpolation is carried out on the estimated impulse response to relate platform-to-range cell distance to the pixel matrix. By using the relationship between the platform distance to each range cell and the estimated impulse response, the pixel distance matrix values are to calculate the value of the impulse response at those positions, creating the 2D image.

A circular SAR platform trajectory has been simulated in the SAR results in this thesis.

The relative parameters used in the simulation are given in the following table:

The parameters used for the scene and relative platform positions were:

Radar System Parameters	Value
Pulse length: τ_c	$3.41\mu s$
Bandwidth: B_c	150MHz
Wavelength: λ	0.03m
Sampling rate: f_s	150MHz
Waveform samples N:	512

Table A.1: *Waveform properties used in simulations*

SAR scene parameters	Value
Platform height: h	1500 m
Range-to-scene centre: R_0	6000 m
Range swath: R_w	512 m
Range resolution: Δ_R	1 m
Range profile samples: K	512
Pulse repetition interval: f_s	150 MHz
Platform velocity:	200 ms^{-1}
Pixel values	256×256

Table A.2: *SAR platform and scene values used in simulations*

A.2   Particle Swarm Optimization

Standard particle swarm optimization (SPSO) has been used in simulated examples in this thesis. SPSO uses swarm intelligence to search a specified solution space for an optimal value [101,115,116]. The optimization problem in Chapter 4 is laid out in (4.4), and the cost function C to be evaluated is

$$C(x) = \text{tr}(\mathbf{X}^H \mathbf{R}_{nn}^{-1} \mathbf{X})^{-1} \tag{A.1}$$

under the constraint that $\mathbf{x}^H \mathbf{x} = E_T$. The optimization is carried out by evaluating the cost function and using the swarm of particles to search for the the smallest value. Each "particle" represents: a potential solution i.e. a position in the search space, a velocity, representing the distance travelled across the search space over a timestep, a cost function evaluation, a memory of the best previous position found up until the current timestep and the best cost function value at this position.

Parameters required in the SPSO algorithm are defined as:

- q_i= current position of particle

- v_i = velocity of particle

- p_i = local best position of particle

- p_g = global best position

- w =inertial weight

- e_1 and e_2 = random number in range: $0 \to 1$

- k= time step (iteration number)

- K_{stop}= total number of iterations

- S= swarm size

Each particle has a position within the solution space according to

$$q_i(k+1) = q_i(k) + v_i \tag{A.2}$$

where the velocity of the particle is given as

$$v_i = wv_i + e_1(p_i - x_i) + e_2(p_g - q_i) \tag{A.3}$$

The solution space spans the possible values which the cost function dependent parameter can take on. In this implementation, a single particle i represents a single solution, but is actually a vector representing the transmitted signal $x_i(t)$. A single solution refers to a series of values forming the waveform vector, and a swarm of S particles would therefore refer to S individual waveforms.

The inertial weight relates to either a exploration of a full search space (high value) or concentrate on local values (low value). There is no clear definitive value for the inertial weight and is largely an empirical value which is simulation dependent. The inertial weight is usually chosen such that $0 < w < 1$ [117]. In this simulated case, the inertial value is set $w = 0.9$, which generally lead to finding the global solution in fewer iterations. The waveform values -i.e. the search space - were constricted to take on values between $-1 < x(t) < 1$ to prevent all the energy gathering around a few samples and to maintain a relatively feasible time-domain waveform.

The standard algorithm is modified slightly to constrain the particle solutions to have energy E_T by rescaling the solutions at the end of every evaluation so that the algorithm block is:

Algorithm 4 Particle Swarm Optimization for GLS

Initialize: set initial guess swarm positions and velocities, choose w and $c1, c2$

1: **for** $k = 1 : K_{\text{stop}}$ **do**
2:     Update velocities
3:     Update positions according to velocities
4:     Enforce constraint by rescaling waveform energy $\mathbf{x}_i^H \mathbf{x}_i = E_T$
5:     Form transmitted signal matrix for each particle $\mathbf{X}_i$ from particle solution $x_i(t)$
6:     Evaluate cost functions for each particle $C_i(x)$
7:     Find new global minimum: check new position costs against current global best
8:     Update local particle position costs: is new position better than previous
9: **end for**
10: Position of global best solution is the optimal waveform $x(t)$

Appendix B

Proofs

B.1 Covariance of Constrained and Unconstrained Impulse Response

Proof that $\text{cov}(\mathbf{H}_u - \hat{\mathbf{H}}_u) = \text{cov}(\mathbf{h}_c - \hat{\mathbf{h}}_c)$ if $\text{cov}(\mathbf{H}_u - \hat{\mathbf{H}}_u)$ is assumed to be diagonal.

The constrained impulse response can be calculated as follows

$$\begin{bmatrix} \hat{\mathbf{h}}_{\mathbf{c}} \\ \mathbf{0}_N \end{bmatrix} = \begin{bmatrix} \mathbf{I} & \mathbf{0}_N \\ \mathbf{0}_N & \mathbf{0}_N \end{bmatrix} \mathbf{F}^{-1} \hat{\mathbf{H}}_{\mathbf{u}} \tag{B.1}$$

To calculate the error in the constrained impulse response

$$\begin{bmatrix} \hat{\mathbf{h}}_c \\ \mathbf{0}_N \end{bmatrix} - \begin{bmatrix} \hat{\mathbf{h}}_c \\ \mathbf{0}_N \end{bmatrix} = \begin{bmatrix} \mathbf{I} & \mathbf{0}_N \\ \mathbf{0}_N & \mathbf{0}_N \end{bmatrix} \mathbf{F}^{-1} (\mathbf{H}_u - \hat{\mathbf{H}}_u) \tag{B.2}$$

The error in the unconstrained frequency domain estimate has been approximated as follows

$$\text{cov}(\mathbf{H} - \hat{\mathbf{H}}) = (\mathbf{\Omega}^H \mathbf{D}^{-1} \mathbf{\Omega})^{-1} \tag{B.3}$$

To estimate the total error the trace is required

$$\text{tr}\left\{ \begin{bmatrix} \text{cov}(\mathbf{h} - \hat{\mathbf{h}}) & \mathbf{0}_N \\ \mathbf{0}_N & \mathbf{0}_N \end{bmatrix} \right\} = \text{tr}\left\{ \begin{bmatrix} \mathbf{I} & \mathbf{0}_N \\ \mathbf{0}_N & \mathbf{0}_N \end{bmatrix} \mathbf{F}^{-1} (\mathbf{\Omega}^H \mathbf{D}^{-1} \mathbf{\Omega})^{-1} \mathbf{F}^H \begin{bmatrix} \mathbf{I} & \mathbf{0}_N \\ \mathbf{0}_N & \mathbf{0}_N \end{bmatrix} \right\} \tag{B.4}$$

Then due to the commutable property of the trace

$$= \text{tr} \left\{ \mathbf{F}^H \begin{bmatrix} \mathbf{I} & \mathbf{0}_N \\ \mathbf{0}_N & \mathbf{0}_N \end{bmatrix} \begin{bmatrix} \mathbf{I} & \mathbf{0}_N \\ \mathbf{0}_N & \mathbf{0}_N \end{bmatrix} (\mathbf{\Omega}^H \mathbf{D}^{-1} \mathbf{\Omega})^{-1} \right\} \tag{B.5}$$

$$= \text{tr} \left\{ \underbrace{\mathbf{F}^H \begin{bmatrix} \mathbf{I} & \mathbf{0}_N \\ \mathbf{0}_N & \mathbf{0}_N \end{bmatrix} \mathbf{F}}_{\text{A}} \underbrace{(\mathbf{\Omega}^H \mathbf{D}^{-1} \mathbf{\Omega})^{-1}}_{\text{B}} \right\} \tag{B.6}$$

Only interested in the diagonal of the product AB to find the trace which is written as

$$\text{tr}\{\mathbf{AB}\} = \text{tr} \begin{bmatrix} \mathbf{a}_1^T \\ \mathbf{a}_2^T \\ \vdots \\ \mathbf{a}_m^T \end{bmatrix} \begin{bmatrix} \mathbf{b}_1 & \mathbf{b}_2 \cdots \mathbf{b}_N \end{bmatrix} \tag{B.7}$$

where $\mathbf{a}_i^T$ is ith row of $\mathbf{A}$ and $\mathbf{b}_i$ is jth column of $\mathbf{B}$ and where A and B are respective parts of equation B.6 as shown.

$$\text{tr}(\mathbf{AB}) = \sum_i \mathbf{a}_i^T . \mathbf{b}_i \tag{B.8}$$

We know that the rows of A are sinc functions. The rows of a and b line up such that only the constant from a_i is needed to give the overall expression. This then dictates that the magnitude of the constant, which is given by the size of the Fourier transform matrix γ gives the relationship between

$$\text{cov}(\mathbf{H}_u - \hat{\mathbf{H}}_u) = \gamma \text{cov}(\mathbf{h}_c - \hat{\mathbf{h}}_c) \tag{B.9}$$

B.2 Sufficient Conditions

For sufficient conditions we consider the bordered Hessian matrix [118] evaluated at the candidate solution; For the bordered Hessian matrix the first row and column are constructed from $\nabla_{\mathbf{E}} g(\mathbf{E})$ and the remaining elements are second-order partial derivatives

of $L(\mathbf{E}, \lambda)$ with respect to the elements of $\mathbf{E}$ [118]. First the constraint, we have

$$\frac{\partial g(\mathbf{E})}{\partial E_i} \quad = \quad 1 \tag{B.10}$$

i.e. a constant as indicated earlier. Then the partial derivatives of the Lagrangian

$$\frac{\partial^2 L(\mathbf{E}, \lambda)}{\partial E_j \partial E_i} \quad = \quad \frac{\partial}{\partial E_j} \left(-\frac{D_i}{E_i^2} + \lambda \right)$$
$$= \quad \begin{cases} \frac{2D_i}{E_i^3} & \text{if } i = j, \\ 0 & \text{otherwise.} \end{cases} \tag{B.11}$$

The bordered Hessian is thus

$$\mathcal{H}_B \quad = \quad \begin{bmatrix} 0 & \mathbf{1}_N^T \\ \mathbf{1}_N & \mathcal{H} \end{bmatrix} \tag{B.12}$$

where $\mathcal{H}$ is an $(N \times N)$ matrix containing the partial derivatives defined by (B.11) and (4.25) and is thus a diagonal matrix with positive terms and $\mathbf{1}_N$ is an N-vector of unity elements arising from (B.10). For a single equality constraint, If a candidate solution is a minimum then

$$\det(\mathcal{H}_{B,k}) \quad < \quad 0, \ 3 \leq k \leq N + 1 \tag{B.13}$$

where $\mathcal{H}_{B,k}$, the kth leading principal minor, is the upper left $(k \times k)$ sub-matrix of $\mathcal{H}_B$. Because of the structure of $\mathcal{H}_B$ all the relevant leading principal minors have the same structure as the bordered Hessian itself. Thus, without loss of generality, we only need to consider $\det(\mathcal{H}_B)$ to infer the rest

$$\det(\mathcal{H}_B) \quad = \quad \det(0 - \mathbf{1}_N^T \mathcal{H}^{-1} \mathbf{1}_N) \det(\mathcal{H}) < 0 \tag{B.14}$$

because $\det(\mathcal{H}) = \prod_{i=0}^{N-1} \frac{2D_i}{E_i^3} > 0$ and $\mathbf{1}_N^T \mathcal{H}^{-1} \mathbf{1}_N = \sum_{i=0}^{N-1} \frac{E_i^3}{2D_i} > 0$. Thus because (B.13) is satisfied, the candidate solution (4.25) is a minimum and we have already shown that it is the only minimum that satisfies the non-negative energy constraint. Hence it is the global minimum for original optimization problem (4.18). Proof by Prof. B.Mulgrew.

References

[1] M. Richards, *Fundamentals of Radar Signal Processing, Second Edition*. McGraw-Hill Education, 2014.

[2] K. Gerlach, M. Frey, M. Steiner, and A. Shackelford, "Spectral nulling on transmit via nonlinear FM radar waveforms," *Aerospace and Electronic Systems, IEEE Transactions on*, vol. 47, pp. 1507–1515, April 2011.

[3] T. Miller, L. Potter, and J. McCorkle, "RFI suppression for ultra wideband radar," *IEEE Transactions on Aerospace and Electronic Systems*, vol. 33, pp. 1142–1156, Oct 1997.

[4] F. Zhou, R. Wu, M. Xing, and Z. Bao, "Eigensubspace-based filtering with application in narrow-band interference suppression for SAR," *IEEE Geoscience and Remote Sensing Letters*, vol. 4, pp. 75–79, Jan 2007.

[5] F. Zhou and M. Tao, "Research on methods for narrow-band interference suppression in synthetic aperture radar data," *IEEE Journal of Selected Topics in Applied Earth Observations and Remote Sensing*, vol. 8, pp. 3476–3485, July 2015.

[6] C. V. J. Jakowatz, D. E. Wahl, P. H. Eichel, D. C. Ghiglia, and P. A. Thompson, *Spotlight-Mode Synthetic Aperture Radar: A Signal Processing Approach*. Springer US, 1996.

[7] A. Golden, Jr., S. A. Werness, M. A. Stuff, S. R. DeGraaf, and R. C. Sullivan, Jr., "Radio frequency interference removal in a VHF/UHF deramp SAR," *Proc. SPIE*, vol. 2487, pp. 84–95, 1995.

[8] M. Soumekh, *Synthetic Aperture Radar Signal Processing with MATLAB Algorithms*. New York: J. Wiley, May 1999.

[9] H. Griffiths, "Where has all the spectrum gone?," in *Radar (Radar), 2013 International Conference on*, pp. 1–5, Sept 2013.

[10] C. Nunn and L. R. Moyer, "Spectrally-compliant waveforms for wideband radar," *IEEE Aerospace and Electronic Systems Magazine*, vol. 27, pp. 11–15, August 2012.

[11] R. T. Lord and M. R. Inggs, "Approaches to RF interference suppression for VHF/UHF synthetic aperture radar," in *Communications and Signal Processing, 1998. COMSIG '98. Proceedings of the 1998 South African Symposium on*, pp. 95–100, Sep 1998.

[12] T. Koutsoudis and L. A. Lovas, "RF interference suppression in ultrawideband radar receivers," *Proc. SPIE*, vol. 2487, pp. 107–118, 1995.

[13] M. E. Davis, *Foliage Penetration Radar: Detection and characterisation of objects under trees.* Radar, Sonar & Navigation, Institution of Engineering and Technology, 2011.

[14] R. Calderbank, S. Howard, and B. Moran, "Waveform diversity in radar signal processing," *Signal Processing Magazine, IEEE*, vol. 26, no. 1, pp. 32–41, 2009.

[15] D. A. Garren, M. K. Osborn, A. C. Odom, J. S. Goldstein, S. U. Pillai, and J. R. Guerci, "Enhanced target detection and identification via optimised radar transmission pulse shape," *IEE Proceedings - Radar, Sonar and Navigation*, vol. 148, pp. 130–138, Jun 2001.

[16] X. Gong, H. Meng, Y. Wei, and X. Wang, "Phase-modulated waveform design for extended target detection in the presence of clutter," *Sensors*, vol. 11, no. 7, pp. 7162–7177, 2011.

[17] M. Bica, K. W. Huang, V. Koivunen, and U. Mitra, "Mutual information based radar waveform design for joint radar and cellular communication systems," in *2016 IEEE International Conference on Acoustics, Speech and Signal Processing (ICASSP)*, pp. 3671–3675, March 2016.

[18] K. Bell, C. Baker, G. Smith, J. Johnson, and M. Rangaswamy, "Fully adaptive radar for target tracking part i: Single target tracking," in *Radar Conference, 2014 IEEE*, pp. 0303–0308, May 2014.

[19] K. Bell, C. Baker, G. Smith, J. Johnson, and M. Rangaswamy, "Fully adaptive radar for target tracking part ii: Target detection and track initiation," in *Radar Conference, 2014 IEEE*, pp. 0309–0314, May 2014.

[20] R. Gui, W. Q. Wang, Y. Pan, and J. Xu, "Cognitive target tracking via angle-range-doppler estimation with transmit subaperturing fda radar," *IEEE Journal of Selected Topics in Signal Processing*, vol. 12, pp. 76–89, Feb 2018.

[21] D. Kershaw and R. Evans, "Optimal waveform selection for tracking systems," *Information Theory, IEEE Transactions on*, vol. 40, pp. 1536–1550, Sep 1994.

[22] S. Sira, A. Papandreou-Suppappola, D. Morrell, and D. Cochran, "Waveform-agile sensing for tracking multiple targets in clutter," in *Information Sciences and Systems, 2006 40th Annual Conference on*, pp. 1418–1423, 2006.

[23] N. Goodman, P. Venkata, and M. Neifeld, "Adaptive waveform design and sequential hypothesis testing for target recognition with active sensors," *Selected Topics in Signal Processing, IEEE Journal of*, vol. 1, pp. 105–113, June 2007.

[24] Y. Wei, H. Meng, and X. Wang, "Adaptive single-tone waveform design for target recognition in cognitive radar," in *Radar Conference, 2009 IET International*, pp. 1–4, April 2009.

[25] A. Aubry, V. Carotenuto, and A. D. Maio, "Forcing multiple spectral compatibility constraints in radar waveforms," *IEEE Signal Processing Letters*, vol. 23, pp. 483–487, April 2016.

[26] A. Aubry, A. D. Maio, Y. Huang, M. Piezzo, and A. Farina, "A new radar waveform design algorithm with improved feasibility for spectral coexistence," *IEEE Transactions on Aerospace and Electronic Systems*, vol. 51, pp. 1029–1038, April 2015.

[27] A. Aubry, A. De Maio, M. Piezzo, and A. Farina, "Radar waveform design in a spectrally crowded environment via nonconvex quadratic optimization," *Aerospace and Electronic Systems, IEEE Transactions on*, vol. 50, pp. 1138–1152, April 2014.

[28] L. K. Patton and B. D. Rigling, "Phase retrieval for radar waveform optimization," *Aerospace and Electronic Systems, IEEE Transactions on*, vol. 48, pp. 3287–3302, October 2012.

[29] S. Kay, "Optimal signal design for detection of Gaussian point targets in stationary Gaussian clutter/reverberation," *Selected Topics in Signal Processing, IEEE Journal of*, vol. 1, pp. 31–41, 2007.

[30] S. Kay, "Representation and generation of non-Gaussian wide-sense stationary random processes with arbitrary PSDs and a class of PDFs," *Signal Processing, IEEE Transactions on*, vol. 58, no. 7, pp. 3448–3458, 2010.

[31] T. Zhang and X. G. Xia, "OFDM synthetic aperture radar imaging with sufficient cyclic prefix," *IEEE Transactions on Geoscience and Remote Sensing*, vol. 53, pp. 394–404, Jan 2015.

[32] S. D. Blunt and E. L. Mokole, "Overview of radar waveform diversity," *Aerospace and Electronic Systems Magazine, IEEE*, vol. 31, pp. 2–42, November 2016.

[33] E. Fowle, "The design of FM pulse compression signals," *IEEE Transactions on Information Theory*, vol. 10, pp. 61–67, Jan 1964.

[34] T. Zhang, X. G. Xia, and L. Kong, "IRCI free range reconstruction for SAR imaging with arbitrary length OFDM pulse," *IEEE Transactions on Signal Processing*, vol. 62, pp. 4748–4759, Sept 2014.

[35] D. Garmatyuk and M. Brenneman, "Adaptive multicarrier OFDM SAR signal processing," *IEEE Transactions on Geoscience and Remote Sensing*, vol. 49, pp. 3780–3790, Oct 2011.

[36] S. Sen, "OFDM radar space-time adaptive processing by exploiting spatio-temporal sparsity," *Signal Processing, IEEE Transactions on*, vol. 61, no. 1, pp. 118–130, 2013.

[37] G. E. A. Franken, H. Nikookar, and P. V. Genderen, "Doppler tolerance of OFDM-coded radar signals," in *2006 European Radar Conference*, pp. 108–111, Sept 2006.

[38] N. Levanon, "Multifrequency radar signals," in *Record of the IEEE 2000 International Radar Conference [Cat. No. 00CH37037]*, pp. 683–688, 2000.

[39] S. Haykin, "Cognitive radar: A way of the future," *Signal Processing Magazine, IEEE*, vol. 23, pp. 30–40, Jan 2006.

[40] J. Ender and S. Bruggenwirth, "Cognitive radar - enabling techniques for next generation radar systems," in *2015 16th International Radar Symposium (IRS)*, pp. 3–12, June 2015.

[41] D. Cochran, S. Suvorova, S. Howard, and B. Moran, "Waveform libraries," *Signal Processing Magazine, IEEE*, vol. 26, no. 1, pp. 12–21, 2009.

[42] C. E. Shannon, "A mathematical theory of communication," *Bell System Technical Journal*, vol. 27, pp. 379–423, July 1948.

[43] P. Woodward, "Theory of radar information," *Transactions of the IRE Professional Group on Information Theory*, vol. 1, pp. 108–113, Feb 1953.

[44] D. DeLong and E. Hofstetter, "On the design of optimum radar waveforms for clutter rejection," *IEEE Transactions on Information Theory*, vol. 13, pp. 454–463, July 1967.

[45] W. D. Rummler, "Clutter suppression by complex weighting of coherent pulse trains," *IEEE Transactions on Aerospace and Electronic Systems*, vol. AES-2, pp. 689–699, Nov 1966.

[46] S. U. Pillai, K. Y. Li, and H. Beyer, "Reconstruction of constant envelope signals with given fourier transform magnitude," in *Radar Conference, 2009 IEEE*, pp. 1–4, May 2009.

[47] M. Bell, "Information theory and radar waveform design," *Information Theory, IEEE Transactions on*, vol. 39, pp. 1578–1597, Sep 1993.

[48] J. Guerci, "Cognitive radar: A knowledge-aided fully adaptive approach," in *Radar Conference, 2010 IEEE*, pp. 1365–1370, May 2010.

[49] R. Romero, J. Bae, and N. Goodman, "Theory and application of SNR and mutual information matched illumination waveforms," *Aerospace and Electronic Systems, IEEE Transactions on*, vol. 47, pp. 912–927, April 2011.

[50] A. Leshem, O. Naparstek, and A. Nehorai, "Information theoretic adaptive radar waveform design for multiple extended targets," *IEEE Journal of Selected Topics in Signal Processing*, vol. 1, pp. 42–55, June 2007.

[51] Y. Yang and R. S. Blum, "Mimo radar waveform design based on mutual information and minimum mean-square error estimation," *IEEE Transactions on Aerospace and Electronic Systems*, vol. 43, pp. 330–343, January 2007.

[52] D. Guo, S. Shamai, and S. Verdu, "Mutual information and minimum mean-square error in gaussian channels," *IEEE Transactions on Information Theory*, vol. 51, pp. 1261–1282, April 2005.

[53] S. Sen and A. Nehorai, "OFDM MIMO radar with mutual-information waveform design for low-grazing angle tracking," *IEEE Transactions on Signal Processing*, vol. 58, pp. 3152–3162, June 2010.

[54] S. Herbert, J. R. Hopgood, and B. Mulgrew, "MMSE adaptive waveform design for active sensing with applications to mimo radar," *IEEE Transactions on Signal Processing*, vol. 66, pp. 1361–1373, March 2018.

[55] F. F. Kretschmer and K. Gerlach, "Low sidelobe radar waveforms derived from orthogonal matrices," *IEEE Transactions on Aerospace and Electronic Systems*, vol. 27, pp. 92–102, Jan 1991.

[56] M. A. Kerahroodi, A. Aubry, A. D. Maio, M. M. Naghsh, and M. Modarres-Hashemi, "A coordinate-descent framework to design low PSL/ISL sequences," *IEEE Transactions on Signal Processing*, vol. 65, pp. 5942–5956, Nov 2017.

[57] S. Mertens, "Exhaustive search for low-autocorrelation binary sequences," *Journal of Physics A: Mathematical and General*, vol. 29, no. 18, p. L473, 1996.

[58] P. Stoica, H. He, and J. Li, "New algorithms for designing unimodular sequences with good correlation properties," *IEEE Transactions on Signal Processing*, vol. 57, pp. 1415–1425, April 2009.

[59] K. Gerlach, "Thinned spectrum ultrawideband waveforms using stepped-frequency polyphase codes," *IEEE Transactions on Aerospace and Electronic Systems*, vol. 34, pp. 1356–1361, Oct 1998.

[60] I. W. Selesnick, S. U. Pillai, and R. Zheng, "An iterative algorithm for the construction of notched chirp signals," in *2010 IEEE Radar Conference*, pp. 200–203, May 2010.

[61] I. W. Selesnick and S. U. Pillai, "Chirp-like transmit waveforms with multiple frequency-notches," in *2011 IEEE RadarCon (RADAR)*, pp. 1106–1110, May 2011.

[62] L. Jackson, S. Kay, and N. Vankayalapati, "Iterative method for nonlinear FM synthesis of radar signals," *Aerospace and Electronic Systems, IEEE Transactions on*, vol. 46, no. 2, pp. 910–917, 2010. CM waveform synthesis.

[63] H. He, P. Stoica, and J. Li, "Waveform design with stopband and correlation constraints for cognitive radar," in *2010 2nd International Workshop on Cognitive Information Processing*, pp. 344–349, June 2010.

[64] L. Patton, D. Hack, and B. Himed, "Adaptive pulse design for space-time adaptive processing," in *Sensor Array and Multichannel Signal Processing Workshop (SAM), 2012 IEEE 7th*, pp. 25–28, 2012. Himed.

[65] G. Cui, X. Yu, Y. Yang, and L. Kong, "Cognitive phase-only sequence design with desired correlation and stopband properties," *IEEE Transactions on Aerospace and Electronic Systems*, vol. 53, pp. 2924–2935, Dec 2017.

[66] H. Subbaram and K. Abend, "Interference suppression via orthogonal projections: a performance analysis," *IEEE Transactions on Antennas and Propagation*, vol. 41, pp. 1187–1194, Sep 1993.

[67] M. S. Lam Nguyen, "Suppression of radio frequency inteference (RFI) for synchronous impulse reconstruction ultra-wideband radar," *Proc.SPIE*, vol. 5808, pp. 5808 – 5808 – 7, 2005.

[68] J. O.Ojowu Jr, "RFI suppression for synchronous impulse reconstruction UWB radar using RELAX," *Int. J. Remote. Sens. Appl.*, vol. 3, pp. 33–46, March 2013.

[69] M. Braunstein, J. Ralston, and A. Sparrow, "Signal processing approaches to radio frequency interference (rfi) suppression," vol. 2230, pp. 2230 – 2230 – 19, 1994.

[70] L. C. P. Timothy R. Miller, John W. McCorkle, "Near-least-squares radio frequency interference suppression," *Proc.SPIE*, vol. 2487, pp. 2487 – 2487 – 12, 1995.

[71] J. K. Abend, "Radio and tv interference extraction for ultrawideband radar," *Proc.SPIE*, vol. 2487, pp. 2487 – 2487 – 11, 1995.

[72] S. Haykin, *Adaptive Filter Theory (3rd Ed.)*. Upper Saddle River, NJ, USA: Prentice-Hall, Inc., 1996.

[73] R. T. Lord and M. R. Inggs, "Efficient RFI suppression in SAR using lms adaptive filter integrated with range/doppler algorithm," *Electronics Letters*, vol. 35, pp. 629–630, Apr 1999.

[74] D. O. Carhoun, "Adaptive nulling and spatial spectral estimation using an iterated principal components decomposition," in *[Proceedings] ICASSP 91: 1991 International Conference on Acoustics, Speech, and Signal Processing*, pp. 3309–3312 vol.5, Apr 1991.

[75] X. Luo, L. M. H. Ulander, J. Askne, G. Smith, and P. O. Frolind, "RFI suppression in ultra-wideband SAR systems using LMS filters in frequency domain," *Electronics Letters*, vol. 37, pp. 241–243, Feb 2001.

[76] J. Tsao and B. D. Steinberg, "Reduction of sidelobe and speckle artifacts in microwave imaging: the clean technique," *IEEE Transactions on Antennas and Propagation*, vol. 36, pp. 543–556, Apr 1988.

[77] F. J. Meyer, J. B. Nicoll, and A. P. Doulgeris, "Correction and characterization of radio frequency interference signatures in l-band synthetic aperture radar data," *IEEE Transactions on Geoscience and Remote Sensing*, vol. 51, pp. 4961–4972, Oct 2013.

[78] A. Reigber and L. Ferro-Famil, "Interference suppression in synthesized SAR images," *IEEE Geoscience and Remote Sensing Letters*, vol. 2, pp. 45–49, Jan 2005.

[79] F. Zhou, M. Xing, X. Bai, G. Sun, and Z. Bao, "Narrow-band interference suppression for SAR based on complex empirical mode decomposition," *IEEE Geoscience and Remote Sensing Letters*, vol. 6, pp. 423–427, July 2009.

[80] F. Zhou, G. Sun, X. Bai, and Z. Bao, "A novel method for adaptive SAR barrage jamming suppression," *IEEE Geoscience and Remote Sensing Letters*, vol. 9, pp. 292–296, March 2012.

[81] F. Zhou, M. Tao, X. Bai, and J. Liu, "Narrow-band interference suppression for SAR based on independent component analysis," *IEEE Transactions on Geoscience and Remote Sensing*, vol. 51, pp. 4952–4960, Oct 2013.

[82] F. Zhou, M. Tao, and Z. Bao, "Suppression of narrow-band interference in SAR data," in *2014 IEEE Geoscience and Remote Sensing Symposium*, pp. 227–230, July 2014.

[83] M. Tao, F. Zhou, J. Liu, Y. Liu, Z. Zhang, and Z. Bao, "Narrow-band interference mitigation for sar using independent subspace analysis," *IEEE Transactions on Geoscience and Remote Sensing*, vol. 52, pp. 5289–5301, Sept 2014.

[84] Z. Liu, G. Liao, and Z. Yang, "Time variant rfi suppression for SAR using iterative adaptive approach," *IEEE Geoscience and Remote Sensing Letters*, vol. 10, pp. 1424–1428, Nov 2013.

[85] M. Tao, F. Zhou, and Z. Zhang, "Wideband interference mitigation in high-resolution airborne synthetic aperture radar data," *IEEE Transactions on Geoscience and Remote Sensing*, vol. 54, pp. 74–87, Jan 2016.

[86] H. Liu, D. Li, Y. Zhou, and T. K. Truong, "Joint wideband interference suppression and SAR signal recovery based on sparse representations," *IEEE Geoscience and Remote Sensing Letters*, vol. 14, pp. 1542–1546, Sept 2017.

[87] M. Pinheiro, M. Rodriguez-Cassola, P. Prats-Iraola, A. Reigber, G. Krieger, and A. Moreira, "Reconstruction of coherent pairs of synthetic aperture radar data acquired in interrupted mode," *IEEE Transactions on Geoscience and Remote Sensing*, vol. 53, pp. 1876–1893, April 2015.

[88] M. Pinheiro and M. Rodriguez-Cassola, "Reconstruction methods of missing SAR data: Analysis in the frame of tandem-x synchronization link," in *EUSAR 2012; 9th European Conference on Synthetic Aperture Radar*, pp. 742–745, April 2012.

[89] J. Salzman, D. Akamine, R. Lefevre, and J. C. Kirk, "Interrupted synthetic aperture radar (SAR)," *IEEE Aerospace and Electronic Systems Magazine*, vol. 17, pp. 33–39, May 2002.

[90] E. G. Larsson, P. Stoica, and J. Li, "Amplitude spectrum estimation for two-dimensional gapped data," *IEEE Transactions on Signal Processing*, vol. 50, pp. 1343–1354, Jun 2002.

[91] S. I. Kelly and M. E. Davies, "RFI suppression and sparse image formation for UWB SAR," in *2013 14th International Radar Symposium (IRS)*, vol. 2, pp. 655–660, June 2013.

[92] G. Turin, "An introduction to matched filters," *IRE Transactions on Information Theory*, vol. 6, pp. 311–329, June 1960.

[93] H. S. Mir and U. K. T. Wong, "Low-rate sampling technique for range-windowed radar/sonar using nonlinear frequency modulation," *IEEE Transactions on Aerospace and Electronic Systems*, vol. 51, pp. 1972–1979, July 2015.

[94] A. Goldsmith, *Multicarrier Modulation*, ch. 12, p. 374?402. Cambridge University Press, 2005.

[95] M. Levin, "Optimum estimation of impulse response in the presence of noise," *IRE Transactions on Circuit Theory*, vol. 7, pp. 50–56, Mar 1960.

[96] H. Wold and P. Faxer, "On the specification error in regression analysis," *Ann. Math. Statist.*, vol. 28, pp. 265–267, 03 1957.

[97] G. Goodwin, G. Goodwin, and R. Payne, *Dynamic System Identification: Experiment Design and Data Analysis*. Developmental Psychology Series, Academic Press, 1977.

[98] S. Sen and A. Nehorai, "Adaptive design of OFDM radar signal with improved wideband ambiguity function," *IEEE Transactions on Signal Processing*, vol. 58, pp. 928–933, Feb 2010.

[99] T. Amemiya, *Advanced Econometrics*. Havard University Press, 1985.

[100] J. J. Shynk, "Frequency-domain and multirate adaptive filtering," *Signal Processing Magazine, IEEE*, vol. 9, pp. 14 – 37, 02 1992.

[101] J. Kennedy and R. Eberhart, "Particle swarm optimization," in *Neural Networks, 1995. Proceedings., IEEE International Conference on*, vol. 4, pp. 1942–1948 vol.4, Nov 1995.

[102] M. Hamidi and J. Pearl, "Comparison of the cosine and Fourier transforms of Markov-1 signals," *IEEE Transactions on Acoustics, Speech, and Signal Processing*, vol. 24, pp. 428–429, Oct 1976.

[103] H. L. Van Trees, *Optimum Array Processing*. John Wiley & Sons, Inc., New York, USA, 2002.

[104] C. Tierney and B. Mulgrew, "Waveform independent range profile reconstruction for SAR," in *2017 IET Radar Conference*, p. To appear, October 2017.

[105] W. Huleihel, J. Tabrikian, and R. Shavit, "Optimal adaptive waveform design for cognitive MIMO radar," *Signal Processing, IEEE Transactions on*, vol. 61, no. 20, pp. 5075–5089, 2013.

[106] T. H. Cormen, C. E. Leiserson, R. L. Rivest, and C. Stein, *Introduction to Algorithms, Third Edition*. The MIT Press, 3rd ed., 2009.

[107] M. Cetin and R. L. Moses, "SAR imaging from partial-aperture data with frequency-band omissions," vol. 5808, pp. 5808 – 5808 – 12, 2005.

[108] S. W. Frost and B. Rigling, "Sidelobe predictions for spectrally-disjoint radar waveforms," in *2012 IEEE Radar Conference*, pp. 0247–0252, May 2012.

[109] P. Broersen, "The abc of autoregressive order selection criteria," *IFAC Proceedings Volumes*, vol. 30, no. 11, pp. 245 – 250, 1997. IFAC Symposium on System Identification (SYSID'97), Kitakyushu, Fukuoka, Japan, 8-11 July 1997.

[110] S. de Waele and P. M. T. Broersen, "The burg algorithm for segments," *IEEE Transactions on Signal Processing*, vol. 48, pp. 2876–2880, Oct 2000.

[111] H. Akaike, "A new look at the statistical model identification," *IEEE Transactions on Automatic Control*, vol. 19, pp. 716–723, Dec 1974.

[112] J. H. Ender, "On compressive sensing applied to radar," *Signal Processing*, vol. 90, no. 5, pp. 1402 – 1414, 2010. Special Section on Statistical Signal & Array Processing.

[113] L. A. Gorham and L. J. Moore, "Sar image formation toolbox for matlab," 2010.

[114] M. D. Desai and W. K. Jenkins, "Convolution backprojection image reconstruction for spotlight mode synthetic aperture radar," *IEEE Transactions on Image Processing*, vol. 1, pp. 505–517, Oct 1992.

[115] T. A. Khan, T. A. Taj, M. K. Asif, and I. Ijaz, "Modeling of a standard particle swarm optimization algorithm in matlab by different benchmarks," in *Second International Conference on the Innovative Computing Technology (INTECH 2012)*, pp. 271–274, Sept 2012.

[116] D. Bratton and J. Kennedy, "Defining a standard for particle swarm optimization," in *2007 IEEE Swarm Intelligence Symposium*, pp. 120–127, April 2007.

[117] R. C. Eberhart and Y. Shi, "Comparing inertia weights and constriction factors in particle swarm optimization," in *Proceedings of the 2000 Congress on Evolutionary Computation. CEC00 (Cat. No.00TH8512)*, vol. 1, pp. 84–88 vol.1, 2000.

[118] M. A. H. Nerenberg, "The second derivative test for constrained extremum problems," *International Journal of Mathematical Education in Science and Technology*, vol. 22, no. 2, pp. 303–308, 1991.